Methods for Optimization of Neutron Detector Performance in Nuclear Power Plants

by

Elnara Nasimi

A thesis submitted to the
School of Graduate and Postdoctoral Studies in partial
fulfillment of the requirements for the degree of

Doctor of Philosophy in Nuclear Engineering

The Faculty of Energy Systems and Nuclear Science
University of Ontario Institute of Technology
Oshawa, Ontario, Canada

August 2018

THESIS EXAMINATION INFORMATION

Submitted by: **Elnara Nasimi**

Doctor of Philosophy in **Nuclear Engineering**

Thesis title: Methods for Optimization of Neutron Detector Performance in Nuclear Power Plants

An oral defense of this thesis took place on March 12, 2018 in front of the following examining committee:

Examining Committee:

Chair of Examining Committee	Dr. Langis Roy
Research Supervisor	Dr. Hossam Gaber
Examining Committee Member	Dr. Shahryar Rahnamayan
Examining Committee Member	Dr. Jing Ren
University Examiner	Dr. Akira Tokuhiro
External Examiner	Dr. Mehrdad Saif, University of Windsor

The above committee determined that the thesis is acceptable in form and content and that a satisfactory knowledge of the field covered by the thesis was demonstrated by the candidate during an oral examination. A signed copy of the Certificate of Approval is available from the School of Graduate and Postdoctoral Studies.

ABSTRACT

Safety of nuclear power plants (NPPs) requires shutdown systems to mitigate design-basis accidents. Shutdown is based on measurements from in-core flux detectors. Thus, this thesis proposes a methodology for managing neutron-detector aging. Detector performance improvement for prompt fraction along with genetic algorithm optimization, risk estimation, and the fault semantic network (FSN) are studied.

Detector models have been developed using circuit models to represent detector behavior in aged conditions. For cases with preprocessed measured data, initial conditions are set to the initial sample value, and an inverse of the transform is applied to reconstruct the signal at the detector. The model's response is compared to the plant data to validate output. Proposed gains have been implemented in the model with the old gain values to compare with FUELPIN code predictions. A genetic algorithm has been selected to solve optimization and search problems where the Dynamic Signal Compensator (DSC) function is the objective function and the detector function is the fitness function. Two new sets of gain constants have been used to solve the power ramp-up case, allowing reduction of maximum margin-to-trip (MTT) loss to 0.8%.

The risk model has been established in the FSN using historical data, and the risk factor for all channels has been identified. The initial channel table and risk prioritization map are updated as information becomes available. This is demonstrated in three case studies where assumed component failure rates were used in a qualitative/quantitative manner for risk estimation.

The results suggest the simulated ramp rate with the optimized DSC gain constants is conservative compared to actual fueling and signal oscillation rates. Further gains in detector prompt fraction were obtained by optimization of the amplifier gain settings through genetic algorithm with no adverse impact on operating margins.

Keywords: neutron detector aging; degradation of detector prompt fraction; fault semantic network; risk-informed decision making; lifetime extensions.

AUTHOR'S DECLARATION

I hereby declare that this thesis consists of original work of which I have authored. This is a true copy of the thesis, including any required final revisions, as accepted by my examiners.

I authorize the University Of Ontario Institute Of Technology to lend this thesis to other institutions or individuals for the purpose of scholarly research. I further authorize University of Ontario Institute of Technology to reproduce this thesis by photocopying or by other means, in total or in part, at the request of other institutions or individuals for the purpose of scholarly research. I understand that my thesis will be made electronically available to the public.

_____ ELNARA NASIMI

STATEMENT OF CONTRIBUTIONS

I hereby certify that I am the sole author of this thesis and that no part of this thesis has been published or submitted for publication. I have used standard referencing practices to acknowledge ideas, research techniques, or other materials that belong to others. Furthermore, I hereby certify that I am the sole source of the creative works and/or inventive knowledge described in this thesis.

ACKNOWLEDGEMENTS

I would like to express my deepest, heartfelt gratitude to Professor Hossam A. Gaber, my thesis advisor. Without his continuous support, my PhD study and related research would not have been possible. I am extremely grateful for his patience, motivation, and tremendous knowledge. His guidance helped me during the research and writing of this thesis. I could not have imagined having a better advisor and mentor.

Next, my gratitude goes to my thesis supervisory committee, Professor J. Ren and Professor S. Rahnamayan, for their insightful comments and encouragement. The hard questions they asked inspired me to widen my research from various perspectives.

I would also like to express a special thank-you and tremendous gratitude to Mr. Todd Stroud, without whose precious support it would not be possible to conduct this research.

Finally, my sincere thanks also go to Mr. Lovell Gilbert, who supported my work and gave me access to the necessary materials, time, and resources.

TABLE OF CONTENTS

List of Tables

CHAPTER 2

CHAPTER 3

CHAPTER 4

CHAPTER 5

LIST OF FIGURES

CHAPTER 2

CHAPTER 3

CHAPTER 4

CHAPTER 5

LIST OF ABBREVIATIONS AND SYMBOLS

1D	One-Dimensional
2D	Two-Dimensional
3D	Three-Dimensional
AECL	Atomic Energy Canada Limited
AF	Amplifier
ANN	Artificial Neural Network
ASMOD	Adaptive B-Spline Modelling
BBN	Bayesian Belief Network
BLW	Boiling Light Water
CaFr	Causal Factor
CANDU™	CANada Deuterium Uranium
CNSC	Canadian Nuclear Safety Commission
COG	CANDU™ Owners Group
CoIm	Impact of Consequence
CoPr	Probability of Consequence
CPPF	Channel Power Peaking Factor
CRNL	Chalk River National Laboratories
CV	Control Variable
D_2O	Deuterium Oxide (heavy water)
DCC	Distributed Control Computers
Dev	Deviation
DRAGON	Transport code for three-dimensional (3D) modelling of reactivity devices
DSC	Dynamic Signal Compensator
EBR	Experimental Breeder Reactor
EFWS	Emergency Feed-Water System
EMI	Electro-Magnetic Interference
EPF	Effective Prompt Fraction
ETA	Event Tree Analysis
FBR	Fast Breeder Reactor

FDI	Fault Detection and Identification
FDS	Fault Diagnostic System
FFS	Fault Forecasting System
FFT	Fast Fourier transform
FL	Fuzzy Logic
FM	Failure Mode
FMECA	Failure Mode, Effects, and Criticality Analysis
FM-ID	Failure Mode Identifier
FP	Full Power
FPr	Probability of Failure
FSN	Fault Semantic Network
FTA	Fault Tree Analysis
FUELPIN	Heat transfer/point kinetics performance code for transient analysis
FUSVAF	Fuzzy Sensor Validation and Fusion
GA	Genetic Algorithms
HAZOP	Hazard and Operability
HCC	Hierarchical Control Chart
HMT	Hidden Markov Tree
HPSW	High Pressure Service Water
HTM	Hidden Markov Tree
HWPR	Heavy Water Pressurized Reactor
HX	Heat Exchanger
I&C	Instrumentation and Control
IAE	Integral Absolute Error
IAEA	International Atomic Energy Agency
ICFD	In-Core Flux Detectors
ID	Identifier
ISA	International Standards Agency
ISE	Integral Squared Error
IST	Industry Standard Tool
ITSE	Integral Time Squared Error

KPCA	Kernel Principal Component Analysis
LBLOCA	Large Break Loss of Coolant Accident
LNG	Liquefied Natural Gas
LOCA	Loss of Coolant Accident
LOPA	Layers Of Protection Analysis
LP	Loading Pattern
LPF	Low-Pass Filter
LT	Level Transmitter
LZ	Liquid Zone
LZC	Liquid Zone Control
MATLAB	Matrix Laboratory (Mathworks, Inc.)
MCNP	Monte Carlo Neutron and Photon transport code
MCNP-REN	MCNP- Random Exponentially distributed Neutron source
MCNPX	Fortran 90 Monte Carlo radiation transport computer code
MLP	Multi-Layer Perceptron
MSE	Mean Square Error
MTT	Margin-to-Trip
MV	Motorized Valve
MVA	Multivariate Analysis
MWT	Morlet Wavelet Transform
NaN	Not a Number
NE	North East
Ni	Nickel
NLPCA	Non-Linear Principle Component Analysis
NN	Neural Network
NOP	Neutron Overpower Protection
NPP	Nuclear Power Plant
NPT	Node Probability Table
NRU	National Research Universal
NW	North West
OPG	Ontario Power Generation

P&ID	Piping and Instrumentation Diagram
PBD	Process Block Diagram
PCA	Principle Component Analysis
PF	Prompt Fraction
PFB	Process Flow Block
PFD	Probability of Failure on Demand
PFD	Process Flow Diagram
PFU	Predicted Future Unavailability
Ph.D	Philosophiae doctor (Doctor of Philosophy)
PHT	Primary Heat Transport
PHWR	Pressurized Heavy Water Reactor
PID	Proportional-Integral-Derivative
PLS	Partial Least Squares regression
PRA	Probabilistic Risk Assessment
PSA	Probabilistic Safety Analysis
PSO	Particle Swamp Optimization
PV	Process Variable
PWR	Pressurized Water Reactor
RBF	Radial Basis Function
RDS	Required Detector Setting
REM	Roentgen Equivalent Man
RF	Radio Frequency
RFSP	Reactor Fueling Simulation Program – Industry Standard Tool
RP	Reactor Power
RPM	Rotations per Minute
RRS	Reactor Regulating System
RSS	Root Sum Square
RTD	Resistance Temperature Detector
RVAR	Restricted Vector Auto-regressive
SAL	Safety Analysis Limit
SDS	Shutdown System

SG	Steam Generator
SIMBRASS	The nuclear safety analysis code used to establish the NOP trip setpoints
SNR	Signal to Noise Ratio
SPND	Self-Powered Neutron Detector
SURE	Stein's Unbiased Risk Estimate
TE	Tennessee Eastman
Temp	Temperature
TP	Test Point
TSA	Time Synchronized Averaging
TSP	Trip Setpoint
UOIT	University of Ontario Institute of Technology
VAR	Vector Auto-regression
VDC	Volt (Direct Current)
WASH-1400	A report produced in 1975 for the US Nuclear Regulatory Commission
WIMS-IST	Transport code for the calculation of lattice-cell properties
wPCA	Weighted Principle Component Analysis
wRMS	Weighted Root Mean Square

NOMENCLATURE

C_v	flow coefficient
DIV	division
e	noise
EPF	effective prompt fraction, in %
eV	electron Volt, approximately 1.6×10^{-19} joules
f	sensor bias
F.P.	full power, in [%] or decade
f_i	transfer function
G	Giga, 10^9
$h^{(u)}$	the decoding layer
$h^{(x)}$	first hidden layer
hr	hour
Hz	unit of frequency, one cycle per second
i and j	subscripts
in	inch
J	the cost function
K	Kilo, 10^3
k	1, 2, …, *n* , a corresponding data axis of y(k)
K	process gain
K_1	constant, adjustable from 0.90 to 1.15
K_2	constant, adjustable from 0.006 to 0.057
K_3	constant, adjustable from 0.031 to 0.093
kg	unit measure
kg/s	flow rate in [kilogram per second]
kPa(g)	gauge-mode pressure, normally measured with respect to ambient pressure
L	Liter, unit measure
l	vector length
L/s	flow rate in [liter per second]
M	Mega, 10^6

m	milli, 10^{-3}
m	the smooth width, selected to be a positive integer
m	number of rows, integer
m	column vector length
m	a number of hidden neurons
m_c	combined smooth width
mk	fraction of k-effective, measurement of sub criticality
mm	millimeter
MTT	margin to trip, in % Reactor Power
mV	millivolt
n	neutron
n	integer
nv	neutron flux, in [n/cm^2/s]
o	noisy observation
o	unit measure, degree
p	Pico, 10^{-12}
p(x)"	prior distribution
Pa	unit pressure
PF	prompt fraction
$Q^T x^{(k)}$	coordinate system
t	time
%	fraction
°C	degrees Centigrade
°F	degrees Fahrenheit
μ	average
μ	micro, 10^{-6}
μsec	micro-second
235-U	Uranium-235
G	Giga, 10^9
$h^{(u)}$	the decoding layer
$h^{(x)}$	first hidden layer

AMP	signal amplitude in Ampere
D	relative detector signal amplitude, in Volt DC
cps	neutron count rate, in [count/sec]
cps/nv	neutron sensitivity in [counts per second/neutron flux]
D_2O	Deuterium Oxide (heavy water)
hr	hour
Hz	unit of frequency, one cycle per second
m x l	weight matrix
Δt	difference between two point of measurement in time
$PF_i(t_1)$	measured EFP of detector *i* at time t_i
t_1	time typically associated with the most recent outage/measurement
$PF_i(t_1 + \Delta t)$	predicted PF value for detector *i* at time ($t_1 + \Delta t$), in %
$t_{\beta, n-1}$	statistical student t distribution for probability β and n-1 degree of freedoms
$\mu^{(1-\beta)}$	the momentum of the statistical distribution resulting from $pf_i = PF_i(t_1) - PF(t_o)$, at confidence 1-β
m	the mean of the sample
s	standard deviation of the sample set on *n* detector deltas
σ	the standard deviation
β	the value of 90% is assumed to be adequate which can be interpreted as single sided probability
PF	prompt fraction , in %
RP	reactor power, in % full power
CPPF	Channel Power Peaking factor, in % reactor power
TSP	trip setpoint, in % reactor power
REM	Roentgen Equivalent Man
MgO	Magnesium Oxide
Pt	Platinum
Vout	output of the dynamic compensator, in Volt DC
DC	Direct Current
T_2	time, in seconds

T	time, in seconds
sec	second
Vin	input to the dynamic compensator, in Volt DC
τ_i	30 seconds, time constant, in seconds
τ_2	2500 seconds, time constant, in seconds
τ_3	time, in seconds
Fp	in a natural uranium fueled reactor, 70% of the gamma flux, assumed to be prompt
γ	gamma
e	electron
I	total current produced by the detector, in μAmp
I(n, γ, e)	current due to (n, γ, e) reactions, in μAmp
I(γ, e)	current due to (γ, e) reactions, in μAmp
N	neutron flux
$\bar{\gamma}$	total delay fraction
$\bar{\gamma}_i$	*ith* delay fraction
λi	*ith* decay constant
d_i	relative amplitude of delay group *i*
τ	filter time constant
R	Resistance, in Ohm
C	Capacitance, in Farad
α_i	the fraction of the *ith* decay component
t	time (step change occurs at time zero)
τ_i	the decay time constant
$\Delta\phi$	step change in flux
Ω	Resistance, in Ohm
V_{TP}	step input at test point, in Volt DC
TP	test point
S_j	central point to on the x-axis
Y_j	point to on the x-axis at position j
n	number of passes for smoothing
w	the w-width smooth

S_{dev}	standard deviation
S	standard deviation of the remaining noise after smoothing
f_i	data value
g_i	linear combination of a data value with itself
n_L	the number of points to the left of the data point
n_R	the number of points to the right of the data point
cn	filter coefficient, where $c_n=1/(n_L+n_{R+1})$
z_p	filter zero pole
α	filter coefficient
y_n	smoothed output from the filter
h	a data sampling interval, in seconds
w_i	weight
i	an amalgamation of the magnitude of error, computed each time the weights are updated
(err)	the error signal
dt	time derivative
$\psi(t)$	main wavelet function, mother wavelet
$\varphi(t)$	scale function in time domain
a	a scale parameter
b	time translation parameter
v_o	constant
β	shape parameter
RDS	required detector setting, in % Reactor Power
Pwr	reactor power, in % full power
π	mathematical constant
$x^{(k)}$	vector where k=1, 2, …n
X	m by n matrix
i	1, 2, …, m
XX^T	covariant matrix
r	rank of the covariant matrix XX^T
$y^{(k)}$	data axis

$S(Y)$	covariant matrix
$W^{(x)}$	m by l weight matrix
$b(x)$	a column vector of length m
u	non-linear principle component
$h_k^{(u)}$	the decoding layer
x	the original data
x'	the output of the neural network
x_{set}	known parameter setpoint
$x(t)$	obtained measurement x at time t
$\hat{x}(t)$	predicted measurement x at time t
err	the difference between the expected and the obtained value
x''	reduced plant data
F_t	tolerable frequency
F_{np}	process demand frequency
$CaFr$	causal factor
$CoPr1$	probability of consequence
$CoIm$	total Impact of Consequence
$P(X\|A)$	prior distribution of X
$P(A)X$	marginal likelihood, i.e. normalizing constant of the density of the posterior distribution
$P(X)$	likelihood function
$P(A)$	posterior distribution of the parameters
PFD_{avg}	probability of failure on demand, average
P	probability or unavailability, 0=P=1
λ_d	dormant failure rate, in failures per 1000 years
λr	running failure rate, in failures per 1000 years
T_m	mission time, typically in hours
T_r	mean time to repair, hours per failure
T_t	test duration where the component is unavailable during test, in hours
f_m	frequency of occurrence, occurrences per year
T_a	administration time in hours per failure,

T_i	test interval in days
$(T_a + T_r)$	the restoration time
RI	risk increment
IR	instantaneous risk
BR	baseline risk
ΔT	duration of risk state
$p(x)"$	prior distribution
eV	electron-Volt
C_v	flow coefficient
f_i-n_L	range to the left of the data point f_i
f_i+n_R	range to the right of the data point f_i

Chapter 1: Introduction

This chapter introduces the thesis subject and motivation for research. The overall research goal is given along with several specific thesis objectives in support of the primary research target. The originality and innovative contributions of this thesis are also presented in this chapter.

1.1. Motivation

Protection against ionizing radiation is an essential safety requirement for any type of research, development, or commercial application of nuclear energy. To ensure public safety, the primary objective of any utility is to demonstrate that it has a safety case that meets site licensing requirements regarding public dose limits under design-basis accident conditions. In Canada, NPP shutdown systems rely on neutron detection systems to implement this mandate. The Canadian fleet of power reactors, constructed in stages from 1966 to 1991, is nearing the end of its design life. Station measurements of detector responses to flux indicate that the detector performance is decreasing with time and at a significantly faster rate than earlier predicted. The investigation identified that degradation of the dynamic response (i.e., a prompt fraction [PF]) of in-core flux detectors is due to changes in the isotopic composition of the detector material from exposure to the core neutron and gamma flux, i.e., a function of aging.

The current methodology for PF measurements ignores the local conditions of individual in-core detectors, which could cause an error in the results and lead to overestimation of the degradation. Thus, there is an opportunity to challenge and revalidate assumptions and approaches for scheduling detector replacements.

In light of the above discussion, the motivation for this thesis is as follows:

- Degradation of in-core neutron detector prompt fractions due to the effects of aging can adversely affect safety analysis assumptions. There is a need for a method that improves the effective prompt fractions (EPF) for aged detectors. A method which provides the option to delay detector replacement or penalties to the trip setpoints would be desirable. Aging detectors exhibit increased noise response and poor signal discrimination properties, and they are also prone to specific types of signal variations called oscillations. These

contributing factors must be analyzed when developing a new methodology for optimization of detector EPF in aged conditions.

- Any new improvement method must be integrated with a risk estimation mechanism. Such an approach could be used as a companion tool for probabilistic risk analysis (PRA). The main advantage, compared to PRA, is that it can address the instantaneous risk increment to determine whether the continuous operation of the system in a particular configuration is too risky or requires immediate compensatory actions. The approach would need to be suitable for NPP staff to make risk-informed decisions in near-real time.

1.2. Research Objectives

The main issue pertaining to this thesis is to propose a new methodology that:

- will improve the effective prompt fractions for aged detectors,
- may delay the need for detector replacement or the application of penalties,
- will not adversely affect the operational margin to trip.

Accordingly, this overall goal can be translated into the following specific research objectives:

1) Develop simulation models for aged in-core neutron detectors. The model should consider plant transient scenarios, detector noise and signal oscillations, encompassing:
   a) the proposal of two noise reduction techniques, namely low-pass filters (LPF) and wavelet transform analysis (WTA),
   b) performing data dimensionality reduction using principle component analysis (PCA), weighted PCA (wPCA), and nonlinear PCA (NLPCA) with artificial neural network (ANN) methods to reduce the model processing time.

2) Improve prompt fraction for aged detectors with minimum design changes and demonstrate that increasing DSC amplifier gains can mitigate the effects of aging for Pt-clad detectors without significant intrusive modifications to the existing instrumentation.

3) Optimize DSC gain settings using a proposed enhanced genetic algorithm to improve detector prompt fraction in aged conditions; compare the obtained results to the existing model to show

improvement in performance. Residual dynamic signal compensation (DSC) error has been selected as the primary criterion for this assessment.

4) Develop a qualitatative/quantitatative risk estimation method to integrate with the proposed approach for estimating instantaneous risk due to detector degradation to enable risk-informed decisions for detector replacements. FSN methodology is used to qualitatively assess risk from fault scenarios and utilize them in risk estimation to support the objective of delaying detector replacement.

1.3. Contributions

As discussed earlier, a reduction in prompt fraction can have an adverse impact on safety analysis assumptions and increase the risk to production and safety. The existing detector models do not account for potential complications from fueling near detectors and flux detector signal oscillations. This thesis helps to resolve these gaps through the following original contributions:

- The existing detector models are enhanced to account for typical plant transients, e.g., fueling near a noisy, aged detector. The proposed approach is validated using real plant data.
- DSC gain constants are increased to their maximum value based on current hardware limitations, and detector response is evaluated using actual plant data for transient cases while satisfying the maximum criteria for residual DSC error. The proposed approach is validated against a limiting criterion of impact on MTT of ≤1 percent.
- Efficiency improvements are realized by implementing stochastic optimization, which involves the use of random probabilities in the iterative search for a solution. Further efficiencies are gained by applying approximations to the fitness test that is otherwise difficult to construct, too complex, and computationally prohibitive. This enhanced genetic algorithm is used to obtain an optimal set of the DSC gain constants while satisfying the same error and validation criteria.
- A new risk management approach based on an FSN is developed and customized for use in the neutron detection systems to their unique aging characteristics. The approach allows for qualitative and quantitative instantaneous and aggregate risk estimation. The proposed method is validated using real plant data for two different transient scenarios, namely a

noisy detector and a prolonged detector signal oscillation. Additional studies on denoising are performed using an LPF and WTA. The two methods are compared in terms of the highest signal-to-noise improvement. The best-performing method is identified, and an option for additional future optimization is proposed.

- Additional studies into data dimensionality reduction are performed using PCA, wPCA, and NLPCA with an ANN approach. The results are validated against the plant data. An option for future optimization of the NLPCA-ANN approach is proposed to improve network run time for real-time application.

1.4. Publications

Sections of this thesis, as well as other supporting work, have been published in the open literature in peer-reviewed journals and conference papers listed below:

1. Emmanuel Boafo, Elnara Nasimi, Luping Zhang, Hossam A. Gabbar, "FSN-Based Co-Simulation for Real Time Safety Verification of Nuclear Power Plants," *Mechanical Engineering Journal* (JSME) 4, no. 2 (2017).
2. Elnara Nasimi, Hossam A. Gabbar, "Application of Safety Instrumented System in Older Nuclear Power Plants," *Nuclear Engineering and Design Journal* 301 (May 2016): 1–14.
3. Emmanuel Boafo, Luping Zhang, Elnara Nasimi, Hossam A. Gabbar, "Co-Simulation for Real Time Safety Verification of Nuclear Power Plants," *ICONE* 23 (May 2015): 17–21 (Chiba, Japan).
4. Elnara Nasimi, Hossam A. Gabbar, "Signal Denoising Methods for Fault Diagnosis and Troubleshooting at CANDU® Stations," *Nuclear Engineering and Design*, Elsevier, 280 (2014): 481–492.
5. Elnara Nasimi, Hossam A. Gabbar, "FSN-Based Fault Modeling in Candu® Stations," *Journal of Annals of Nuclear Energy* 65 (March 2014) 325–337.
6. Elnara Nasimi, Hossam A. Gabbar, "Application of Principal Component Analysis for Diagnosis of Neutron Overpower System Oscillations in CANDU Reactors," *Journal of Nuclear Engineering Design* 270 (April 15, 2014): 238–248.
7. Elnara Nasimi, Hossam A. Gabbar, "Optimal Steady State Identification of Liquid Zone Control in Nuclear Power Plants," *Journal of Engineering*, Article ID 450161 (2013): 12 pages.

8. Elnara Nasimi, Hossam A. Gabbar, "Application of Principal Component Analysis for the Diagnosis of Neutron Overpower System Oscillations in CANDU Reactors," Annual Conference of Canadian Nuclear Society Conference, Toronto, Canada (June 9–12, 2013).

Please note that due to an official name change, two different surnames are used to refer to Dr. Hossam Gaber, e.g., Hossam Gaber and Hossam A. Gabbar.

1.5. Thesis Organization

Organization of the remainder of this thesis is as follows:

Chapter 2: Background information on PF and results of the conducted literature review are presented. In this chapter, previously published research work was considered for its applicability to this study.

Chapter 3: The proposed methodology for mitigation of declining PFs, emphasizing the need to denoise plant data and reduce dimensionality before the analysis, is discussed. LPF and WTA methods are used to determine the most suitable alternative in terms of the resultant signal-to-noise ratio. Dimensionality of data is reduced with PCA and two of its derivatives, namely weighted PCA and nonlinear PCA. An algorithm for optimization of the gain setting constants is developed using a GA approach. The proposed method considers increasing trends in detector noise and spurious unexplained variation in detector signals. Finally, methods for quantifying operational risk using the FSN approach are discussed.

Chapter 4: Representative case studies where detectors show poor signal discrimination properties, increased noise response, unexpected trips, decreasing prompt fraction, and other spurious behavior are provided in this chapter.

Chapter 5: Selected methods are applied to the case study data, and comparisons between the theoretical cases and the obtained results are made. Finally, a summary of the main results of this work is given.

Chapter 6: Chapter 6 summarizes the main conclusions of this work in relation to the research objectives and the obtained results. Areas for future work are identified, providing the groundwork for further research.

Chapter 2: Background and Literature Review

This chapter summarizes previously published research work applicable to this study. In some cases, the listed citations present only overall knowledge developed in the academic community up to date. They are listed nonetheless as they aid in the identification of already available methods and overall trends, even if not directly used in this work. Where direct relevance to the current research exists or where this work directly builds upon prior research, appropriate citations are made.

2.1. Terminology and Definitions

Prompt Fraction:

The intrinsic response of a detector to a neutron flux change consists of a prompt and delayed component and is based on the detector material. The prompt response of Inconel detectors is mainly due to neutron capture by 59Ni (n, γ, e) and is nominally over-prompt (i.e., overestimates the thermal power). The introduction of platinum cladding causes an additional gamma reaction, 195Pt (γ, e), which reduces neutron sensitivity, and platinum-clad detectors are nominally under-prompt (i.e., underestimate the thermal power). The fraction of the total response that occurs immediately is called the prompt fraction (PF).

Effective Prompt Fraction:

To provide a more accurate representation of thermal power, a dynamic signal compensator (DSC) was included in the design. The output signal from each detector passes through a DSC circuit, which applies predetermined gain factors and time constants. The output from the DSC is called the effective prompt fraction (EPF). The EPF values are used in the safety analysis.

2.2. Calculation of Prompt Fraction

Prompt fractions of in-core neutron detectors at Canadian NPPs were calculated following the initial five-year development program at the Chalk River Laboratories [1]. It was expected that platinum-clad detectors' PF would decrease from ~90 to ~85% over twenty years [2]. Subsequent measurements of detector responses caused confidence in predictions of detector dynamic response for a twenty-year service life. An additional study performed in 1985 by the industrial collaboration project suggests that PFs will decrease from 89 to 82 [3]. Another industry-driven

study done in the 1990s predicted that PFs would remain above 85% after twenty years in service and should not decrease below 77.4 % [4].

The method used in these studies consists of determining a conservative rate of degradation using two (2) consecutive tests performed at a two- or three-year interval during planned maintenance shutdowns. An average degradation rate is established to bound the slowest detector, with a probability of at least 95% (i.e., adding 2σ). This can be shown as the future value of the prompt fraction, starting from the most recent test performed at t_1, and considering the previous test performed at t_o:

$$PFi(t1 + \Delta t) = PFi(t1) + (\mu - 2\sigma) * \Delta t \qquad \text{[Equation 2. 1]}$$

$$\mu(1-\beta) = m - t\beta,\ n-1 xs/sqrt(n) \qquad \text{[Equation 2. 2]}$$

where:

- $PF_i(t_1)$ – is measured EFP of detector *i* at time t_i;
- t_1 – is time typically associated with the most recent outage/measurement;
- $PF_i(t_1 + \Delta t)$ – predicted PF value for detector *i* at time $(t_1 + \Delta t)$;
- $t_{\beta, n-1}$ – is the statistical student t distribution for probability β and n-1 degree of freedoms;
- $\mu^{(1-\beta)}$ – is the momentum of the statistical distribution resulting from $pf_i = PF_i(t_1) - PF(t_o)$, at confidence 1-β;
- m – is the mean of the sample;
- s – is the standard deviation of the sample set on *n* detector deltas;
- σ – is the standard deviation;
- β –the value of 90% is assumed to be adequate which can be interpreted as single sided probability.

The resultant $PF_i(t1 + \Delta t)$ is then used to determine penalty factors or schedule detectors replacement. A penalty for an in-core detector is used to compensate for detectors that have low prompt fractions to maintain the same trip coverage, i.e., trip time. This can be expressed in terms of the margin-to-trip (MMT) as follows:

$$CPPFpenalty = MTT/[1+(MTT-1)*PF'/PF] \qquad \text{[Equation 2. 3]}$$

The relationship between the (MTT) and the trip set points (TSP) can be defined as:

$$MTT = TSP/(RP*CPPF) \quad \text{[Equation 2. 4]}$$

where:

- RP – is the reactor power.

Therefore, equation 1.2 can be expressed in terms of PF' as a function of the CPPF when the penalty is applied:

$$PF' = (MTT')/(MTT-1)*PF \text{ where } MTT'=MTT/CPPFpenalty \quad \text{[Equation 2. 5]}$$

Therefore, for RP of 90%, a nominal case with MTT=1.2 and PF=1.0485 is equivalent, i.e., same trip time, to a PF' of 0.812 with MTT' reduced to 1.165. Using equation 1.4, the PF' is calculated as 0.865. Using this approach, equation 1.3 can be used to implement a tradeoff between non-PF penalties applied to detector calibration and PF degradation rate. To determine the PF degradation at operating reactors, detector response to changing field conditions is measured during planned reactor shutdowns.

2.3. Prompt Fraction Degradation due to Aging

The Canadian fleet of power reactors, constructed in stages from 1966 to 1991, is nearing the end of their design life. Station measurements of detector responses to flux indicate that the detector performance is decreasing with time and at a significantly faster rate than predicted earlier. The investigation identified that degradation of the dynamic response (i.e., PF) of in-core flux detectors is due to changes in the isotopic composition of the detector material from exposure to the core neutron and gamma flux—a function of aging. These changes are also often referred to as detector burnout. It is important to point out that the method for measuring prompt fraction described above results in data with a wide variance, both in the past and during more recent tests obtained over ten (10) years, as shown in Figure 2.1 below.

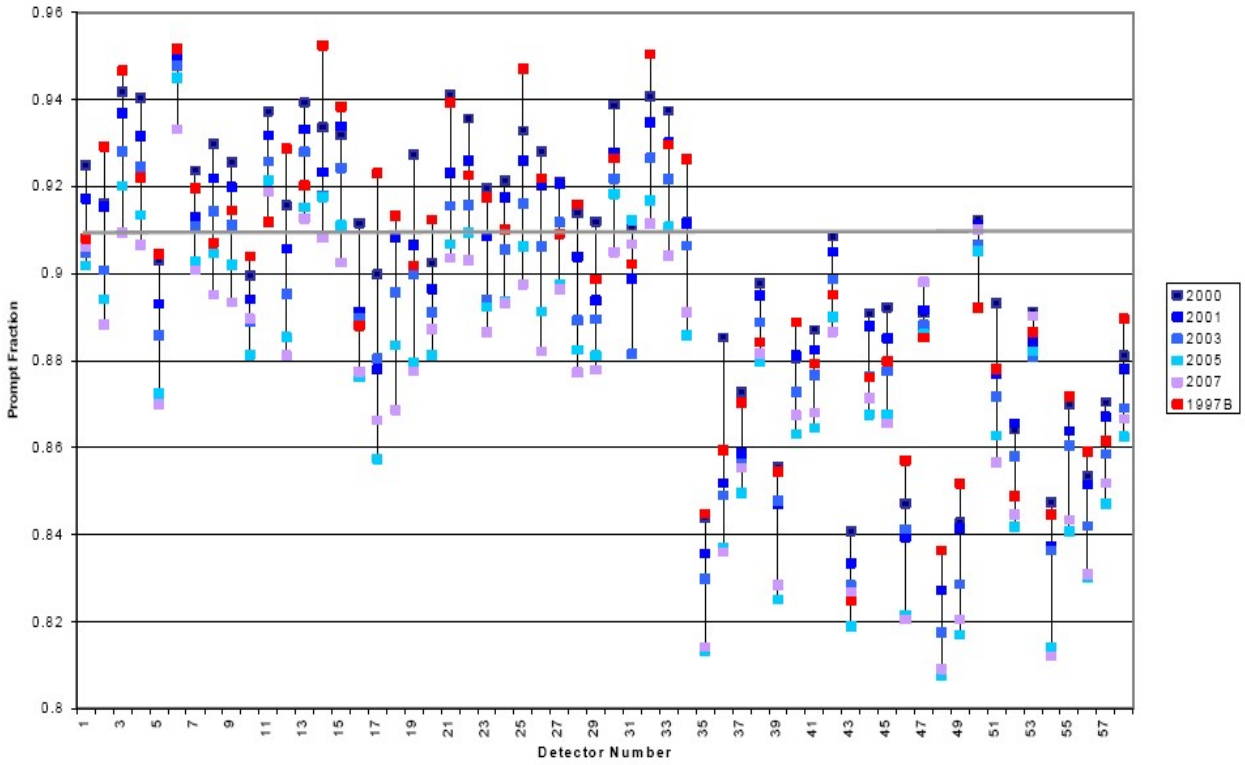

Figure 2. 1: Variation of PFs in Pt. Lepreau ICFDs for various shutdowns, (curtesy of Pt. Lepreau NPP).

Figure 1.1 shows that the PF values vary between 0.81 (81%) and 0.96 (96%). However, the overall trend in PF degradation is increasing over time. Following tests in 2000 to 2007, eight (8) detectors failed with PF values below 85% and were replaced. An additional twenty-five detectors were determined to have low PFs and were scheduled for replacement. Detector replacements can only be performed during planned maintenance outages and require significant lead-in time to enable design work, regulatory approvals, and parts and tools to be prepared. Compensatory measures such as reactor power de-rates are implemented as an interim solution during preparation for replacements.

Similar issues with PF degradation due to detector aging affect other utilities in Canada. For example, the graph in Figure 2.2 shows an example of PF values for three (3) detectors at a different NPP.

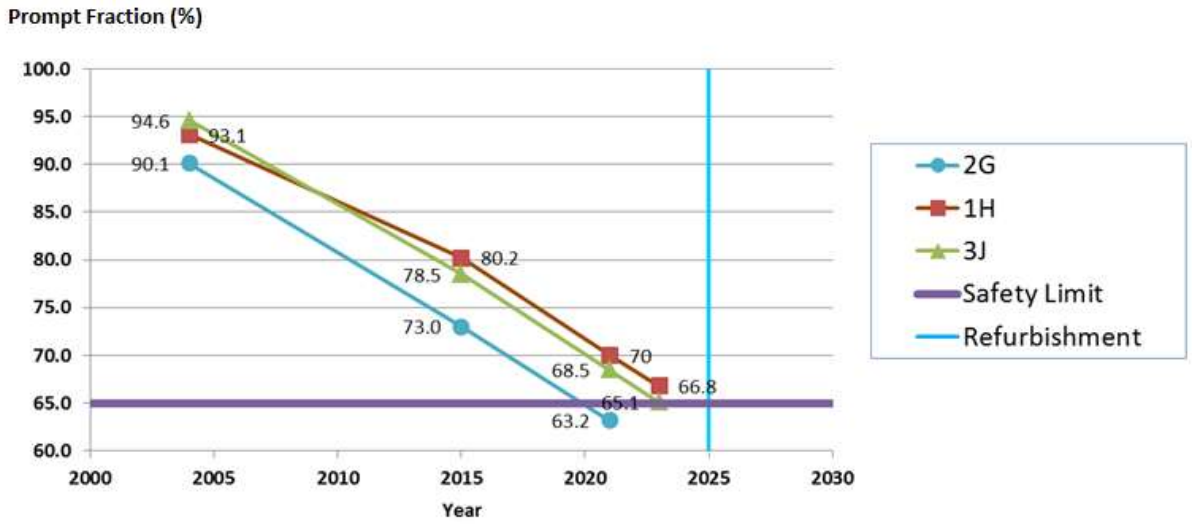

Figure 2. 2: Example of PF degradation of three (3) detectors (designated as 2G, 1H, and 3J). The safety analysis limit (SAL) is shown as a purple horizontal line. The scheduled replacement is shown as a blue vertical line.

The trend shown in Figure 1.2 indicates that the detectors 2G, 1H, and 3J are all expected to degrade below the safety analysis limit of 77.4% and the design limit of 65% set up by this operating utility. Due to the uncertainty in the assumptions used in the current PF measurement approach, each utility sets these criteria based on best practices for detector replacements and operating experience with pressurized heavy water reactors in Canada. Although not supported by academic research in the open literature, it is accepted as a suitable practice by the Canadian Nuclear Safety Commission and is documented in the utilities' safety analysis. The principle used here is that the safety analysis is performed at limiting conditions. However, the safety limit is evaluated considering actual conditions implemented in specific NPP reactor unit operation. One can observe in Figure 1.2 that by the year 2020, the three (3) detectors shown above will no longer be considered fit for duty. Similarly to the case discussed earlier, this will require the detectors to be removed from service until the scheduled refurbishment in 2025. The resultant loss of redundancy in the neutron overpower protection will cause a need for compensatory actions, such as reactor power de-rates and other penalties.

Interviews with the site staff and correspondence with experts on this subject matter confirm a significant concern about degradation of the dynamic response of in-core neutron detectors due to long-term neutron irradiation as well as other failures attributed to aging. Most

recent assessments indicated that thirty-five in-core detectors were deemed to have values below the safety analysis limit of 65%. Ongoing changes in detector performance affect critical trip parameters for safety systems and raise new safety and licensing issues for the NPPs, which often results in financial losses. The current PF safety analysis limit at the NPP in question is determined to be 65%, and no operational margins can be utilized this time. A portion of the required compensatory actions to enable operation of the detectors with PFs (shown in Figure 2.1) is listed in Table 2.1:

Table 2. 1: CPPF penalties for in-core neutron flux detectors with low EPF values.

System	Detector	Penalty	Expiry
Shutdown System	Pt-clad	1.003	01-Feb-18
Shutdown System	Pt-clad	1.004	01-Nov-18
Shutdown System	Pt-clad	1.005	01-Jul-19
Shutdown System	Pt-clad	1.006	01-Apr-20

The penalties shown in Table 2.1 will have to be continuously recalculated and applied until 2025, at which point the detector replacements can be performed, which is the only approach used by the industry to address PF degradation due to aging. Extensive documentation, testing, and regulatory approvals are required to support detector removal and replacement tasks. This type of maintenance is costly and involves significant radiation exposure:

- High gamma fields in the range of REM/hr exist around the neutron detector assemblies.
- It is expected that replacement of detectors will contribute a dose of 1 REM per person during a typical maintenance outage.

Also, as discussed earlier, the current methodology for PF measurements ignores the local conditions of individual in-core detectors, which could introduce an error in the results and lead to overestimation of the degradation.

2.4. Assumptions

The following assumptions are used in this thesis:

1. The magnitude of the detector response to fueling is based on historical observations at a particular NPP, namely 10% of full power (FP) plus a signal oscillation of 6%. These

values are NPP-specific and will differ at other utilities. The simulation models may need to be adjusted if used for analysis at other NPPs based on the relevant historical data.

2. Since the exact degradation mechanism of the detector prompt fraction is not confirmed (as discussed in Section 1.1), it is not known which delayed component is affected as the detectors age. However, it is expected that the detector prompt fraction with aging can be simulated by adjusting the fastest delayed fraction, which will maximize the potential reduction in in MTT. The results of the proposed approach will be compared to the theoretical predictions by FUELPIN code to validate the accuracy of this assumption.
3. The prompt fraction for aged detectors in this study will be assumed to be 0.75, or 75%, based on the safety analysis pertaining to this case study. The same value is applied in the FUELPIN code simulations used for validation of the results of this approach. The simulation models and FUELPIN inputs may need to be adjusted if used for analysis at other NPPs based on the relevant safety analysis case.

The neutron detector signal is filtered by a dynamic signal compensator (DSC) to better approximate the power of the fuel during transient conditions as shown in Figure 2.3 below.

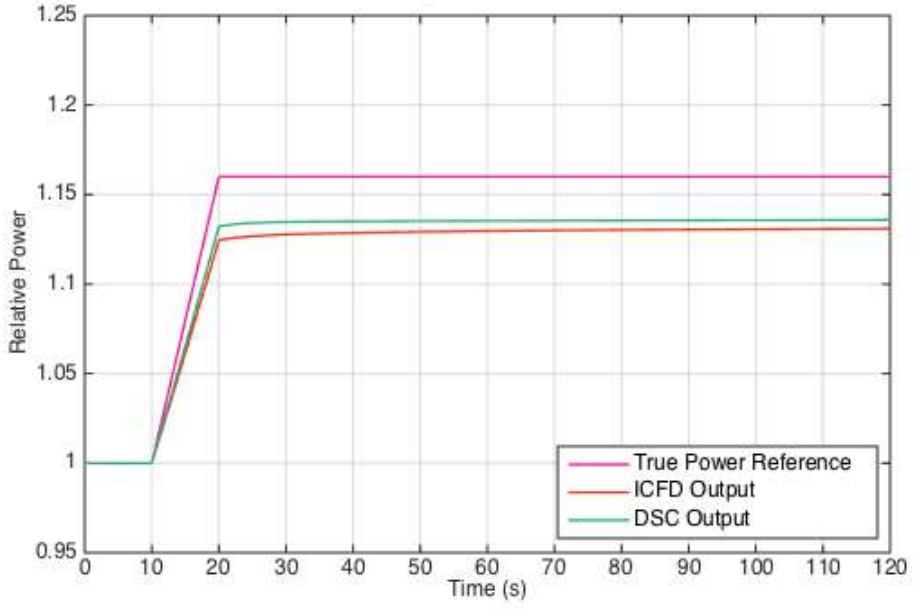

Figure 2. 3: True power reference (magenta), in-core neutron flux detector (ICFD) output (red), and the DSC output (green) are shown.

This case shows the impact of a fuelling transient coincidental with the detector signal oscillation. The graph in Figure 1.3 shows that the simulated ramp rate is conservative compared to actual changes in reactor power due to fuelling and oscillation rates. It can also be observed that the result is under-prompt, as expected. However, it can be noted that there is a discrepancy between the actual reactor power (shown in magenta) and the detector output with the current DSC gain settings (shown in green). Ideally, the signal after the DSC should be compensated such that the signal matches the fuel power. The residual error between fuel power and compensated signal, in this case, is in the order of -1.64% FP.

2.5. Detector Models, Degradation and Prompt Fraction Measurements in NPPs

At the time when neutron detection systems were designed and installed for earlier generations of domestic NPPs, a complete and accurate analytical model of detectors was not available. The decision to proceed with Inconel and Inconel-clad detectors was made based on an understanding of the then-current producing mechanisms, mostly based on experimental data, such as those obtained during a two-year study at Chalk River Nuclear Laboratories [1]. Some additional testing and design work were done at the Gentilly HWPR-BLW reactor, as well as experiments at the Argonne Experimental Breeder Reactor II (EBR II) described in [2].

The early design of neutron detectors in use in domestic nuclear power plants consisted of coiled coaxial cables with MgO as an insulator [1] and Inconel®600 [3] as the main core wire and outer sheath material. This solution is based on the work of a pioneer of detector design, as described in [3]. The original intent of this work was to satisfy the need for a new generation of sensors capable of long-term continuous operation in a reactor core. Initial detectors had slow responses and were used primarily for flux mapping. Subsequently, the primary objective in detector technology was for a faster response that can be used in larger reactors for fast control and safety systems [4, 5, and 6]. Detector response to both neutron and gamma, particularly to the delayed components, became an important consideration.

Additionally, the long-term impact of harsh service conditions and continuous exposure to radiation on detector sensitivity had to be examined. A few emitter materials were considered, e.g. cobalt detectors were studied in [7]. Researchers also looked at the option of zirconium detectors in [5], but these designs did not possess all the desired characteristics regarding sensitivity, noise susceptibility, and response to prompt and delayed components. Examination of detector emitter

materials in the hot cells at Chalk River Laboratories [8] showed that even with Inconel®600 material, irradiation-induced embrittlement in PHWRs resulted in detector failures after only several years of service [8]. Even when the detector assemblies were normally maintained in an inert helium atmosphere, some failures occurred due to an incorrect operating environment, i.e. loss of the cover gas [8]. Another possible cause of low insulation resistance is deterioration of MgO insulation due to radiation effects [8].

In addition to material properties and service conditions, several other factors affecting in-core flux detector performance have been identified. A known issue affecting early stages of system development was the design of Vanadium in-core flux detectors. These types of detectors were initially proposed for use in flux mapping routines but were determined to be unacceptably slow due to their inherent design features [3].

As detectors age, they become more sensitive to neutron activation and electronic noise, known as the burn-up effect [9]. The impact is manifested in the main control room as an increased frequency of low MTT alarms. Another aging effect is inherent to the detectors themselves. Detector effective PF degradation and potential mitigation methods have been studied for the past two decades [10, 11, and 12] to mitigate the known issue of loss of sensitivity due to detector aging and burn-up. The current methodology used to calculate the prompt fractions of in-core flux detectors is based on ion chamber rundown signals during a trip test [13, 14, and 15]. This methodology ignores the local conditions of individual in-core detectors, which could introduce an error in the results [16, 17]. The results obtained have a wide variation, which is difficult to explain based on current understanding of the physical process of detector long-term neutron irradiation [16, 17].

To improve uncertainties in PF values, a combined Owners Group project (COG-95-449) was formed, and the findings are far more credible [18]. Measured and predicted PF values for Pt-clad ICFDs were examined and evaluated. Another approach that uses an absorber to apply a local flux perturbation repeatedly, on power, could be employed for a PF measurement. In 2004, an at-power method for determining PF was presented in [18]. It is based on noise analysis and does not require a reactor power perturbation. Instead, it makes use of the fluctuations in neutron flux caused by the reactor control system (e.g., PHWR liquid zone levels, 0.25 Hz). The in-core neutron detectors can measure the induced neutron noise, but only the prompt component of the detectors can follow the fluctuations. A comparison of the measured signal to the noise source allows the

PF to be determined. This method is particularly attractive in practice because it has minimal impact on plant operation.

2.6. Tools and Methods for Modeling Detector Response

There are two aspects to the discussion of the detector model. First, it is a physical model, e.g., the physical dimensions of the detector, emitter, and collector materials, source-detector distance, or the type of the insulation used for cable shielding. The other aspect is the detector behavior, or the model of the response to the neutron interaction. As discussed in section 2.1, in the early days of NPPs in Canada, a complete comprehensive detector model was not available. With the ongoing research and development, a set of safety analysis codes, which potentially could be used in accident analyses and parametric assessments, was established. Some of the commonly used codes currently include WIMS-IST and DRAGON to perform 2D and 3D lattice cell calculations in support of the reactor physics core equilibrium calculations, RFSP to perform reactor physics core equilibrium calculations for use in large break loss of coolant (LBLOCA) analysis, and FUELPIN and SIMBRASS codes for use in loss of reactivity control (LORC) and neutron overpower analysis [19]. In Canada, point kinetics models in FUELPIN code have been widely used to calculate the impacts of the design change on predicted reactor physics characteristics of the fuel and the core as a whole and to assess the loss of reactivity control. FUELPIN simulates point reactor kinetics given a constant rate of reactivity insertion or constant rate of reactor power increase [20]. It also simulates the thermal response of a fuel element and the response of the neutronic trips [20]. A trip parameter is considered effective in preventing fuel melting if it is initiated at least 1.5 seconds prior to fuel center-line melting time predicted by the code [19].

WIMS-AECL, DRAGON, and RFSP codes are currently utilized in most industrial applications as the primary 3D transport software. The end goal of the simulations is to produce two sets of cross sections for the system with the control device removed and fully inserted. The cross sections are homogenized for the full height and depth over the inner area of the model from the center of the left fuel channel to the center of the right fuel channel, including the control device [19]. The differences in the two sets of homogenized cross sections are then computed, producing the incremental cross sections for the specific control devices that are required for the diffusion calculation. These incremental cross section values are included as an additional input in the

diffusion calculation to adjust the reference lattice cell cross sections appropriately account for the control device configuration at any one time [20]. This 3D transport solution is quite complex and is computationally intensive; as such, the geometry of the fuel channel and some of the control devices are simplified for the calculation.

Other work performed recently in collaboration between Lancaster University and Innovative Physics Ltd. in the United Kingdom focused on the comparison of CdZnTe neutron detector models using MCNP6 and Geant4 codes [21]. Initially, both the MCNP and Geant codes were developed to specialize in neutral particle models and accelerator models, respectively [21]. Following additional studies, there is now a greater overlap of the capabilities of the two codes so that MCNP can be used as a validation tool for comparative studies.

The MCNP suite of codes deserves a special mention in the literature review. Monte Carlo-based tools have been extensively used in the predictions of detector response in conjunction with the point reactor model for the development of neutron detectors. Since the point reactor model fails to accurately predict detector response in common applications, the general Monte Carlo code was developed at Los Alamos National Laboratory and modified specifically to simulate the pulse streams that would be generated by a neutron detector and normally analyzed by a shift register [22]. A variant of the MCPN code, namely MCNP-Random Exponentially Distributed Neutron Source (MCNP-REN), along with the Time Analysis Program, predicts neutron detector response without using the point reactor model, making it unnecessary for the user to decide whether or not the assumptions of the point model are met for the application. The work described in [22] demonstrate that MCNP-REN is capable of simulating standard neutron coincidence counting as well as neutron multiplicity counting [22]; its applications can also be used for other detector design tasks. Findings of this work show that the method used in MCNP-REN is fundamentally sound and can eliminate the need to use the point model for detector performance predictions.

Results of neutron detector efficiency modeling for several detector designs have been collected and studied, as shown in [23]. The focus of this analysis was on the incident neutron spectra, detector efficiency, and count rate at the detector location [23]. Functional dependence on the source-detector distance, experimentally observed in 2014, was compared to MCNP/MCNPX simulation data [23].

The efforts to develop a simulation model of the detector dynamic response have continued to the present day. A unified framework for modeling slow-response, self-powered neutron

detectors with discrete-time state-space representation for Vanadium and Rhodium emitters is described in [24]. As discussed in section 2.1, these slow-response detectors are typically used for flux mapping. To be useful for trip protection in safety systems, the signals must be augmented with time compensation to counteract the delay due to beta decay. A majority of these compensation techniques are based on Laplace and z-transformations, which inevitably requires some kind of approximation to map from s-domain to z-domain. The authors argue that the prevailing approaches are neither straightforward nor accurate due to complex manipulations of representations in different domains. Moreover, the reported methods are generally developed in a case-by-case fashion, without addressing the issue with a generalized approach that applies to all kinds of slow-response in-core detectors. The approach proposed in [24] is a derived discrete-time state-space model, which readily facilitates application of state-of-the-art signal processing algorithms such as Kalman filtering.

Development of 3D neutronic kinetic models and control for the control system of PHWR is carried out in [25], using a modal synthesis method. The reactor space-time-dependent neutron flux is synthesized by a time-weighted series of precalculated neutron flux modes, which are Eigen-functions of the governing neutron diffusion equation at reference steady-state operating conditions. The performance of the developed 3D model is compared with that of a traditional coupled point kinetic model in a closed-loop environment of a reactor regulating system (RRS). The 3D reactor model is implemented by a MATLAB/Simulink software environment, and the accuracy is validated against actual plant measurements under transient conditions.

A semi-empirical dynamic model, devoted to simulation of the Inconel lead cables in Ontario Power Generation's Darlington Nuclear Generation Station and able to simulate the lead cables' response to arbitrary neutron-flux transients, was developed in 2013 and is described in [26]. This model was developed using a MATLAB/Simulink toolbox, where the model's parameters were obtained by fitting simulation results to measured lead-cable signals acquired during reactor shutdown. The functionality of the Simulink model was demonstrated for arbitrary neutron flux transients, and simulation results were found to agree within 1.2% with measurements for reactor trip transients [26]. Although some discrepancies were identified, further investigation of the observed differences was not performed at the time.

Further review of published research, not shown here, shows that the MATLAB/Simulink package provides a flexible environment for solution of the time-differential or integral problems.

A variety of numerical time-integration algorithms in Simulink allows for obtaining results for the transient analysis without developing routines for each case. Instead, the space-time coupled problem can be converted into space-dependent only, where the MATLAB/Simulink tools are used to solve the time-only-dependent problem.

Furthermore, the MATLAB/Simulink environment has been widely used for simulation of dynamic systems both in and outside the nuclear industry. This simulation tool was chosen for the current study. To predict the transient reactor fuel power, a FUELPIN code will be used. This code incorporates a neutron point kinetics model and can, therefore, be used to simulate the effects of reactivity changes due to burnup. Although MCNP is a well-developed, state-of-the art transport code, used globally for radiation-transport or reactor physics calculations, it is unable to perform burnup calculations, so to assess burnup-dependent power distributions, additional codes are required. The output of the FUELPIN code is used in this thesis to validate the MATLAB/Simulink results to demonstrate that the proposed design change has minimal impact on the reactor physics aspects of the various reactor power transients and therefore has minimal impact on the timing of neutronic trips credited during the transient analysis.

2.7. Noise Reduction and Data Preprocessing Methods

Noise in process signals is not just unwanted disturbance affecting system performance. It also negatively affects the ability to analyze plant transients by masking true process deviations or corrupting useful data signals. Despite recent advances in hardware and instrumentation technology, various forms of noise still affect signal readings and make fault detection challenging.

Application of various denoising techniques based on statistical methods has been proposed for source separation in industrial data at Électricité de France power plants with the objective to separate vibration modes [27] and reduce the flattening noise using a two-order statistical algorithm.

Various types of filters are commonly used for recovery of objects from noisy and incomplete signals as well as for data denoising. Typical filters assign coefficients corresponding to specific details of process data so that dimensionality of data sets can be reduced by omitting some data points without negatively affecting the overall trends in the process [28]. A similar method is proposed where all coefficients are evaluated against a particular threshold and are set to zero if they are not significant enough [29]. Standard and median nonlinear filters are a common

technology used for resolution of Gaussian noise. While they smooth the data well and remove noise, they do so at the expense of losing high-frequency details and are best suited to work with data that is heavily contaminated with spikes [30] rather than low-energy noise dispersed throughout the data.

Application of traditional digital filters, matched filters, discreet wavelet transforms, and the second-generation wavelet transforms was proposed for denoising the measurement of insulation conditions in power plants [31]. Similarly, application of the Kalman filter as a denoising technique was proposed for noise-contaminated data in air preheater systems and performed well, but only white noise was involved in the computation [32].

Time domain averaging methods, such as time synchronize averaging (TSA), and fast Fourier transform (FFT) techniques, have been proposed to mediate the effects of background noise [33, 34, and 35] in rotating equipment affected by vibration. By using an FFT, the vibration signal amplitude, which is a function of time, can be represented by the amount of signal information at different frequencies. A similar method was proposed for reducing random noise in hydroelectric generator control systems [36]. The generator response [36], particularly its dynamic response, was simulated using a time-averaging algorithm [36], which was applied under disturbance conditions. In this study, it was necessary to minimize noise disturbances during the process of data collection. The proposed methodology was extended so that outlying data points could be ignored while calculating the average responses. Use of the FFT method was also considered for identification of the dynamic response time of a nuclear plant pressure transmitter [37] to detect sensing line blockages. The limitation of all these methods is the loss of important information present in the signal, requiring a tradeoff between noise-filtering capabilities and quality of results.

Time domain filtering is a method that has been proposed for tuning filters to avoid the averaging process [38, 39]. Although the results appear to be much improved, this method has the drawback of increased computation time and therefore does not appear suitable for real-time fault diagnostic applications at present.

The fuzzy sensor validation and fusion (FUSVAF) [40] algorithm uses nonlinear dynamic validation curves and a weighted average aggregation. This algorithm was proposed for removal of noise and sensor failure data from measurements in a gas turbine at power plants. In this study,

a nonlinear system was subject to both noise and outliers. Different types of noise were considered, including non-Gaussian noise.

A similar approach was used for analysis of temperature signals from the Experimental Breeder Reactor II [41]. The upper plenum of the reactor is investigated during a startup from 0% to 100% full power [41]. This method compares features from redundant and related signals. Research shows that it is possible to determine whether the noise is the consequence of an equipment anomaly or a process abnormality [41]. This work suggests that a similar technique can have wide applicability across other plant systems and applications, e.g. monitoring of instrument calibration.

A feed-forward multilayer artificial neural network (ANN)-based approach has been proposed to model nonlinear systems and was tested for two target applications in reactor power level monitoring using system output data at various operating points [42]. In one case the instantaneous position of the control rod, reactor power, and rod drop distance were input to the neural network [42], while the resulting instantaneous power was the output. A similar approach was used for modeling the behavior of the control system AC servo motor position to predict the instantaneous rod position. The results suggest that the multilayer feed-forward, ANN approach can be successfully used to represent a system's original nonlinear behavior [42].

Data denoising using wavelet analysis is a novel technique for improving data quality and reliability. Wavelets are functions that can be described by certain mathematical parameters and can be used for representing data or other functions. Wavelet analysis methods have not been widely applied in process industries where discretely sampled time-series data needs to be analyzed [43, 44, 45, and 46]. Application of wavelet transform technique has been proposed for denoising generator output data [47]. A multilevel 1-D wavelet in level-5 decomposition was used in this experiment and proved useful for minimizing fluctuation of the data. A fault detection method based on wavelet denoising and Scholkopf's kernel principal component analysis (KPCA) method [48] was proposed for application in chemical industry for denoising data and removing disturbances. When applied to the Tennessee Eastman (TE) process, it proved superior in fault detection. Wavelet domain Hidden Markov Tree (HMT) was recently proposed for use at smaller power plants in China [49] to denoise the flame image of boilers so that boiler characteristics, such as combustion rate and flame temperature, can be optimized. This method proved very successful for white Gaussian noise and performed better than other denoising techniques.

Signal decomposition using wavelet methods for the purpose of eliminating drafting noise was studied for the in-service eddy current inspection of steam generators [50], where recognition of a defect in the obtained image heavily depends on the separation of mixed signals and removal of wobbling noise. This study produced satisfactory extraction and classification results for all measured signals.

Application of wavelet analysis in power system disturbance modeling was described in [51], where wavelets were used to model a variety of power system transients, which can be used for developing a fault classification method. Another application of wavelet transform analysis is troubleshooting voltage variations in power systems [52], where it was demonstrated to be useful for classifying power system failures. Minimizing the effect of randomness in the reactor power transient data by using different classes of smoothing was investigated in feed-water control of a large pressurized heavy water reactor (PHWR) [53, 54].

The use of various denoising methods for troubleshooting in-core neutron detection systems at nuclear power plants was discussed by the current author in [55]. This work examined the development of an intelligent digital filter methodology based on low pass filters and a wavelet transform approach.

2.8. Dimensionality Reduction with Multivariate Techniques/Principle Component Analysis

Principle component analysis (PCA) is one of the oldest and most versatile methods of multivariate analysis (MVA). Many applications of multivariate techniques have been made in the behavioral and biological sciences [56, 57, 58, 59, and 60], but they have also been used in other applications, e.g., in the pharmaceutical industry for tablet development and manufacturing [61]. It is commonly used in various industries for dimensionality reduction for detecting and diagnosing faults [62, 63, and 64]. MVA methods have been proposed for application in industrial, chemical, and water treatment processes [65, 66, 67, and 68] and will be considered for this study.

The use of PCA methods for analysis of transients in neutron detection systems was discussed by the current author in 2014 [69]. This work studied the development of an intelligent troubleshooting methodology for NPPs that required dimensionality reduction of process data using intelligent PCA and weighted PCA algorithms. A similar approach was proposed by another research group in 2015, where the methodology of PCA is utilized to construct the mathematical

models among various in-core flux detectors [70]. The proposed fault detection approach is validated with four types of simulated detector faults and the results are positive; however, only simulation data was used in this study.

2.9. Optimization Methods and Algorithms

In general, optimization involves finding an alternative with the most cost-effective or best achievable performance, which is typically accomplished by maximizing desired factors and minimizing undesired ones under the given constraints. In the nuclear industry, the ongoing desire to improve power plant performance and safety records is one of the drivers for optimizing plant efficiency through development and application of innovative tools. Methods for mathematical modeling and optimization of NPPs were proposed as early as 1975 [71, 72].

In 2003 the International Atomic Energy Agency (IAEA) established a technical working group on life management of NPPs [73]. This group is tasked with the managerial and engineering aspects of NPP maintenance, particularly with its optimization process for condition monitoring and maintenance strategies [73]. In its 2003 report, the IAEA defined the objective of the optimization of NPPs as a systematic improvement in the overall performance and competitiveness of NPPs while preserving and enhancing safety through the application of technological and engineering best practices [73]. This report established the foundation for the optimization methodologies that have since been proposed for the nuclear industry.

In the 2010 study, a combined simulation-optimization tool was developed and used to optimize the secondary loop of an HWPR NPP (in Gentilly-2 nuclear station) [74]. The simulation package was used to estimate the behavior of the power plant and to allow the best tradeoff for the operating conditions [74]. The results showed that there is an opportunity to improve the overall performance of the power station.

A novel method for optimization of the maintenance activities in the NPP while considering the plant safety is developed in [75]. The objective function of the optimization is the mean value of the selected risk measure, which is assessed from the minimal cut sets identified in the probabilistic safety assessment (PSA) [75]. The proposed method is applied to the PSA model of a safety system to show that optimization of maintenance decreases the risk and improves the plant safety [75].

Particle swarm optimization (PSO) is a population-based stochastic optimization technique first proposed in 1995 [76] for improvement of nonlinear functions. Instead of using genetic operators, the individuals in each population pool are "evolved" by cooperation and competition among the individuals themselves through generations [76]. A new parameter, called inertia weight, is introduced into the original particle swarm. Based on this approach, an algorithm has been developed to optimize the fuel core loading pattern in a typical light water-cooled reactor [76]. The proposed algorithm presents a simple social model, while a modified version of the algorithm for discrete variables has been developed and implemented successfully for the multi-objective optimization of fuel-loading pattern design with constraints [76]. The simulation results suggest that the proposed methodology can help in the acquisition of a new pattern without contravention of the limitations [77].

Monte Carlo neutron transport codes have been applied for reactor analysis where large-scale neutron transport simulations require large-scale computations. An example of this approach was demonstrated in [78], where the researchers implemented and tested several algorithms using a simple Monte Carlo communication kernel intended to mimic the behavior of the full Monte Carlo code [78]. A quantitative evaluation method for the maintenance plan for NPPs based on scientific approach was then proposed. The computer simulation of maintenance planning for boiling water reactor (BWR) systems was carried out and showed that the proposed method can produce a new maintenance plan that meets the conservation targets corresponding to maximum support [78].

A new hybrid mutation in the GA was proposed in [79] for designing the loading pattern (LP) in pressurized water reactors. A GA and crossover techniques were used to optimize an objective function in this study. The flattening of power inside a reactor core was chosen as an objective function, and the results showed a significant improvement [79].

In general, the literature review suggests that optimization provides greater flexibility concerning specifying additional design requirements while maintaining compliance with the predetermined set of constraints. Thus, optimization algorithms could provide the benefit of tuning the model parameters to implement the best performance of the system.

2.10. Risk Estimation and Mapping to Operational Decision Making

Concerns about depletion of nonrenewable natural resources, carbon emissions, and environmental and societal impacts of dependency on fossil fuels were important factors in the initiation of the nuclear program in the United States in the mid-1960s and in Europe in the mid-1970s. To progress to large-scale nuclear energy production worldwide, the introduction of NPPs required that safety analysis, risk assessment, and safety barriers be evaluated for all potential hazards associated with atomic energy. The Event Tree Analysis (ETA) method was proposed circa 1974 by a committee of specialists under Professor Norman Rasmussen to estimate the radiological consequences and the probability of occurrence of events that might arise during a serious accident. In this work, known as WASH-1400 report [80], a probabilistic risk assessment (PRA) approach was used for a large, light water reactor. Although, with time, the initial findings of the WASH-1400 were much debated [81], the PRA approach became widely adapted in the nuclear industry and Fault Tree (FTA) and Event Tree (ETA) Analysis techniques became standard tools used by risk assessment professionals in the nuclear industry.

The approach used in ETA and FTA is basically the same and is based on analysis of possible causes for any top event or combination of causes and their propagation [82]. The two approaches involve the use of graph techniques called event trees and fault trees. This, in turn, requires identification of all potential hazards and a thorough understanding of the plant design, operation, maintenance, and testing. Furthermore, the ability to translate that understanding into a model of the plant that captures the logic of the possible sequences of events is critically important [83]. The complexity and tight coupling of nuclear plant processes make it imperative that the search for accident sequences be conducted in a systematic and structured manner. This logic development can be conducted in either an inductive or a deductive manner, or both.

The inductive method starts with a given initiating event, usually a plant malfunction. Then all the ways in which that malfunction can progress are traced until an end state. The outcome of the end-state failure is determined based on consequences such as economic factors, public health, or equipment damage. The deductive method, on the other hand, first postulates the existence of the end state of concern and then, step by step, establishes the various ways in which that end state can occur.

Both ETA and FTA methods have been successfully used in the nuclear power industry for risk assessment applications. However, these methods are not particularly suitable for real-time

operational support. The processes of collection of fault data, fault typing, and model updates are time-consuming and resource-intensive. It is understood that plant-specific data should be selected over a sufficient time period to provide statistically meaningful results. Therefore, there is typically a year of delay between the in-use models based on historical values and the current real-time system failure data. Once all the fault data is collected for a year, the probabilistic risk assessment (PRA) database needs to be updated. The Bayesian methodology is used to incorporate the plant-specific observed failures with generic failure rates. The applicable models (unavailability/risk) are evaluated after the failure rate update. The analyst must solve the applicable unavailability and risk models with the updated PRA database. The new frequency for the risk models and predicted future unavailability (PFU) values, i.e., the probability that at a future time a system will be found in a state in which component faults prevent it from operating with acceptable effectiveness, are determined. The PFU and frequency are compared with previous baseline, targets, and limits and compared with the most up-to-date unavailability targets. It is not uncommon that when a decision is made to revise the failure rates in the PRA model with plant-specific data, the overall probability numbers change (increase or decrease), sometimes in a statistically significant way, indicative of the current plant performance. A significant failure rate change analysis is typically performed annually, following the PRA updates. The present year's mean failure rate for a certain group and failure mode is compared to the previous year's failure rate fifth percentile and ninety-fifth percentiles. If the present year's failure rate is greater than the previous year's ninety-fifth percentile, then the failure rate change is considered a statistically significant failure rate increase, thus challenging the system unavailability assumptions and decision-making process.

Another approach for fault identification and analysis is based on statistical methods such as in [84, 85]. The presence of a fault is determined by comparing the current status of the system with the predefined state, and the solution is narrowed down to the fault detection and identification (FDI) with no forecast capabilities [86], particularly for the future system upsets [87], i.e., fault prediction. Methodologies based on rule-based methods [88], decision trees, or Bayesian networks [89] have been proposed. The approach involves the establishment of correlations between previous events and fatal events to predict potential failures in the future [90, 91, 92, 93, and 94]. One of the main limitations of these methods is the practical difficulty of managing a large number of variables, and relationships among them, especially in high-dimensionality datasets. Therefore, it is often required to apply sophisticated mathematical techniques to relatively simple knowledge

structures to reduce the dimensionality of data and efficiently establish correlations between defined behaviors. This equation-based approach has been criticized on theoretical as well as on empirical grounds [95].

A significant amount of research effort is directed toward developing and implementing intelligent automated tools based on various pattern-recognition schemes, knowledge-based systems, or artificial neural network systems. Solutions based on intelligent computational methods, such as GAs, Fuzzy Logic (FL), and Artificial Neural Network (ANN), have been developed for various industries, such as automotive [96], geophysical [97], and intelligent online performance monitoring of electronic circuits and systems [98]. Such applications are also widely considered in computer science, electrical engineering, computer engineering, mathematics, and physics [99, 100, and 101]. These methods gained popularity with many professionals as an alternative to the modeling of some physical and nonphysical systems. This approach can be based on a scientific or mathematical foundation. Power production industries have also looked into the applicability of these methods for fault detection in power plant instrumentation [102] to assess system status and the possible need for component maintenance. Similar solutions based on FL techniques have been proposed for solar thermal power plants [103, 104]. The application of similar techniques in nuclear steam generator level control is described in [105, 106, and 107]. It has been proposed for groundwater pumping at a coal-fired unit [108], a hybrid fuel cell-gas turbine facility [109], and a combined cycle power plant [110, 111].

Failure mode, effects, and criticality analysis (FMECA) is a technique often used to analyze the consequences of a failure within a complex system and the severity of those consequences and is somewhat related to the Bayesian approach for diagnostic of the system status. Unlike the FMECA, Bayesian networks can be tuned to model the relationships between components of a complex system and estimate their probabilities of failure with time. This approach is fundamentally different from the PRA system unavailability models when used for calculations of operational reliability and making risk-informed decisions for maintenance. One of the limitations of the current PRA methods is due to the assumption that the probabilities of all failure modes of a particular component remain the same during the calendar year. The models are recalculated only after the failure data is collected for the entire year. Bayesian-based methods can be used to reason forward and backward, work with missing data, and extend to include decisions made. For the purpose of this thesis study, comparison of system unavailability statistics based on the

assumed component failure rates and actual real-time component failure rates is critical for risk-informed and cost-effective safety-driven decisions. Therefore, a companion tool to the PRA methods is needed to enable risk estimation, both qualitatively and quantitatively, for the instantaneous status and risk assessment of the fast, dynamically changing neutron detection systems, particularly when affected by aging.

2.11. Fault Semantic Networks (FSN) for Qualitative/Quantitative Risk Estimation

2.11.1. Fault Semantic Network Overview

The work that laid the initial steps for the concept of an integrated FSN methodology started with a practical experiment conducted at Okayama University, Japan, in 2009 [112, 113, and 114]. In this work, it was proposed to analyze and forecast faults based on monitoring of a large set of process variables in a large, complex chemical control system. The experimental plant consisted of tanks, pumps, sensors, alarms, control valves, and manipulated valves. The measuring equipment consisted of sensors measuring temperature, pressure, and vibration levels at different locations in the plant, and alarms were set on the limits of process variables (PVs), e.g., water level in the tank [114]. The proposed model applied subset modeling strategy and Bayesian approaches (the Restricted Vector Auto-Regressive Model [RVAR] and Bayesian Vector Auto-Regression [BVAR]) to decrease dimensionality of the process variables and determine the suitability of fit over the forecasting interval. The results were compared to an unrestricted Vector Auto-Regression (VAR) model for each variable in each equation. For short forecasting intervals, RVAR provides better performance than BVAR, but this changes if applied over longer test intervals, where BVAR performs better.

The main advantages of the proposed approach for fault forecasting were its ability to work offline, the flexibility of setting the runtime, and the ability to estimate faults accurately. Both RVAR and BVAR algorithms performed well compared to the other approaches in their ability to forecast faults before they occur, not simply detect faults after the fact.

This work also highlighted the problem with over-parameterization and the need for parameter reduction to improve the forecasting performance. Application of sophisticated mathematics for this purpose may not be ideal due to restriction on the type of inputs, and a different approach based on modern computing methods is suggested to take advantage of the

simplicity of individual relationships within the data. This work also suggested that a proposed fault forecasting system (FFS) should be linked with an intelligent fault knowledge base where mitigating barriers and actions can be stored so that the users of this system can get immediate support during early stages of fault development.

2.11.2. Development of FSN Knowledge Base

Development of a knowledge base and acquisition system for failure and accident analysis was explored for applications at gas processing facilities [115], particularly at liquefied natural gas (LNG) plants. In this work, accident models are structured using FSN and are linked with lessons and controls to assist during design and operation phases due to the presence of known hazards such as fire, explosions, and health and environmental impacts. In addition to exploring knowledge base design, this work examined the associated accident risk estimates. Deviations are modeled using a qualitative approach, i.e., parameter behavior is described by terms such as "high" or "low." For example, a high temperature is modeled as an association of process variable = "temperature," and deviation is "high."

Next, faults are defined in the generic form and associated with all possible causes and consequences. A fault model is related to plant equipment, which is associated with a unique equipment tag or ID. The user can further tune and enhance the fault models for the equipment class. Next, a causation model is formulated from the cause or causes of the final accident, as suggested by the authors. This work proposes to collect accident data for each equipment class. Next, causes, consequences, and the fault locations are assigned using this system.

Development of the knowledge base and acquisition system for failure and accident analysis is described in [116] for gas processing facilities. The authors suggest that risks can be calculated for each fault propagation model and aggregated for each piece of equipment, process, and scenario. The systematic analysis of a knowledge base and acquisition system to support the analysis of faults and accidents for gas plants was the main contribution of this study. The researchers did not provide any comparative studies on how this approach compares to alternative existing or experimental methods.

A similar approach was investigated by the author in [117], where a methodology for a new intelligent and highly automated hierarchical control chart (HCC) approach was proposed. The main objective of this study was to develop an operations mapping solution that provides

control system designers, developers, and operators with a single view of all elements and systems [117]. The HCC approach is designed with integrated interactive data access and information retrieval capabilities to enable faster fault diagnostics [117].

2.11.3. Qualitative Hazard Analysis Technique Based on FSN Methodology

Another application of FSN for LNGs was explored in [118] with the main focus on developing a qualitative hazard analysis technique. In this work, the authors proposed to use historical accidents at LNG facilities to establish accident propagation steps and to link those with related process variables.

The main objective was to propose an algorithm for early identification of process failures that can be used to support plant operation in real time. In this resultant study [119, 120], an FSN is designed with causes, while faults and consequences are modeled as network nodes. The accidents are treated as a sequence of events. The proposed approach suggests that prediction of accidents can be achieved by integrating related state variables (SVs), i.e., process data, and possible deviations and failure modes with process models. All PVs are assumed to be in several predefined states described using qualitative values, e.g., “N” for normal, “L” for low, or “H” for high, as given in [120]. Next, the PV state is compared with each accident fault model to decide whether the accident is likely to occur and to map it to the closest accident scenario. This approach was demonstrated in the case study of an unknown accident in the flush drum process. This work, however, did not give statistics on how this approach compares to other popular fault and accident prediction techniques.

2.11.4. Use of FSN with Genetic Programming for Batch Process Analysis

The application of the FSN for the Tennessee Eastman (TE) process, introduced by Downs and Vogel in early 1990 [121], was proposed in conjunction with genetic programming for chemical and other industrial processes that use hazardous and flammable materials in [122, 123]. FSN describes relationships between variables using directed graphs, where causes, faults, and consequences are shown as nodes in the network connected by directed links according to the predefined rules. However, there are many cases where uncovering relationships and patterns between process variables may be challenging. This condition may have a detrimental effect on the ability of FSN to find the cause or causes of the disturbance and their accurate mapping to

consequences. The focus of this work was on suggesting the optimal method of uncovering relationships between process variables that would be involved in the FSN analysis.

In the subsequent work presented in [124, 125, 126], it was proposed that many different approaches can be used to qualitatively and quantitatively describe these relationships, e.g., a probabilistic approach, FL, or mathematical formulations. The authors explored the applicability of genetic programming algorithms for this purpose using the TE process as a case study. Tuning of FSN performance for the TE process is expected to improve the overall approach to implementing automated hazard identification algorithms.

2.11.5. Industrial Applications of FSN

Application of the FSN as an integrated approach was proposed as a novel technique for modeling fault, failures, hazards, and accident models at LNG plants [119]. Similar to chemical and batch production plants, LNG facilities are prone to faults and failures and have hazards that could potentially develop into accident scenarios if left unmitigated [119]. Fault development and fault scenario analysis was the main topic of the work where FSN design was discussed.

Development of FSN starts with an analysis of plant structure, behavior, operation, control, and functions, where all plant equipment is described in a hierarchical manner, i.e., all equipment is arranged into a set of parent-child classes. Selection of classes is based on the equipment function, components, and related process variables. For example, the "pump" class is treated as a parent class that may include various child classes, e.g. "centrifugal pump." Faults are treated as a combination of a normal process variable (PV) behavior and unwanted deviation. All PVs are identified and linked to the associated potential fault or failure propagation scenario.

Next, causational models are built for the associations between process equipment PVs and information about hazards, faults, and failures from previous accidents and maintenance data. Thus, the static layer of FSN is based on known historical data. Next, dynamic FSN is constructed using real-time process data and can be updated as new fault data become available. The authors argue that this method can be further used to estimate safety measures for each operational step since a process model validated with process conditions allows accurate risk estimation for different accident scenarios [124, 125, and 126]. The main advantage of this approach is that it allows integration among various scenarios in multiple fault propagation models and includes degradation and process condition information. Integration among these scenarios in a qualitative

and quantitative manner provides an additional advantage where risk-informed decisions need to be made both during design and operational phases. This work, however, did not give statistics on how this approach compares to other popular fault and accident prediction techniques performed on a specific case study.

2.11.6. FSN Methods for Transient Analysis in Neutron Detection Systems

The use of FSN methods for troubleshooting neutron detection systems was discussed by the author in [127]. This work analyzed the development of intelligent troubleshooting methodology for NPPs based on an FSN with risk estimation. The underlying Bayesian network is used to continually recalculate the real-time system risk status. It enables the user to define very complex workflows where hundreds of potential parameters can be analyzed and compared. The incoming information is inserted as evidence into the Bayesian network and results in dynamic updates to the knowledge base.

In this thesis, a similar approach is applied. The FSN network is constructed as a dynamic, self-adapting decision tree that keeps learning over time. This is unlike the traditional decision trees, which are static structures that don't adapt to the situation and learn over time. Similar to the earlier application in [127], the proposed method is easy to construct and is highly scalable.

Chapter 3: Methodology

This chapter describes methodology proposed in this thesis. First, the approach looks at validation of the maximum amplifier gain increase based on the existing hardware limitations. Subsequently, optimization of gain settings using an enhanced GA is proposed. Finally, a risk-estimation tool based on the FSN is developed to assess the risk and mitigate detector aging effects without adversely affecting the operational MTT. All proposed methods are demonstrated using plant data collected using a plant information (PI) system at an NPP. The scope and overview of this approach are both shown below in Figure 3.1 and are described below for each step.

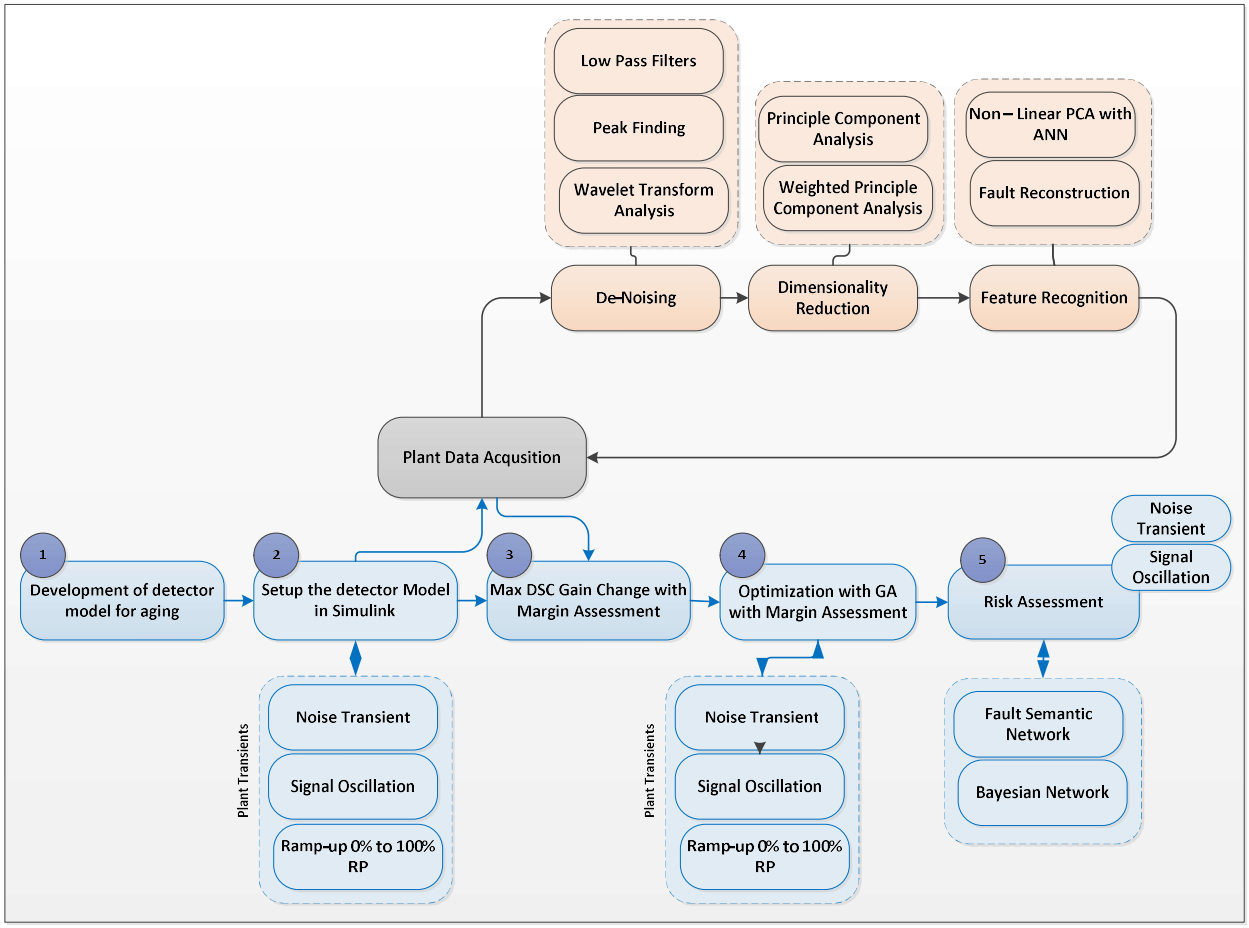

Figure 3.1: Research methodology in this thesis.

Step 1: This thesis starts with the analysis of an existing detector model, followed by a new model extension for validation purposes. Detectors and their components are presented both as mathematical models and control circuits. First, the existing detector model is studied and analyzed. This step is required to develop understanding of the detector behavior and to determine

whether the existing detector model is suitable for accurately showing degradation due to aging, specifically fueling near high-response detectors, signal oscillations, and ramp-up after a prolonged outage.

Additionally, this step allows the development of familiarity with the hardware implementation of the dynamic signal compensation (DSC) module. This step is important to determine the limitations of the current hardware components and to evaluate the magnitude and the impact of possible changes to the DSC design. For example, assuming that the overall DSC drift impacts each individual parameter (i.e. K_1, K_2, and K_3) as a percentage based on the gain value, it is necessary to evaluate the impact on instrument uncertainty calculation, e.g., drift, setting tolerance, temperature effect, etc. The analysis of the existing detector model was also important to confirm in that the time constants are not adjustable, and therefore cannot be calibrated with the current design. Finally, a proposed methodology for new model development with optimization of the transient conditions is discussed, and an example of the new detector model is shown.

Step 2: A detector model that accounts for aging is set up in Simulink and customized for three transient scenarios that are common at the NPP, namely, noisy detector signals, signal oscillations during normal operation, and a full power ramp-up. Plant data is acquired at this step to be used in the analysis. The detector signals appeared to be contaminated with random noise spikes, both positive and negative, lasting for very brief time intervals. Low-pass filters (LPF) and wavelet analysis transform (WTA) methods were explored for the purpose of denoising and smoothing the data. Based on the performance comparison, the best method was selected and used.

Next, methods for dimensionality reduction of plant data were explored. Dimensionality reduction is considered an important step for systems where multiple, fast-changing process variables must be analyzed simultaneously to establish the main contributing factors to system faults. It is necessary to identify the initiating cause of process variation to establish a mapping between the affected equipment and PVs. PCA is used in this thesis for identification of variables of particular interest. Weighted PCA (wPCA) is used without modifications to improve the robustness of the algorithm. Feature extraction for fault identification and reconstruction is investigated at this stage. The PCA and wPCA algorithms used for dimensionality reduction are modified to work with nonlinear data, particularly due to liquid zone (LZ) control valve challenges, to support real plant processes where the linearity of data is not known in advance. Feature

reconstruction was performed using nonlinear PCA with the auto-associative neural network (ANN). The algorithms available from open research are customized for research objectives in this thesis. All the above were considered helpful in addressing the general concern with data visualization and presentation.

Step 3: Existing detector gain setting methodology is discussed first. The main limitation of this methodology is that it does not account for potential complications from fueling near detectors, high-response detectors, signal variability, or reactor power maneuvers following a prolonged outage. This thesis proposes to extend a detector gain setting methodology to include operational transients. The methodology for denoising and dimensionality reduction of plant data is discussed at this step. Next, new detector models for particular cases of interest are developed in MATLAB/Simulink. The models are tested using plant data to confirm detector response versus the safety analysis limits for MTT, which allows extension of the gain setting methodology for actual operating transients.

Step 4: Optimization of the detector gains setting values using an enhanced GA is proposed in this step. The optimization is performed to determine whether additional gains could be obtained with minimal modification to the amplifier circuit boards. This new knowledge is a significant original contribution of this thesis and constitutes advancement in knowledge that can be useful to others.

Step 5: Methods for assessing risks due to detector aging are analyzed at this step. First, the FSN approach is described. Next, it is proposed to develop a qualitative/quantitative risk estimation mechanism to quantify the risk associated with aged detector system performance. This approach will allow accurate risk estimation for different transient scenarios and is equipped with the corresponding risk mitigation barriers to aid in operational risk-based decision making. All the above steps are further described in subsections below.

3.1. Existing Detector Model

A review of the related literature found that neutron detector dynamic response has been studied for several decades, as discussed in Chapter 2. First, the detector signal is converted into current and voltage format by the current amplifier. The current reading is compared against a trip

set point (TSP) as well as a low MTT marker. Trip logic identifies a suitable behavior, e.g., on the indication of high neutron power, a signal to activate a safety system is issued. If the process signal did not reach the TSP but is approaching an upper control limit, then an alarm will be issued to notify the operator that a low MTT condition has occurred, as shown in Figure 3.2.

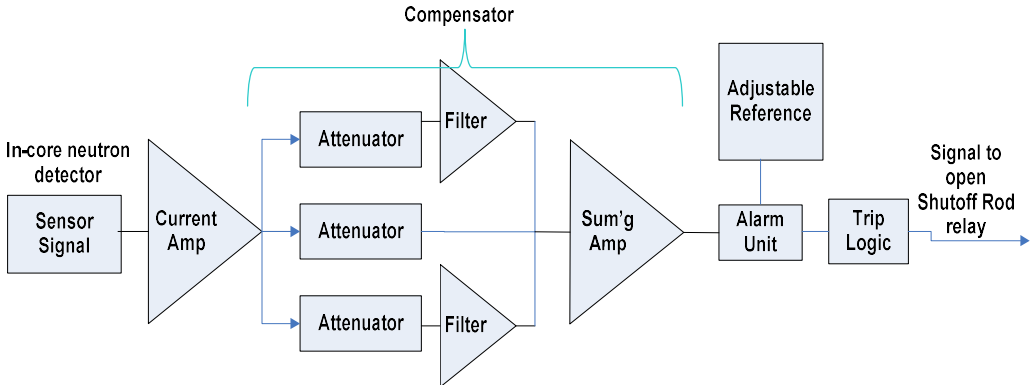

Figure 3.2: Instrumentation loop block diagram.

There are two (2) first-order filters in the instrumentation circuit, as shown in Figure 3.2, each with a compensation time constant. A summing amplifier adds the two (2) filter outputs and a direct, unfiltered signal. It is assumed that the time constant and fixed delay measurement account for all the instrumentation from the flux detector to the trip logic circuit.

As new knowledge became available, to provide a more accurate representation of thermal power, a DSC was included in the amplifier assembly. The DSC is designed to help match the in-core detector signal to thermal fuel power. This circuit compensates for a portion of the difference between the detector signal and the transient power response. The output signal from each detector passes through a DSC circuit, which applies predetermined gain factors and time constants. There is no combination of the DSC time constant components because the three DSC elements act in parallel, and the one (1) with the largest gain is a direct component (no delay, dominating for the limiting accident) that makes the time constant of the two (2) filters irrelevant. New detectors have an initial response to neutron power changes of about 104% (over-prompt). For natural uranium fuel, which has a 94% response (under-prompt), it follows that the detectors overestimate fuel power by about 10% immediately after a step increase in neutron flux. The introduction of platinum cladding causes an additional gamma reaction, 195Pt (γ, e), which reduces neutron

sensitivity, and platinum-clad detectors are nominally under-prompt. The circuit can be modeled as follows:

$$V_{out} = \left(K_1 + \frac{K_2}{1+T_2} + \frac{K_3}{1+T_3}\right) \times V_{in} \qquad \text{[Equation 3.1]}$$

where:

- K_1, K_2, and K_3 are the adjustable gain coefficient for the input and output voltages;
- K_1 is the static gain, and K_2, K_3 are dynamic gains.

During normal DSC operation there, the two (2) integrating amplifiers (30-second and 2,500-second time constants τ_2 and τ_3 and gain K_2 and K_3, respectively) subtract their gain from the gain of K_1 over time to attain the steady state gain of 1.0 (i.e., K_1-K_2-K_3=1.0).

The compensation has an effect only under a dynamic situation, i.e., when the reactor power is changing. At a steady state, the compensator has a negligible effect on the detector signal. The output from the DSC is termed the effective PF and is used in the safety analysis, as discussed in chapter 1. The background contribution of the lead cable, which depends on the concentrations of impurities, is usually less than 3% of the total signal, while the detectors themselves depress the local thermal neutron flux by about 2%.

3.2. Development of the New Detector Models in Simulink

The Pt-clad detector is sensitive to the local radiation intensity. For fixed reactor geometry in a steady-state core, the neutron and gamma fluxes are proportional to one another. Both are related to the fission rate of reactor power. The detector response to the radiation is almost totally prompt. However, since the gamma signal in a reactor is partially delayed (approximately 30% from β-active fission products), the response of the detector to changes in power is delayed. Results from CRNL [1, 3] indicate that neutron capture is the source of 70% of the current generated in the Pt-clad detector. Approximately 30% of the response is due to reactor gamma radiation. With irradiation, the gamma-ray induced current will remain approximately constant. The neutron-induced current *I(n, γ, e)* from platinum will burn out with a cross section of approximately 27 barns, while the current from Inconel will increase initially as 58Ni transmutes to 59Ni. Eventually, the Inconel component will burn out with a cross section of approximately 4.6 barns. The predicted

variation, based on an extrapolation of CRNL data, is an increase of total sensitivity by about 15% during the first three years, followed by a decrease to about 85% (of the initial sensitivity) after twenty years. Thus, in this thesis, the following assumptions are used:

- During a reactor's normal operation, a self-powered neutron detector is always subject to both neutron and gamma flux, and around 30% of its signal is due to delayed gamma rays.
- Since in a natural uranium-fueled reactor, 70% of the gamma flux is assumed to be prompt, it can be expressed as:

$$F_p = \frac{I(n,\gamma,e)}{I} + \frac{0.7I(\gamma,e)}{I} \qquad \text{[Equation 3.2]}$$

where:

- I – total current produced by the detector;
- $I(n,\gamma,e)$ – current due to (n,γ,e) reactions;
- $I(\gamma,e)$ – current due to (γ,e) reactions.

This can be represented in Laplace domain as follows:

$$I(s) = K\left(F_p + \sum_i \frac{a_i}{1+s\tau_i}\right)\phi(s) \qquad \text{[Equation 3.3]}$$

Detector response, including PF and delayed components, is well known for the nominal detectors. The same cannot be said about aged detectors. Measurements of detector performance in all literature studies focus on assessing detector PF. Reliable information related to how the various delayed components of the detector response change with time is not available. For the purpose of this thesis, the assumption is made as follows:

- A proportional increase of all delayed components occurs due to the changes in the detector PF.
- Only the fastest delayed component is impacted by aging effects.

One of the approaches for analysis of the detector response in aged conditions is based on FUELPIN simulations. FUELPIN is a computer code that was developed to predict the transient reactor fuel and clad temperatures based on a lumped parameter model of a fuel pin. The code incorporates a neutron point kinetics model and can, therefore, be used to simulate the transient

changes in fuel power. In FUELPIN, fhe functions, shown in the Laplace domain with the "s" as a Laplace variable, relating the DSC output signal to the input signal from the amplifier output can be described as:

$$D = (1 - \bar{\gamma}) \cdot N + \sum_{i=1}^{Ngroups} d_i \qquad \text{[Equation 3.4]}$$

$$\overset{*}{d}_i = \bar{\lambda}_i \cdot (\bar{\gamma}_i \cdot N - d_i) \qquad \text{[Equation 3.5]}$$

where:

- D – is relative detector signal amplitude;
- N – is the neutron flux;
- $\bar{\gamma}$ – total delay fraction;
- $\bar{\gamma}_i$ – *ith* delay fraction;
- λ_i – *ith* decay constant;
- d_i –relative amplitude of delay group *i*.

The dynamically compensated signal *D'(s)* is calculated using Laplace transform:

$$\frac{V_2(s)}{V_1(s)} = K_1 - \left[\frac{K_2}{(1+\tau_2 s)}\right] + \left[\frac{K_3}{(1+\tau_3 s}\right] \qquad \text{[Equation 3.6]}$$

where:

- V_2 – output of compensation network;
- V_1 – input to compensation network;
- K_1 – is a constant, adjustable from 0.90 to 1.15;
- K_2 – is a constant, adjustable from 0.006 to 0.057;
- K_3 – is a constant, adjustable from 0.031 to 0.093;
- τ_2 – is a 30 second time constant;
- τ_3 – is a 500 second time constant.

With this approach as the basis, the detector model in this thesis was developed in Simulink. The assumptions used in the model development are as follows:

- DSC input is modeled as the output of the amplifier stage,
- The output from the dynamic compensation circuit, which represents the compensated flux detector signal, is fed into the input of the voltage comparator,
- The DSC transfer function has a proportional gain term and two first-order lag terms each of which has an adjustable gain,
- All detectors are assumed to be aged in this analysis.

3.3. Calculation of Nominal and Maximum DSC Gain Settings

Thus, a typical self-powered in-core detector can be modeled as a current source shunted by a resistor and a capacitor to represent cable insulation as shown below in Figure 3.3.

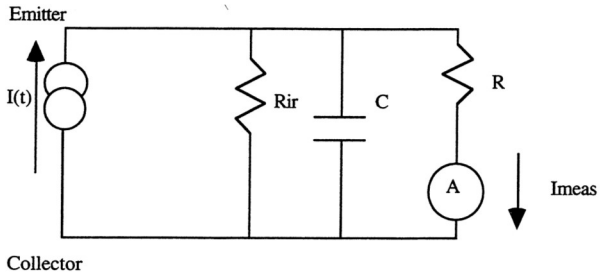

Figure 3.3: In-core flux detector modeled as a current source.

The linear amplifier with filtering is assumed to have a single pole response with a time constant of τ, i.e. $\tau = RC$ as demonstrated in Figure 3.4.

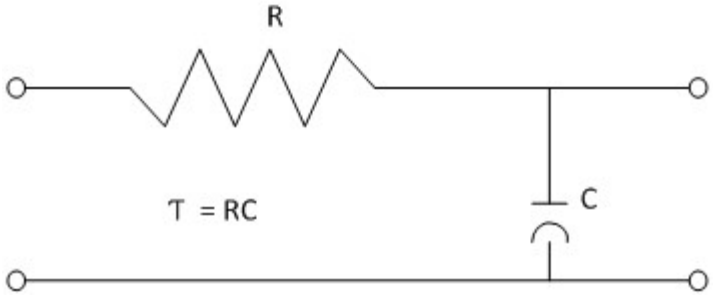

Figure 3.4: Schematics for the linear amplifier with filtering.

The system can then be represented as follows in Figure 3.5:

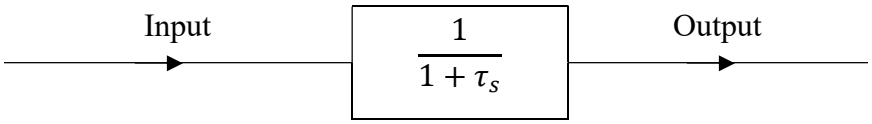

Figure 3.5: Linear amplifier system representation.

The capacitance depends on the length of the lead cable. The detector current can be modeled as a PF and a sum of all delayed fractions (equal to unity):

$$\Delta I(t) = K(F_p + \sum_i a_i(1 - e\frac{-t}{\tau_i}))\Delta\phi \qquad \text{[Equation 3.7]}$$

where:

- K – calibration constant;
- F_p – prompt fraction;
- a_i – the fraction of the *ith* decay component;
- t – time (step change occurs at time zero);
- τ_i – the decay time constant;
- $\Delta\phi$ – step change in flux.

A portion of the schematic for the main Printed Circuit Board (PCB), which houses the circuitry for the DSC, is shown in Figure 3.6.

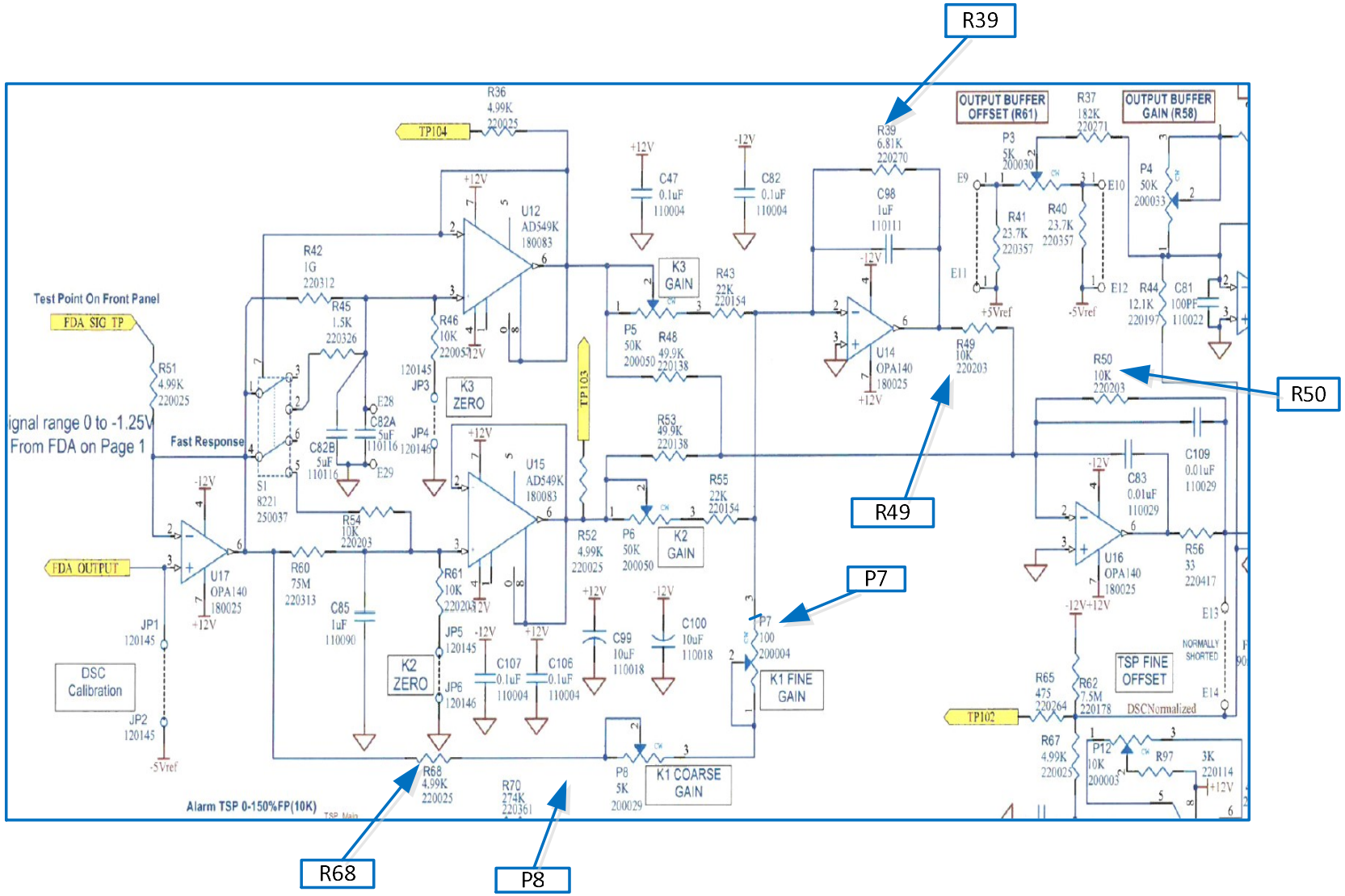

Figure 3.6: A portion of the main PCB schematic for detector amplifier is shown.

Using the assumptions discussed earlier, K_1 gain can be calculated with the following formula:

Gain = (R39*R50)/(R68*R49) [Equation 3.8]

where:

- *R39 (6.81KΩ)*, *R49 (10KΩ), R50 (10KΩ),* and *R68* (4.99K*Ω)* - are resistors shown in Figure 3.6.

This yields the nominal values between 0.68 and 1.36, depending on the positions of P7 and P8 resistors (shown in Figure 3.6) which are installed in series with R68. To account for resistor tolerances, the maximum allowance for K_1 gain is, therefore, set to be 0.75 to 1.25.

Case 1: Steady State Response

As discussed earlier, the DSC modifies the in-core amplifier signal to compensate for the under-prompt characteristics of the detectors and is given by the Equation 3.9 below:

$$\frac{V_2(s)}{V_1(s)} = K_1 - \left[\frac{K_2}{(1+\tau_2 s)} + \frac{K_3}{(1+\tau_3 s)} \right] \quad \text{[Equation 3.9]}$$

where:

- V_2 – is the output of the compensation network;
- V_1 – is the input to the compensation network;
- K_1 – is a constant, adjustable from 0.90 to 1.15;
- K_2 – is a constant, adjustable from 0.06 to 0.057;
- K_3 – is a constant, adjustable from 0.031 to 0.093;
- τ_2 – is a 30 second time constant;
- τ_3 – is a 2500 second time constant.

The gain coefficients K_1, K_2, and K_3 are determined based on the assumption that a 6.00 VDC input is used to the DSC. This measurement corresponds to 120% full power (FP). The 6.00 VDC is at the amplifier output and corresponds to a 0.720 amp current generated by a calibrator source. Table 3.1 documents the voltage values at a steady state corresponding to the old DSC gains. The steady-state tolerances for the individual gains

are ±1 mV and for the sum of the three gains is ±10 mV. To account for the instrumentation uncertainties during calibration, the tolerance for the sum of all three gains can be calculated as the root sum of squares (RSS) of the individual tolerances of K_2 and K_3, i.e. ±14.4%.

Table 3.1: Steady state voltages corresponding to current DSC gain configuration for a 6.00 VDC input.

DSC Gain	Gain Value	Measurement location across the test points (TP)	Voltage Calculation (VDC)	Expected Voltage (VDC)	Tolerance (VDC)
K_1	1.082	+TP10 to -TP5	(1.082*6)/2	3.246	3.245 to 3.247
K_2	-0.008	+TP3 to -TP5	(-0.008*6)/2	-0.024	-0.023 to -0.025
K_3	-0.074	+TP4 to -TP5	(-0.074*6)/2	-0.222	-0221 to -0.223
$K_1+K_2+K_3$	1.000	+TP2 to -TP5	(1.082-0.008-0.074)*6	6.000	5.990 to 6.010

Table 3.2: Steady state voltages corresponding to current DSC gain configuration for a 6.00 VDC input.

Case 2: Transient Response

During normal operation, there are two (2) integrating amplifiers (30-second and 2,500-second time constants, τ_2 and τ_3 , and gain K_2 and K_3, respectively) that subtract their gain from the gain of K_1 over time to attain the steady-state gain of 1.0 so that K_1-K_2-K_3=1.0. Transient response to a step input can be verified by checking the DSC output at specific points in time, as follows:

$$V_{TP3}(t) = 0.5K_2V_{TP1}(1-e^{-\frac{t}{\tau_2}}) \qquad \text{[Equation 3.10]}$$

$$V_{TP4}(t) = 0.5K_3V_{TP1}(1-e^{-\frac{t}{\tau_3}}) \qquad \text{[Equation 3.11]}$$

$$V_{TP2}(t) = V_{TP1}(K_1 - K_2(1 - e^{-\frac{t}{\tau_2}}) - K_3(1 - e^{-\frac{t}{\tau 3}})) \quad \text{[Equation 3.12]}$$

where:

- V_{TP1} = 6.0 VDC , step input at time zero;
- t – is the time;
- τ_2 = 30 seconds, time constant;
- τ_3 = 2500 seconds, time constant;
- *TP1, TP2, TP3*, and *TP4* – test points for measurements;
- K_1, K_2, and K_3 are per gain values in Table 3.2 and 3.3.

Table 3.2 documents the voltage values at a steady state corresponding to the new proposed DSC gains.

Table 3.3: Steady state voltages corresponding to the new recommended DSC gain settings for a 6.00 VDC input.

DSC Gain	Gain Value	Measurement location across the test points (TP)	Voltage Calculation (VDC)	Expected Voltage (VDC)	Tolerance (VDC)
K_1	1.150	+TP10 to -TP5	(1.15*6)/2	3.450	3.449 to 3.451
K_2	-0.057	+TP3 to -TP5	(-0.057*6)/2	-0.171	-0.170 to -0.172
K_3	-0.093	+TP4 to -TP5	(-0.093*6)/2	-0.279	-0.278 to -0.280
$K_1+K_2+K_3$	1.000	+TP2 to -TP5	(1.15-0.057-0.093)*6	6.000	5.990 to 6.010

As time increases the voltage at test points TP3, TP4 and TP2 will approach the steady state voltages tabulated in Table 3.4 and 3.5 below.

Table 3.4: Transient voltages corresponding to the old DSC gain settings for a 6.00 VDC input.

Elapsed Time (sec)	Test Points	Expected Voltage (VDC)	Tolerance (VDC)
30	+TP3 to -TP5	-0.015	-0.012 to -0.018
600	+TP4 to -TP5	-0.047	-0.042 to -0.052
720	+TP2 to -TP5	6.332	6.298 to 6.366

Table 3.5: Transient voltages corresponding to the new DSC gain settings for a 6.00 VDC input.

Elapsed Time (sec)	Test Points	Expected Voltage (VDC)	Tolerance (VDC)
30	+TP3 to -TP5	-0.108	-0.101 to -0.114
600	+TP4 to -TP5	-0.060	-0.054 to -0.065
720	+TP2 to -TP5	6.418	6.436 to 6.402

The new gains for each detector are set to their maximum values, given in Table 3.2, and are applied to every DSC module as shown below:

Table 3.6: The existing and recommended DSC gains

DSC Gain Coefficient	Existing (PF=0.772)	Recommended (PF=0.75)
K_1	1.082	1.15
K_2	0.008	0.057
K_3	0.074	0.093

Next, the impact of the proposed DSC gain changes is assessed by using the neutron detector DSC Simulink model.

3.4. Calculation of Residual Error for Transient Scenarios

The following transient scenarios were used in FUELPIN for aged detectors with the DSC gains at nominal and modified values as shown in Table 3.3:

- Ramp increase in power from 0% to 100% at rates of 0.1%/sec and 1%/sec.
- Ramp decrease in power from 100% to 70% and 10% at a rate of 0.8%/sec. These transients are used to find the amount of undershoot in the compensated detector signal. On power reduction, it appears to be lower than it is.
- Power increase of up to approximately 10% over time periods ranging from 10 sec to 2 minutes. These stylized transients are used to set up bounds for the worst expected detector response following a refueling and allow for estimation of the impact of changes in DSC gains on operating margins during refueling.

For all cases, the simulations were performed for a total of a one hour period. The maximum residual errors for aged detectors (PF=75%) is shown below in Table 3.7.

Table 3.7: Maximum Residual Errors for detectors, aged (PF=75%), from FUELPIN.

Cases	Error (nominal DSC gains)	Error (max DSC gains)
K_1	1.066	1.150
K_2	-0.028	-0.057
K_3	-0.038	-0.093
Ramp Down (decrease in power)		
100% to 10%, at 0.8%/sec	10.45	9.04
100% to 70%, at 0.8%/sec	3.49	3.02
Ramp Up (increase in power)		
0% to 100%, at 0.1%/sec	-11.54	-9.81
0% to 100%, at 1%/sec	-11.62	-10.04
Refueling (power increase)		
10% , in 10 sec	-1.18	-1.00
10% , in 30 sec	-1.17	-1.00
10% , in 60 sec	-1.17	-1.00
10% , in 90 sec	-1.17	-1.00
10% , in 120 sec	-1.17	-1.00

Here, the residual error is calculated as the difference between the compensated signal and fuel power in percentage of power. For refueling and ramp increases of power, the positive residual error means that the detector is overcompensated and MTT decreases by the amount of error. Conversely, the negative residual error means the detector is undercompensated. For ramp decreases in power, the negative residual error means that detector is overcompensated by the amount of error. Conversely, the positive residual error means the detector is undercompensated.

For all scenarios considered, the maximum reduction in MTT for the worst fueling transient is found to be less than 1.0%. This criterion is used in this thesis to validate the proposed approach for optimization of the DSC gain settings using a GA.

3.5. Denoising Plant Data for Analysis

The methodology for plant data de-noising and smoothing used in this thesis is explained below. These steps are not a primary focus of the thesis but were considered significant enough for development of an overall framework. Low-pas filter (LPF) and WTA algorithms are described first, along with a discussion on the extension of the best-performing method. These methods were chosen based on the ease of implementation. No attempts are made in this thesis to customize or tune filters. The scope of this section is to estimate the overall impact of noise reduction and overall feasibility of these methods for managing detector degradation due to aging. Application of the most promising method on a case study is also presented in this section.

3.5.1. Selection of Approach

The methodology for PF optimization proposed in this thesis considers increasing trends in detector noise, particularly during fueling and coincidental detector signal oscillations. Processing large time-series data from a noisy process is a significant challenge. Thus, a need for additional techniques for noise reduction and signal smoothing prior to subsequent analysis was identified. The chosen method must be able to support a high volume of input data without dramatically increasing processing time or negatively impacting computational complexity. Another major factor is the potential data losses associated with the chosen method. This is particularly critical for applications in fault detection for neutron detector systems. This thesis proposes a mitigating strategy based on denoising or filtering the output signals from each detector before it passes through the DSC circuit and the application of predetermined noise reduction factors using LPF and WTA.

3.5.2. Overview of Low-Pass Filter Methodology

Smoothing, differentiation, and peak sharpening of the signal and its frequency spectrum were performed using low-pass filter methods. The literature review, highlights of which are given in chapter 2, shows that LPFs typically perform well as data smoothers. A low-pass conventional filter approach was chosen for this thesis because of its previous high success and relative ease of implementation. More importantly, low-pass filters are

known to provide a certain degree of data smoothness while preserving the independence of the components, which is a critical criterion for this study. This thesis is mainly concerned with the spikes in the positive direction since these can have an adverse impact on safety analysis assumptions. If not mitigated, random high-frequency noise can result in a much more severe impact on MTT calculations.

Removal of evident disturbances, such as spikes and steps, was accomplished using a filter model established in MATLAB to produce theoretical results. Next, an experimental temporary modification was installed for one detector at a power plant to compare actual results to the predicted response. In this modification, the detector readings were captured using data-logging equipment connected to the buffered output of the flux detector amplifier. The obtained data was used for analysis of the filter performance, e.g., comparison of the unfiltered versus the filtered signal. The use of a buffered output and a signal isolator of the data logger allows the implementation of this and subsequent modifications without any safety impact on the plant operation.

3.5.3. Application of the LPF Approach in This Thesis

Commonly used smoothing algorithms are rectangular, triangular, pseudo-Gaussian, and the Savitzky-Golay algorithm [128], sometimes also referred to as the least-square method. The first three methods are based on replacing each point in the signal with the average of *m* adjacent points. Typically, *m* is selected to be a positive integer, called the *smooth width*, and is chosen to be an odd number. This method ensures that the smooth coefficients are symmetrically balanced around the central point to preserve the x-axis position of peaks.

$$S_j = \frac{Y_{j-1} + Y_j + Y_{j+1}}{m} \qquad \text{[Equation 3.13]}$$

The *smooth width* can be adjusted to obtain the optimum results, and smoothing can be applied several times resulting in a multi-pass smoothing with a combined smooth width of:

$$m_c = n * w - n + 1 \qquad \text{[Equation 3.14]}$$

where:

- n is the number of passes;
- w is the w-width smooth.

If the raw data is not corrupted, smoothing should not distort the signal. For white noise, i.e., noise evenly distributed over the entire frequency spectrum of the signal without sharp steps or peaks, the standard deviation of the noise remaining in the signal can be approximated as:

$$S_{dev} \approx \frac{S}{\sqrt{(m)}} \qquad \text{[Equation 3.15]}$$

where:

- S is the standard deviation of the remaining noise after smoothing,
- m is the smooth width.

For cases when the smooth width is substantial or signal distortion is highly undesirable, the Savitzky-Golay [128] algorithm can be applied. This method is developed on the principle of least-square fitting of polynomials to segments of the data. In its simplest form, it can be described as a nonrecursive filter. This filter replaces each data value f_i with a linear combination gi of itself and some number of adjacent neighbors, i.e., the average of the data points from f_i-n_L to f_i +n_R:

$$g_i = \sum_{n=-n_L}^{n_R} c_n f_{i+n} \qquad \text{[Equation 3.16]}$$

where:

- n_L - is the number of points to the left of the data point;
- n_R - is the number of points to the right of the data point;
- c_n - is the filter coefficient, where $c_n=1/(n_L+n_{R+1})$.

The Savitsky-Golay algorithm identifies filter coefficients c_n such that the moving window averaging preserves the area under a spectral line, the mean position in time, the so-called first moment, and the higher moments. This method is less effective at reducing noise but is better at preserving the shape of the original signal.

3.5.4. Peak Finding Method

When the data set is contaminated with noise or the signal-to-noise ratio (SNR) is extremely low, false peaks can be expected. One of the ways to process a real peak in the signal is first to identify where the actual peaks are, and then measure the peak amplitude, i.e., height, width, and position. A conventional method for peak finding is to look for a negative slope zero-crossing of the first derivative and then determine the position, height, and width of each peak by least-squares curve fitting about the maximum.

Certain smoothing filters can distort signals, as discussed earlier, thus affecting the peak heights and width. Therefore, it could be useful to establish specific threshold criteria for slope parameters so that only signals that exceed this threshold are taken into consideration [129]. This approach should provide accurate results even for heavily smoothed first derivatives with known noise distortion since the peak parameters extracted by curve fitting are not distorted.

3.5.5. Proposed LPF Algorithm Optimization

For this study, the low-pass filter appears to be a suitable approach since it provides the compromise between the required degrees of smoothing versus latency. It is important to note that in this study, only past and current detector input signal x_n is available to produce output signal y_n. Thus, the poles of the filter reside in the unit circle $|z_p|<1$. Since a single-pole filter is proposed, $z_p = (1-\alpha)$ where α is a filter constant, then $|1-\alpha| < 1$ and the range of α where the filter is causal and stable can be shown as $0 < \alpha < 2$. The area of interest is the high-frequency noise. Thus, the pole is along the positive side of the line, and α needs to be in the range between 0 and 1. The filter can be tuned so that very little smoothing occurs (α is close to 1). However, there is almost no latency in the detector amplifier output. Conversely, if a higher degree of smoothing is required, the value of α can be reduced to be closer to zero. This, however, will result in higher latency. At time n, the smoothed output y_n can be given as:

$$y_n = \alpha * y_{n-1} + (1-\alpha) * x_n \text{ for } 0 < \alpha < 1 \qquad \text{[Equation 3.17]}$$

$$\alpha = \frac{\tau}{\tau + h} \qquad \text{[Equation 3.18]}$$

where:

- h - is a data sampling time interval, e.g., two (2) seconds;
- τ - is the time constant.

As discussed earlier, the high frequency noise affecting detector signal varies in the frequency spectrum, amplitude and time of occurrence. Thus, it is proposed to modify the least mean squares filter design algorithm so that it is possible to continually update a set of weights that change the output of the system to adaptively cancel the noise in a rapidly changing environment as shown in Figure 3.7:

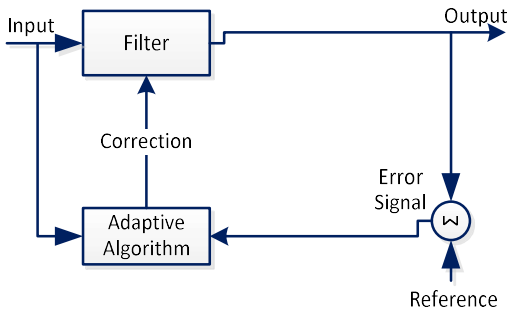

Figure 3.7: A block diagram for the proposed algorithm.

In this figure, the error signal is fed back into the filter which modifies its weights according to the ultimate desired signal. The value of α defines the weight given to the previous data versus the raw data. Thus, the output signal y_n can be computed by summing the product of weights w_i and previous inputs:

$$y_n = \sum_{i=0}^{n} x_i w_i \qquad \text{[Equation 3.19]}$$

The weights can be adapted such as:

$$w_{n+1} = w_n + (err)\frac{x_n}{2^i} \qquad \text{[Equation 3.20]}$$

where:

- *i* - is an amalgamation of the magnitude of error, computed each time the weights are updated;
- *(err)* - is the error signal, i.e., the output.

The check for filter stability can be performed by comparing the output with the previous output. This approach initially estimates the correction coefficient, and then iteratively updates it in the appropriate direction, which optimizes accuracy. As time goes by, the correction coefficients should reach their optimal values. For example, if the error is a quadratic function that never goes negative, minimizing the mean squared error means moving along this quadratic function. The objective here is to get to the minimum of the function where the error is minimized. An integral absolute error (IAE) approach can be used to achieve this goal. In this case, the error is integrated over time without placing weight on any of the errors in the overall response.

$$I_{IAE} = \int_0^{\infty} | err(t) | dt \qquad \text{[Equation 3.21]}$$

This approach tends to produce a slower response, which may not be acceptable if the filter latency is a critical performance characteristic. It can be improved by application of an integral squared error (ISE) function where the square of the error is integrated over time:

$$I_{ISE} = \int_0^{\infty} err^2(t) dt \qquad \text{[Equation 3.22]}$$

The ISE will penalize large errors more than smaller ones since the error is squared. The system optimized for ISE will tend to eliminate large errors quickly but will tolerate small, persistent errors for an extended period. This will produce fast responses but with considerably low amplitude and oscillation. Since the reduction in latency is a desirable feature in this filter application, this can become a viable option for implementation.

There are many other functions that can be considered for filter optimization. They will not be further explored in this thesis.

3.5.6. Overview of Wavelet Analysis Methods – Morlet Wavelet

Based on the literature review in Chapter 2, the main challenge expected with LPF filter methods is the poor SNR and losses in signal shape and amplitude. The in-core detectors in this study (e.g., located in the horizontal flux detector assemblies) have roughly similar noise (amplitude and pattern) as an SNR of approximately 110/1 at full power. The SNR values decrease significantly during low power operation, and shutdowns and any

additional losses due to filtering are highly undesirable. Therefore, application of the WTM, as an alternative approach to LPF, is also investigated in this thesis. Wavelets are well suited to represent signals with discontinuities [130], which is a critical factor for applications with real-time data. Also, WTMs are a novel intelligent filtering technique with a promising future potential for development. This criterion was also a deciding factor in the selection of this approach. Using the governing equations, a model was established in MATLAB to produce theoretical results.

A family of wavelets is comprised of a main wavelet *ψ(t)*, or the so-called mother wavelet, and daughter wavelets (also called window functions), defined by the main wavelet and a scale function φ(t) in time domain [131]. These daughter wavelets are themselves functions with different regions of support and are used in the transformation process to extract information from the raw data. The wavelet transform is a product of the data signal and the wavelet family. The scaling function can be used to filter out the lowest level of the transform. It also ensures the entire spectrum is covered:

$$\psi_{a,b}(t) = \psi(t - b)/a \qquad \text{[Equation 3.23]}$$

where:

- $\psi(t)$ – is the mother wavelet;
- $\varphi(t)$ – is a scaling function;
- a – is a scale parameter;
- b – is a time translation.

Because wavelet analysis combines both time and frequency analysis of the incoming signals, the wavelet function is in effect a band-pass filter. It can also be applied for data smoothing by using adaptive thresholding, where wavelet coefficients can be selected to correspond to undesired frequency components [132].

A wavelet first needs to be selected, and the process data is then converted into the wavelet domain. Next, a threshold for the wavelet coefficients is determined based on the selected threshold rules. Finally, the transform is inverted so that the wavelet is reconstructed using the original approximation coefficients and the modified detail

coefficients. Denoise filters must be selected carefully to obtain the shape of the wavelet closely matching the faulty signal pulse.

The Morlet wavelet transform belongs to the class of continuous wavelet transforms, where a wavelet function multiplies the signal and the transform is computed separately for different segments of the time-domain signal. The MWT is based on the real-valued wavelet function and scaling function, but unlike conventional wavelet transforms, the MWT is complex, with real and imaginary parts, where the exponential carrier is multiplied by a Gaussian window [131]. Using ν_o as a constant, the Morlet mother wavelet can be defined as:

$$\psi(\mathrm{t}) = \exp(-2\pi^2(\nu - \nu_o)^2) \qquad \text{[Equation 3.24]}$$

The real part of the Morlet wavelet can be shown as a cosine signal that decays exponentially on both sides:

$$\psi_r(\mathrm{t}) = \frac{1}{\sqrt{2\pi}}\exp(-\beta^2 t^2/2)\cos(2\pi\nu_o t) \qquad \text{[Equation 3.25]}$$

Here the exponent term helps determine the shape of the wavelet, and a shape parameter β is used to optimize a trade-off between time resolution and frequency resolution.

3.5.7. Potential for MTW Optimization

The frequency resolution increases, whereas time resolution decreases, with the reduction of β and will become a cosine function with the finest frequency resolution when β is equal to 0. Similarly, when β the parameter reaches infinity, the Morlet wavelet obtains the finest time resolution. From the mother wavelet, a daughter Morlet wavelet can be derived as follows:

$$\psi_{a,b}(\mathrm{t}) = ex(-\beta^2(t-b)^2/2a^2)\cos(\frac{\pi(t-b)}{a}) \qquad \text{[Equation 3.26]}$$

where:

- a – is the scale parameter for dilation;
- b – is a time translation.

Thus, when the signal is convolved with the designed Morlet Wavelet, noise and faults present in the signal can be identified from the filtered signal. Using this approach, a shape parameter β can be used to optimize a trade-off between time resolution and frequency resolution to make the proposed method suitable for a near-real time processing at the plant.

3.6. Data Dimensionality Reduction Prior to Analysis

The methodology for dimensionality reduction and pattern recognition in this thesis is presented below. The main reason for the use of PCA in this thesis is for reduction in the dimensionality of the dataset and pattern identification. These steps are not a primary focus of the thesis but were considered significant enough for development of an overall framework. PCA, wPCA, and nonlinear PCA algorithms are described first, followed by a discussion on the extension and application of these methods in the thesis.

3.6.1. Selection of Approach

As discussed in Chapter 1, the methodology for PF optimization of aged detectors must account for typical plant transient scenarios. In addition to noisy detectors, potential complications to data collection and analysis result from fueling near noisy detectors with the coincidental occurrence of signal oscillations with transient zone levels, as shown in Figure 3.8.

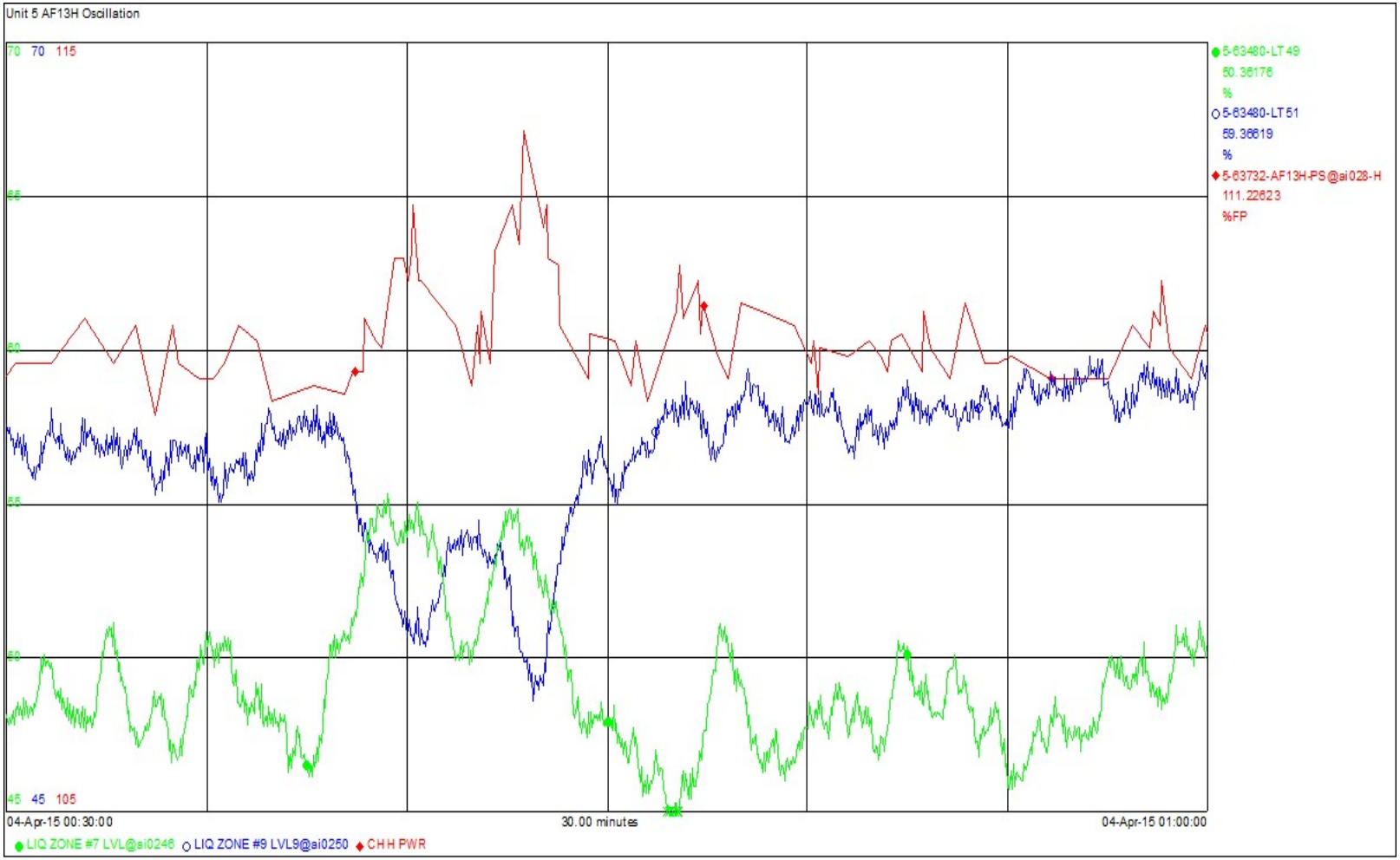

Figure 3.8: Typical detector signal oscillation—a trend of a detector (designated as AF13H) signal is shown in red, and the coincidental zone level transient is shown in blue and green.

This behavior is unexpected because the detector signals and liquid zone controller levels are not synchronized. A similar phenomenon (shown below in Figure 3.9) was noted at several nuclear power plants in Canada. For example, from 1999 to 2003, a neutron detector (designated here as detector 4F) was showing steady performance with relatively little noise present. At midyear of 2003, an unexplained adverse change in the detector signal occurred. A high rate of signal variations persisted until January 2010, when the detector signal returned to its previous performance with minimum disturbances.

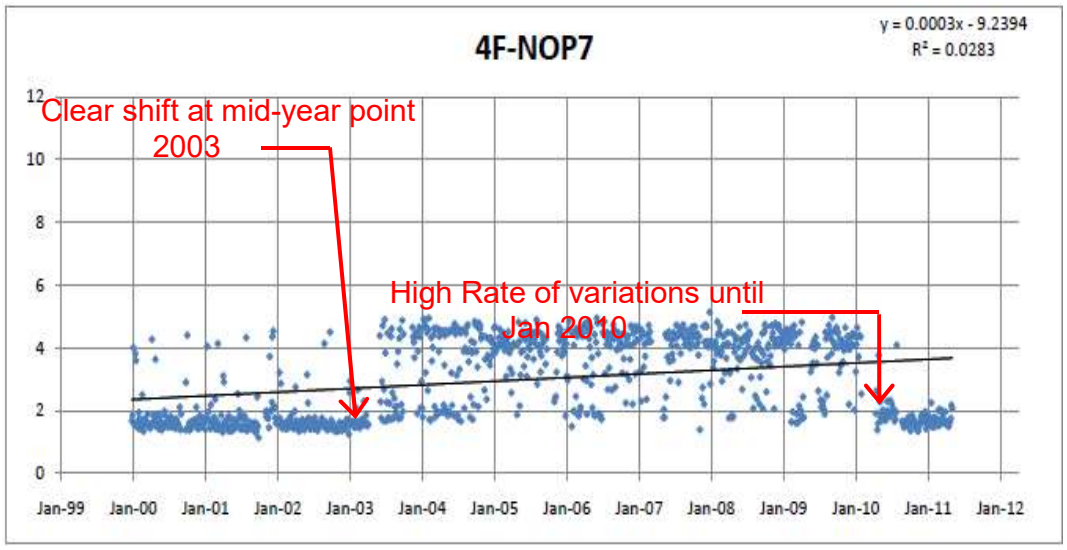

Figure 3.9: Detector performance trend example for January 1999 – January 2011.

The main concern in this case is the impact on MTT, both during normal operation and particularly during refueling. A trend of typical MTT at normal full power operation sampled every five (5) minutes across four reactor units is shown below in Figure 3.10.

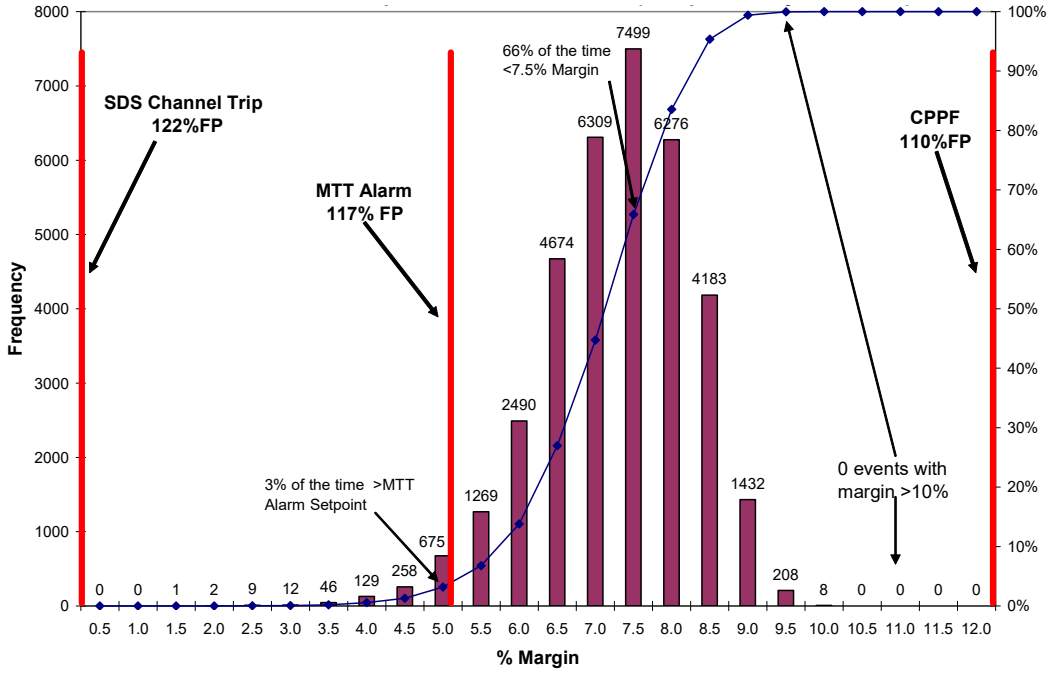

Figure 3.10: A typical MTT at full power.

Analysis of plant data shows that during a typical high-power operation, 66% of the time there was less than 7.5% margin available and no events where margin exceeded 10%. Thus, to maintain the required margin, reactor power de-rates were required. In an ideal case, e.g. with 105 in-core detectors randomly distributed with 2-out-of-3 trip logic, the required detector setting can be shown as:

$$RDS = CPPF \times Pwr = 110\% \qquad \text{[Equation 3.27]}$$

where:

- CPPF – is the minimum issued channel power peaking factor = 1.10;
- trip setpoint = 122%;
- all units operating at 100% full power (FP).

Thus, the maximum achievable margin is 12% when a reactor is operating at 100%.
The impact of margin reduction due to oscillation can be seen by comparing Figures 3.11 and Figure 3.12 where the margin was reduced by 2% on average due to signal variation.

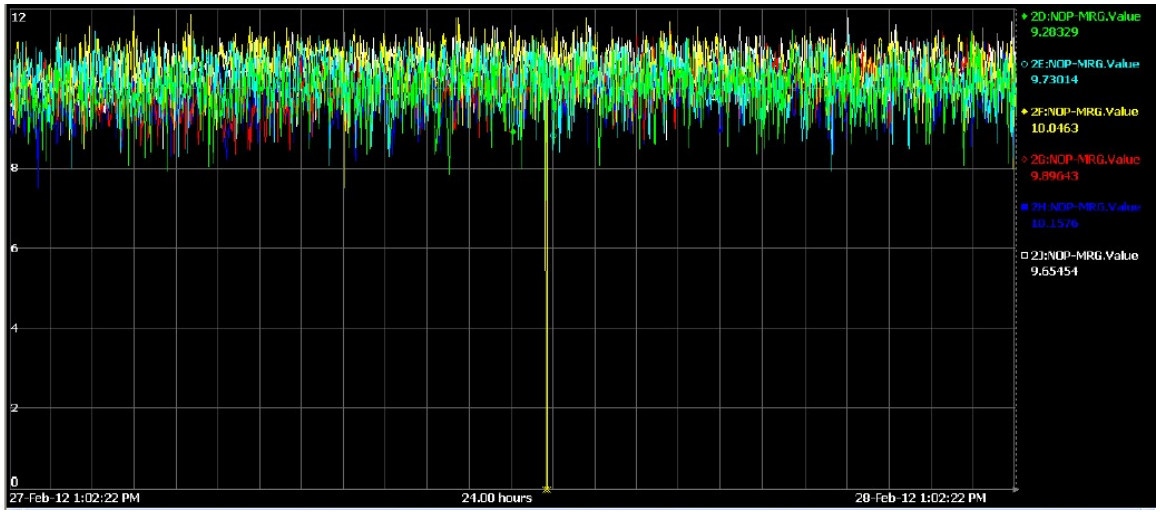

Figure 3.11: MTT in the absence of signal variations, February 20, 2012.

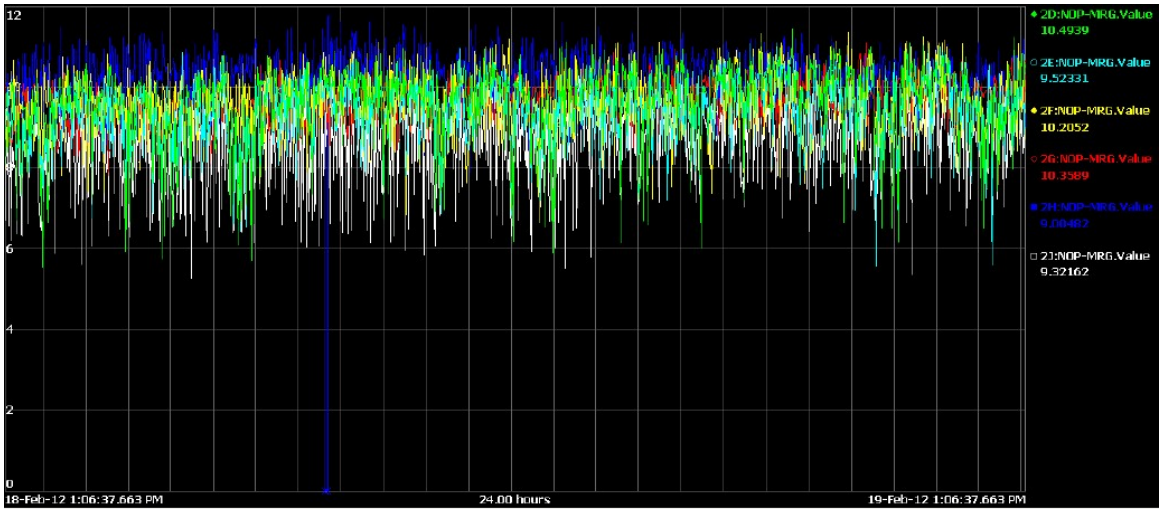

Figure 3.12: Impact on MTT when signal variations are present, February 19, 2012.

The unexplained signal behavior is always present during high power operation at greater than 86% FP and typically results in a 2 to 3% decrease in MTT. Previous engineering analysis confirmed that the detector loops and zone controllers operated correctly in every case where signal oscillations were present but failed to identify the root cause of unexpected system performance due to a large number of potential suspects, i.e., potential variables that could affect detector output.

Thus, plant data dimensionality reduction is important in this case. There appear to be multiple, fast-changing process variables that must be analyzed simultaneously to

establish the main contributing factors of system behavior. It is essential to understanding the variations and grouping structure of a dataset, as well as to find the most important features that explain the most variance in the data.

A comparison of dimensionality reduction techniques, given in Chapter 2, indicates that the best method is problem dependent, e.g., the topology of the embedded data, size of the dataset, noise versus signal, sparseness versus curvature, and the scale of interest. However, a review and systematic comparison of the many dimensionality reduction techniques show the superiority of the variants of PCA algorithms on the most heterogeneous classes. In this study, an unsupervised PCA method is used to discover the structure in the input variables. A supervised learning approach would not be suitable in this case since the relationships in the input data are not known in advance. Another advantage of using a PCA algorithm is that it can also be used to significantly speed up unsupervised feature learning. This aspect is essential for the current case study since the dataset has no target variable or response value and is unlabelled. The other important consideration for selection of a PCA for this study was the opportunity for future optimization, which should be computationally and numerically feasible to implement in practice.

The PCA and wPCA algorithms used for dimensionality reduction need to be modified to work with nonlinear data to support real plant processes. For example, nonlinearity of the zone control valves at the NPP in this study has been speculated to be a probable cause for detector signal oscillations. In some cases, a response to a unit step change resulted in a high degree of signal oscillation exceeding ±15%. This is consistent with the field observations of cases where the zone oscillations of up to 20% have been noted in the worst-case scenarios.

A variety of nonlinear dimensionality reduction techniques have been proposed to address the limitations of traditional techniques such as PCA and classical scaling for nonlinear dimensionality reduction, such as in this case. A literature review of different data modeling methods (given in chapter 2), e.g., PLS, back-propagation multilayer perceptron (MLP) neural networks, radial basis function (RBF) neural networks, and an adaptive B-spline modeling algorithm (ASMOD), indicates that all these methods can identify and represent general nonlinear dependencies in the data without a priori

specifying which particular nonlinear dependencies to look for. However, the PLS approach needs active interaction from the data analyst to identify nonlinear dependencies.

In this thesis, comparisons of the prediction accuracy and performance characteristics, such as computation time and simplicity of use, were the basis for the selection of non-linear PCA with an ANN approach. A feed-forward multilayer ANN is proposed to model nonlinear systems and has already been tested for two target applications in reactor technology, as discussed in the literature review.

3.6.2. Dimensionality Reduction with PCA

A principal component calculated by PCA is a single axis in space. The second and third principal components are other axes in space, perpendicular to the first. Each unit is assigned a set of scores to show the magnitude of its effect on the rest of the components. For all vectors in the dataset, each row position in a vector always corresponds to the same type of observation.

$x^{(k)}$ k=1, 2, …, n $\qquad x^{(k)} = [x_1^{(k)}, x_2^{(k)}, x_3^{(k)}, ...x_m^{(k)}]^T$ [Equation 3.28]

Assuming each of the *m* rows contains values that are independent and identically distributed instances of process variables, *m* by *n* X-matrix can be set up as follows:

$$X = [x^{(1)}, x^{(2)}, x^{(3)}, ...x^{(n)}] = \begin{bmatrix} x_1^{(1)}, x_1^{(2)}, x_1^{(3)}, ...x_1^{(n)} \\ x_2^{(1)}, x_2^{(2)}, x_2^{(3)}, ...x_2^{(n)} \\ x_m^{(1)}, x_m^{(2)}, x^{(3)}, ...x_m^{(n)} \end{bmatrix}$$ [Equation 3.29]

The mean of the attributes in each row to get *m* mean values is given, and each entry in the data matrix is replaced by its difference with the mean; the data average vector can be defined as follows:

$$\bar{x}_i = \frac{1}{n} \sum_{k=1}^{n} x_i^{(k)}$$

[Equation 3.30]

where:

- i=1, 2, …, m.

Next, covariance matrix can be computed:

$$XX^T = \frac{1}{n-1}\sum_{k=1}^{n}(x^{(k)} - \mu)(x^{(k)} - \mu)^T \qquad \text{[Equation 3.31]}$$

Then the eigenvector/eigenvalue pairs of XX^T can be determined as $XX^T\{(q^{(j)}, \lambda_j)\}_{j=1}^{r}$ where r is the rank of XX^T. For each $x^{(k)}$ k=1, 2, …, n a corresponding data axis of $y^{(k)} = Q^T x^{(k)}$ can be calculated to represent the new coordinate system. Finally, the PCA algorithm will produce the n-vectors $y^{(1)}, y^{(2)}, ..., y^{(n)}$ such that for $Y = (y^{(1)}, y^{(2)}, ..., y^{(m)})$ the covariant matrix S(Y) has nonzero diagonal entries and all off-diagonal elements are zero.

It is assumed that all the principal components, as a whole, form an orthogonal basis for the space of the data. Thus, PCA algorithm is used to decompose a data table with correlated detector and process system measurements into a new set of uncorrelated orthogonal variables, i.e., principal components. This approach will allow mapping of the affected equipment to process variables with the main contribution to the process upset.

3.6.3. Improving Robustness of Algorithms—Weighted PCA

To improve the robustness of the PCA algorithm, a recently proposed generalization of PCA, or so-called wPCA, can be used. The application of a wPCA increases robustness by assigning different weights to data objects based on their estimated relevance. The weights are selected by using the inverse variances of the ratings. This approach standardizes sample data by assigning weights to the mean and the outer products that form the covariance matrix. Also, this puts a weight factor on every point in the training data, which makes it easier to identify extreme points in a large sample set.

3.6.4. NLPCA-ANN Approach

Feature reconstruction is a process similar to dimensionality reduction and is used in cases where data of interest is large and complex. The data of interest is selected and transformed into a much-reduced representation set of features that correspond to particular attributes within the original data. A collection of such observations or a feature set can be shown as a feature vector. This principle allows elimination of redundant measurements and reduces computational demands and burden on the processing hardware [133]. A variety of nonlinear dimensionality reduction techniques have been proposed that aim to address the nonlinearity effects where input and output have a nonlinear relationship or the linearity of the process data is not known in advance. In some such cases, a nonlinear system can be modeled using linear equations. The results of this approximation or so-called linearization may not be sufficient for all cases, mainly when the accuracy of a system model can have a high impact on the results.

A novel extension of PCA is known as nonlinear PCA (NLPCA) [134]. In this method, the principal components are generalized from straight lines to curves using ANNs. The introduction of hidden layer(s) makes it possible for the network to exhibit nonlinear behavior. NLPCA using an ANN allows mapping between x to the first principle component. The original data space is curved by applying an MLP [135] to perform identity mapping. The network has three (3) hidden layers of variables between the input and output layers of variables as shown in Figure 3.13:

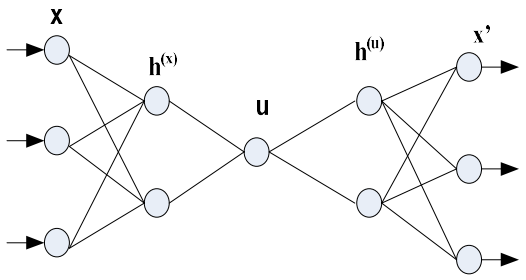

Figure 3.13: Neural network model for calculating NLPCA.

Transfer function f_1 maps from x, the input column vector of length l, to the first hidden layer (the encoding layer), represented by $h^{(x)}$, a column vector of length m, with elements given as:

$$h_k^{(x)} = f_1\left[\left(W^{(x)}x + b^{(x)}\right)_k\right] \quad \text{[Equation 3.32]}$$

where:

- $k = 1, \ldots, m$;
- $W^{(x)}$ – is an $m \times l$ weight matrix;
- $b(x)$ – is a column vector of length m.

Bias parameters are contained in the column $b(x)$. Transfer function f_1 is nonlinear, typically a hyperbolic tangent. A second transfer function f_2,, also called identity function, maps from the encoding layer to the bottleneck layer. This layer has one neuron representing the nonlinear principal component u, given by:

$$u = f_2\left(w^{(x)} \cdot h^{(x)} + \bar{b}^{(x)}\right) \quad \text{[Equation 3.33]}$$

The third transfer function f_3 maps from u to the final hidden layer, $h^{(u)}$, also called the decoding layer, as shown:

$$h_k^{(u)} = f_3\left[\left(w^{(u)}u + b^{(u)}\right)_k\right] \quad \text{[Equation 3.34]}$$

where:

- $k = 1, \ldots, m$.

Next, transfer function f_4 maps from $h^{(u)}$ to the output column vector x' of length l as given:

$$x_i' = f_4\left[\left(W^{(u)}h^{(u)} + \bar{b}^{(u)}\right)_i\right] \quad \text{[Equation 3.35]}$$

The cost function is given as:

$$J = \left\langle \left\| x - x' \right\|^2 \right\rangle \quad \text{[Equation 3.36]}$$

where:

- x –is the original data;
- x' –is the output of the Neural Network.

The cost function is minimized by finding the optimal values, which necessitates that the mean square error between the neural network (NN) output (x') and the original data (x) is

minimized as well [135]. Hyperbolic tangent function for f_1 and f_3 and identity function for f_2 and f_4 can be shown as follows:

$$u = w^{(x)} \cdot h^{(x)} + \bar{b}^{(x)} \quad \text{[Equation 3.37]}$$

$$x_i^{'} = (W^{(u)} h^{(u)} + \bar{b}^{(u)})_i \quad \text{[Equation 3.38]}$$

Imposing constraint and normalization conditions as $<u>=0$ and $<u^2>=1$, the following is true:

$$\bar{b}^{(x)} = -\left\langle w^{(x)} \cdot h^{(x)} \right\rangle \quad \text{[Equation 3.39]}$$

The number of free parameters becomes $2lm+4m+l$, where m is the number of hidden neurons. $m \geq 2$ condition is required for nonlinear solutions, where a higher number of m improves nonlinear modeling solution. Thus, linear relation $u(t)=a*x(t)$ with a linear combination of x_i is generalized to $u=f(x)$, where f is a nonlinear function. As a result, the output of MLP is identical to the input, while the reduction in data dimension is still achieved in the bottleneck of the network, which provides the desired component scores. A further iteration of the same process is used to input the residual $x-g(u)$ back into the same network to obtain the second NLPCA node and so forth.

In this thesis, it is assumed that behavior of parameters in time series is not understood in advance. Initially, only PCA and wPCA algorithms were used in the preliminary studies. Later, it was realized that the approach had to be adjusted to accommodate complex ranges, minimize computing demands, or address time complexity. Additionally, parameter distributions can potentially significantly deviate from multivariate normal or other standard parametric distributions. Thus, a generic nonlinear PCA algorithm available from the open research is customized to optimize the overall solution to account for nonlinear relationships in the detector and plant data. Sample data is analyzed using feature extraction tools to isolate patterns of interest. New representation is established regarding model learning so that mapping can be done between features and pattern groups. After a pattern is identified, confidence in decisions can be evaluated.

3.6.5. Proposed Modification of NLPCA Algorithms

During early stages of this work, it became evident that one of the challenges of PCA and NLPCA algorithms is the model size. A large number of plant parameters change coincidental in time with detector response. Even after some of the detector behavior has been explained using the logical data models for correlation, there is still a significant number of process variables to be included in the analysis. This situation became particularly prominent during the NLPCA portion of this study, where the required computational effort presented challenges during network training runs. Since the proposed algorithm is suggested for near real-time use, it is desired to reduce computational demands. Therefore, this study proposes to modify the NLPCA algorithm to reduce the model size. The main idea in this proposal is based on the assumption that the process variables in this study are obtained at predefined intervals (e.g., two (2) seconds sampling frequency) and typically do not change significantly between samples unless an unexpected failure of the process occurred. Thus, it is hypothesized that it is possible to apply minimization of the cost function (given in Equation 3.36) to reduce the model size. This will result in a small impact on the network performance in terms of accuracy but may significantly reduce model run times. This approach is described next.

The measurements x used in Equation 3.36 are obtained from the various field devices and systems that measure and acquire process data within the plant. These data are obtained from plant system interfaces synchronized to the utility's time servers, so all plant data has a common time source, which allows easy correlation of events between the various data sources, such as Distributed Control Computers (DCCs). The plant information system reads each data point at a specific frequency. Thus, the original data x can be presented as a series of measurements at time instance of t and can, therefore, be presented as $x(t)$. Rather than including each instantaneous reading of x, the algorithm can be set up to forecast future process readings and only use the exception events (i.e., when the measurements exceed a predefined value). The proposed approach can be shown as a series of steps in the flowchart, as in Figure 3.14:

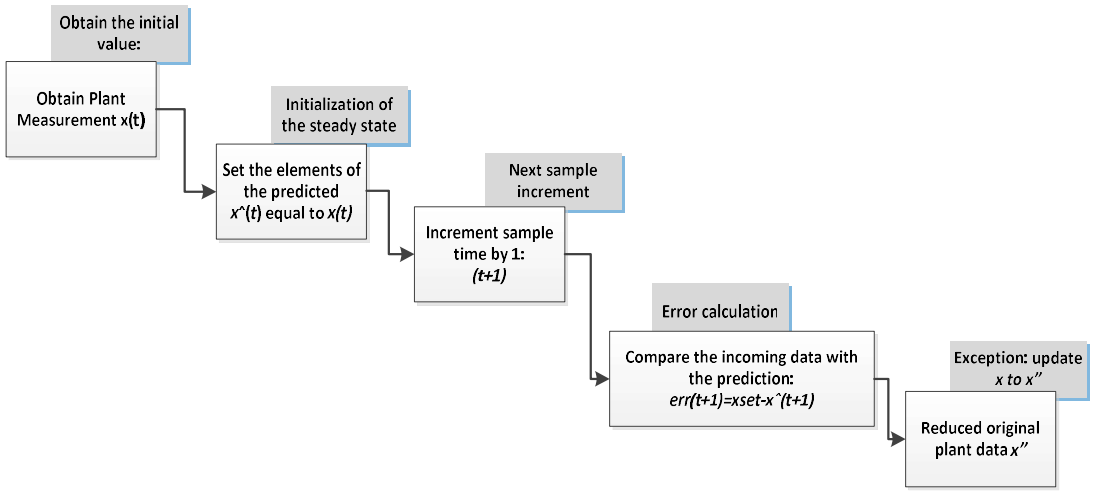

Figure 3.14: A proposed approach to model reduction by minimizing the number of the original data points x.

Each process variable *x(t)* can be shown as a vector of values that should follow a particular predetermined setpoint within the control band. Thus, the number of *x(t)* 's could be reduced such that only significant changes in the instantaneous process variable (PV) readings are used in the model calculation. The error between the predicted and the measured value of the PV can be calculated as:

$$err(t+1) = x_{set} - \hat{x}(t+1) \qquad \text{[Equation 3.40]}$$

where :

- *x(t)* – obtained measurement *x* at time *t*;
- $\hat{x}(t)$ – predicted measurement *x* at time *t*;
- x_{set} – known parameter setpoint;
- err – the difference between the expected and the obtained value;
- t – time.

The error threshold can be established for each PV based on the engineering equations and the desired system performance accuracy, e.g., different weight coefficients could be set up for each process parameter, e.g., weight coefficient w_{xi} set up for process variable x_i. The same approach can be used for the control inputs, e.g., control parameters u_i affecting specific input measurements x_i. Next, the computed error can be added from the first

change of the measurement to the current measurement. This, in effect, will update the vector of the past changes in the PV and correct the prediction, i.e., generate estimates of what system behavior should be when presented with data of current system behavior. The accuracy of the input data will be dependent upon the error threshold that is placed on the point but will effectively reduce the amount of data used to solve the objective function *J* per modified Equation 3.36:

$$J = \left\langle \| x'''' - x' \|^2 \right\rangle \qquad \text{[Equation 3.41]}$$

where:

- x'' - is the reduced plant data;
- x' - is the output of the Neural Network.

Reduced plant data is processed in the NLPCA to solve the modified objective function J, as shown in Figure 3.15.

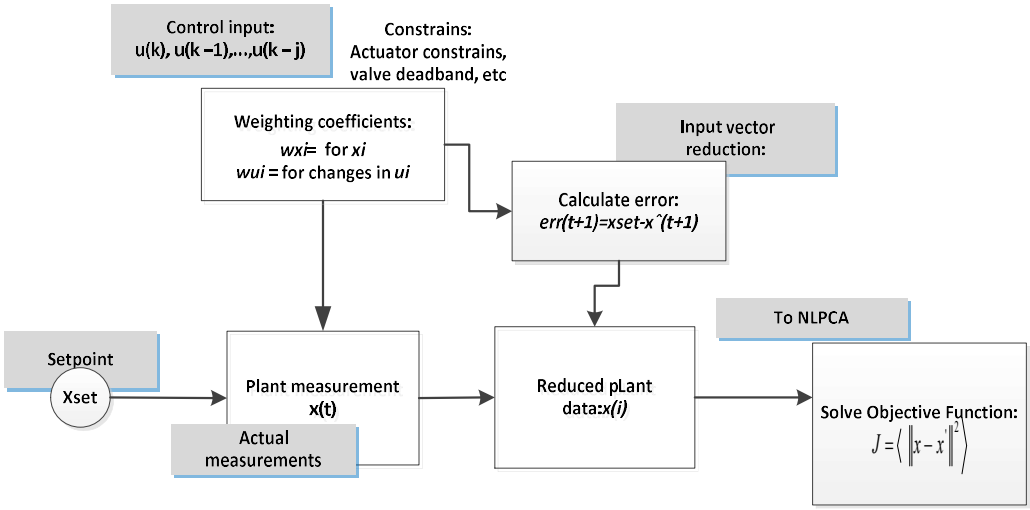

Figure 3.15: Reduced plant data is processed in the NLPCA to reduce the amount of data used to solve the objective function J per Equation 3.41.

This proposal is conceptual and is intended to provide a high-level overview of one of the many possible approaches. It can be further developed in the future work.

3.7. Optimization of the DSC Gain Settings with GA

The focus of the DSC gain setting methodology discussed earlier in Sections 3.4 and 3.5 is on a few selected theoretical cases. Operational constraints, particularly combined with aged conditions, are not considered. Thus, the limiting scenarios may not in fact be bounding, effectively rendering the overall results inconclusive. In this thesis, it is proposed to use an enhanced GA to obtain the optimum set of the *K*-values. As discussed in Section 3.4, the assumptions used in this approach are as follows:

- DSC input is modeled as the output of the amplifier stage,
- The output from the dynamic compensation circuit, which represents the compensated flux detector signal, is fed into the input of the voltage comparator,
- The DSC transfer function has a proportional gain term and two first-order lag terms, each of which has an adjustable gain,
- A typical DSC has three (3) amplifier gains that may be tuned,
- The maximum reduction in MTT for the worst fueling transient needs to be less than 1.0%.

As discussed in Chapter 2, GAs belong to the class of evolutionary algorithms (EA) and are a way of solving problems by mimicking the process of natural selection. The methodology consists of five (5) basic parts: initialization, fitness, selection, generation, and termination. New generations of solutions are iteratively produced and evaluated until a termination condition is reached. For example, if the desired fitness level has been attained and the allocated number of generations reached, a convergence criterion is met, or a computational time limit is passed. The collection of generations is referred to as a genome.

In applied mathematics, a GA is a heuristic technique for solving optimization and search problems. Heuristic methods may be used to reduce the amount of computational effort required to find an acceptable solution to a problem. A solution may not be found, or a solution may not be optimal. Efficiency improvements are realized by implementing stochastic optimization, which involves the use of random probabilities in the iterative search for a solution. Further efficiencies may be gained by applying simplified assumptions or approximations to the fitness test. This may involve the construction of a fitness model and making use of prior knowledge and experience. A surrogate fitness test

is called a fitness approximation and is used in lieu of a fitness test that is otherwise difficult to construct, incomplete, complex, or computationally prohibitive.

The rationale for the selection of the GA method is that a heuristic approach can be useful to reduce the amount of computational effort required to find an acceptable solution to a problem. The following steps illustrate the scenario under consideration:

- Suppose there is a step change in power from zero to 100%FP, and suppose there is no DSC compensation,
- Thus, the reactor regulating system (RRS) will move the reactor power until the detector feedback indicates 100%FP,
- However, since the detector is only seeing 70% of the actual power (i.e., PF = 70%), the actual power is too high initially,
- As the detector delayed components are introduced, the detector power increases and RRS will bring it back to setpoint in small steps until equilibrium, at which point the actual power matches.

This can be represented as a function for the detector response and another function for the DSC. In this case, the DSC function is the objective function, and the detector function is the fitness function. Note that the MATLAB terminology is different: MATLAB calls the objective function the fitness function and fitness function is the constraint function. The DSC must compensate for the detector delayed components, i.e., the DSC gains must be selected so that the DSC function minus the detector function is greater than zero or some small value (e.g., 3% so there is time to get to the detector replacement timeline). To produce a time-dependent DSC curve in the time domain, the inverse Laplace transform is applied to the DSC transfer function.

A similar idea should hold for the detector curve, and then the two functions are entered into the GA solver. However, it is important to point out that there is no guarantee that a solution will be found or that a solution will be optimal. The following steps describe the proposed algorithm:

1) Determine the Objective Function:

   This is the transfer function that represents the physical system under consideration. For the case study in this work, the neutron detector signal is processed by the DSC

according to the following transfer function model. A neutron detector signal processed by a DSC can be shown according to the following transfer function model:

$$H(s) = K_1/s + K_2\left(\frac{1}{1+\tau_2.s}\right) + K_3\left(\frac{1}{1+\tau_3.s}\right) \qquad \text{[Equation 3.42]}$$

where:

- K_1 - is the static gain;
- K_2, K_3 - are dynamic gains;
- τ_2 and τ_3 - are time constants;
- *t*- time variable, greater than zero (the fitness function must be met at all times).

The analytical solution to the above Laplace transform (1) in the time (t) domain is the objective function:

$$F(t) = K_1 + K_2\left(\frac{1}{\tau_2 * \exp\left(\frac{t}{\tau_2}\right)}\right) + K_3\left(\frac{1}{\tau_3 * \exp\left(\frac{t}{\tau_3}\right)}\right) \qquad \text{[Equation 3.43]}$$

2) Determine the parameters to be optimized from the Objective Function:

This is typically the circuit gains but may also include the time constants. The set of optimized parameters represents the solution, and in this study are the three (3) DSC gains (K_1, K_2, and K_3). Thus, the solutions set to the objective function consists of three (3) DSC gain values (K_1, K_2, and K_3).

.

3) Determine the Constraint Function(s):

Constraint functions are additional linear or nonlinear requirements that must be met by the solution. For example, it is desirable that the DSC not apply an overall bias to the flux detector signal, accomplished by the constraint ($K_1 + K_2 + K_3$) = 1.

4) Assumptions:

Solutions are not restricted by potential amplifier design specifications. Currently, the circuit board design limits the ability of the GAIN potentiometer value that can be

selected. Subsequently, the gain cannot be increased to more than the maximum allowable values discussed earlier.

5) Determine the Boundary Conditions:

Boundary conditions may be imposed to help ensure the solution is feasible. In this study, the following conditions were applied:

i) $1.00 \leq K_1 \leq 1.20$; to ensure the DSC can compensate for the prompt fraction.

ii) $-0.20 \leq K_2, K_3 \leq 0$; to ensure the DSC can compensate for the delayed components.

Boundary conditions may be tightened during subsequent GA runs based on past solution results. Boundary conditions may also be used to ensure the solution will meet DSC hardware limitations; this was not applied in this study.

6) Select a Fitness Function:

The Fitness Function is used to determine the relative quality of potential solutions in each generation. In terms of instrumentation and control, a Fitness Function is often called a Performance Function. The goal of the GA approach is to minimize the Performance Function. The following are some Performance Functions that are often cited in relation to optimizing control system parameters:

i) Integral Squared Error (ISE)

$$I_{ISE=} \int_0^\infty e^2(t)dt \qquad \text{[Equation 3.44]}$$

Here, the square of the error over time is integrated by ISE. ISE will penalize large errors more than smaller ones (since the error is squared). Control systems optimized to ISE will tend to eliminate large errors quickly but will tolerate small persistent errors for a long period of time. Often this leads to fast responses but with considerable low-amplitude oscillation.

ii) Integral Absolute Error (IAE)

$$I_{IAE=} \int_0^\infty |e(t)|dt \qquad \text{[Equation 3.45]}$$

IAE integrates the absolute error over time. It doesn't weigh any of the errors in a system's response. Therefore, it tends to produce slower responses than ISE optimal systems but usually with less sustained oscillation.

iii) Integral Time Absolute Error (ITAE)

$$I_{ITAE=} \int_0^\infty \mathrm{t}|e(t)|dt \qquad \text{[Equation 3.46]}$$

ITAE integrates the absolute error over time. What this does is more heavily weigh errors that exist after a long time than those at the start of the response. ITAE tuning produces systems that settle more quickly than other methods.

iv) Integral Time Squared Error (ITSE)

$$I_{ITSE=} \int_0^\infty \mathrm{t}e^2(t)dt \qquad \text{[Equation 3.47]}$$

v) Mean Square Error (MSE)

$$MSE = \frac{1}{n}\sum_{i=1}^{n} e_i^2(t) \qquad \text{[Equation 3.48]}$$

vi) Weighted Root Mean Square (wRMS)

$$\mathrm{wRMS} = \sum_{\mathrm{i=1}}^{\mathrm{n}} (\mathrm{E_i^{calc}(w)\text{-}E_i^{exp}})^2 \qquad \text{[Equation 3. 49]}$$

vii) Zeigler-Nichols (Z-N) [137]

The Zeigler-Nichols technique is a practical process for the tuning of PID controllers, based on trial and error. The technique is based on sustained oscillations. Z-N is also known as online (or sometimes called continuous cycling) tuning. The design criterion for this method is one-fourth decay ratio. The Z-N method may result in a process with marginal stability.

viii) Settling Time

This is the time taken for a response to settle within some band around the setpoint. This time can be defined for the setpoint and the disturbance changes. Shorter settling times are best, although they can lead to long rise times and generally sluggish response.

The performance function used in this study is ITAE. To facilitate its computation in MATLAB, the function was discretized using the multiple application version of Simpson's 1/3 Rule.

7) Determine the Reference Function:

The reference function represents the desired system response. It may be theoretical (e.g., step disturbance) or derived from design specifications and safety requirements. In this study, the reference function was chosen as the system response with a 2% improvement of the PF safety limit, equivalent to operating with the DSC at its design limit. This function was chosen to determine if the GA solution can optimize the design values.

8) Create a Simulink model of the system:

This is achieved by using a transfer function representation of the DSC to visualize the gain parameters.

9) Code the objective and constraint functions:

The GA solver, options, and bounds form the main script, which calls the objective function to run the Simulink model. The performance function is then evaluated and the result returned to the GA solver. Depending on the complexity of the problem and computing resources, execution time may be considerable. Nonlinear constraints significantly increase runtimes. The GA solver has a parallel computing option to improve runtimes if desired.

3.8. Risk Estimation with FSN

Detection of faults depends on the nature of what is causing them, e.g., calibration drifts are detected by monitoring equipment while degradation of the detector itself is identified during PF testing. Faults can be caused by a variety of reasons starting with design deficiencies, ingress of moisture and corrosion due to assembly structure failure, or inadequate or incorrect maintenance strategy. A sample fault-to-accident propagation scenario is shown in Figure 3.16 for the neutron detector system. Ingress of moisture into the detector assembly may occur due to a manufacturing defect, incorrect handling/storage, or maintenance. Resultant corrosion will, in turn, lead to faults where regional neutron power signals provide misleading readings. Faulty performance can result in reduction or loss of trip coverage, which, in turn, can lead to overpowering of fuel in that particular zone. Once the fuel sheath fails, the resultant release of gaseous fission products into the primary heat transport system (PHT) leads to hazardous conditions at the plant. If overheating is not mitigated, it may further propagate into fuel failure, failure of PHT and calandria tubes, and a complete disintegration of the reactor core.

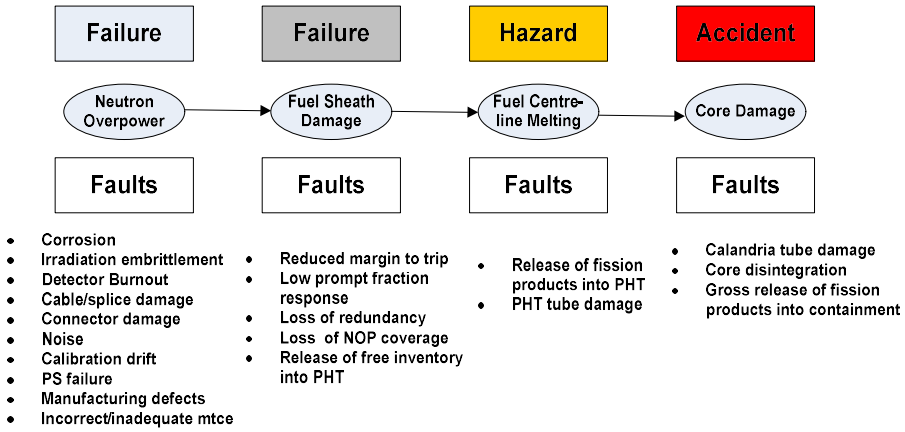

Figure 3.16: Example of Fault, Failure, Hazard and Accident Model for a Neutron Detection System Failure.

As demonstrated in Figure 3.16, faults in the system (e.g. detector failure due to corrosion) result in failure to trip, leading to fuel sheath damage, fuel centerline melting and core destruction. Table 3.7 below shows classification of faults and groups/systems for the

selected case study at different times from the design concept stage to operation and maintenance.

Table 3.8: A data acquisition cycle for faults, starting from design stage through to ongoing operation and maintenance.

	Fault	**Failure**	**Hazard**	**Accident**
Design	Y	Y	Y	N
Manufacturing	Y	Y	N	N
Procurement	Y	Y	N	N
Storage	Y	Y	N	N
Installation	Y	Y	Y	N
Operation	Y	Y	Y	Y
Maintenance	Y	Y	Y	Y

An FSN approach is proposed in this thesis for estimation of risk due to degraded detector performance (e.g., noise and signal oscillations) and to aid in risk-informed decisions for detector maintenance and replacements. In general, a semantic network is a structure where nodes show states, and lines between nodes show transitions between the states. In that sense, an FSN is a method of representing fault knowledge based on relationships between objects, where nodes represent various faults, causes, and consequences. Their interconnections are shown by links to show relations between concepts. Using network diagrams to represent the connections and process flows of the system makes it easier to understand the relationships between various events, especially in a larger system where the impact of activities may not be explicit. In these cases, system modeling based on FSN may be useful to narrow down the problem areas for analysis or to break a large system into smaller components and analyze the linkages between them. This approach is also helpful in identification of the correct process variables for analysis. For example, it can assist in identifying the manipulated process variables (PVs) versus the control PVs.

The ontology structure of the system represents how various components of the system interact to produce a particular outcome, e.g., how various failure modes impact the system performance. Every piece and class of equipment may have more than one potential fault associated with it, each due to different hazards. Each unmitigated fault may lead to more than one accident scenario. The main objective of the FSN methodology is to construct these fault propagation scenarios qualitatively and to use them in risk estimation in different design and operation activities.

First, a selected set of equipment classes is identified along with their parent class, e.g., "detectors" and "sensors." Each class has its associated identifier (ID) and description. Equipment class is related to function, component, and process variables. Failure and faults are represented at a generic and equipment level, and failure mode identification (FM-ID) is used to describe both faults and failures. Every modern power plant will have some built-in protection or control barriers, whether passive or active, to provide a defense against known failures. To increase effectiveness, protections barriers are typically implemented with built-in redundancy. These barriers could be used for prevention, detection, or mitigation purposes and could comprise engineering, administrative, or operational activities. Resulting hazards and accidents are modeled in header and details entities and are linked with "lessons learned" and protection barriers (or controls) available at each step in the causation mode, as shown in Figure 3.17:

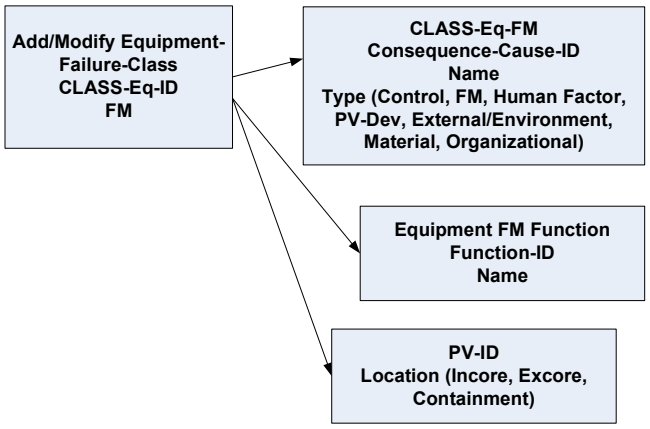

Figure 3.17: Data Acquisition Process Framework.

The ontology structure of fault models needs to be constructed such that each failure mode (FM) is described using symptoms, enablers, process variables, causes, and consequences, shown in Figure 3.18:

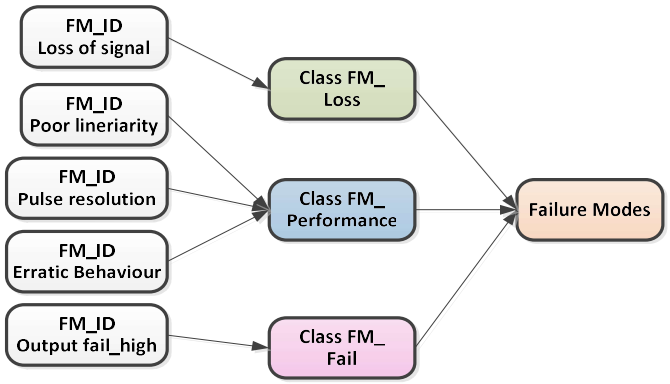

Figure 3.18: Grouping of Failure Modes into Failure Mode Classes.

This approach accounts for the fact that failure modes of the same system may, in conjunction with failures of other systems, lead to significantly different consequences, as seen in Figure 3.19.

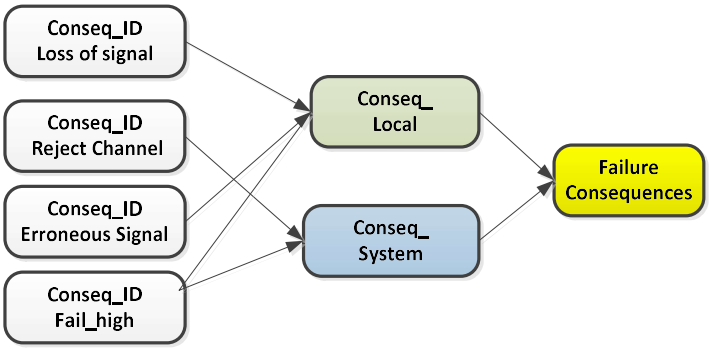

Figure 3.19: Failure consequences are assigned to a failure consequences class based on whether they affect the system on a local level.

A basic causation model of a sample accident progression and control barriers can be developed next, as in Figure 3.20:

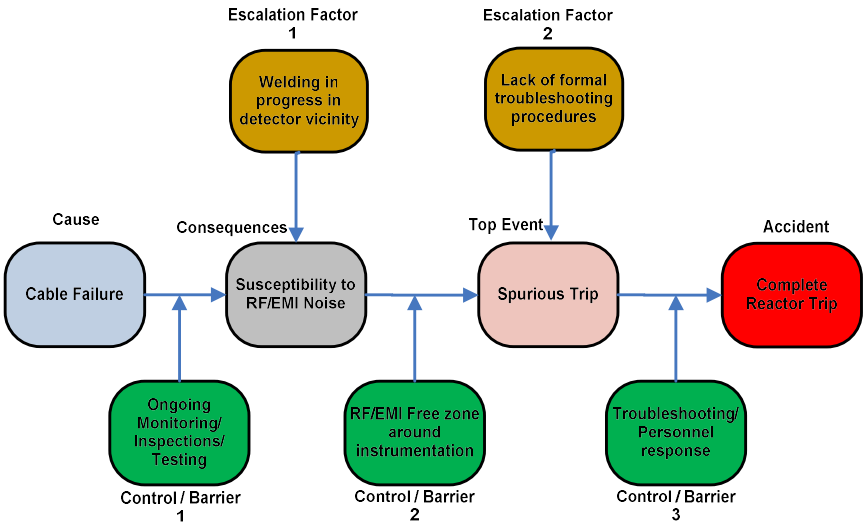

Figure 3.20: Causation model for a sample accident progression in a detector system.

In this causation model, cable failure was selected to be the initiating event or the primary cause. This failure resulted in the increased susceptibility of the system to radio frequency (RF), EMI, and other noise sources. In the absence of escalating factors such as welding or other maintenance in the vicinity of the instrumentation, this event can be mitigated by regular monitoring and inspections. Negative trends in the system response would be caught early, and progression of further accident steps could be prevented.

However, should barrier 1 fail, the system will continue to be affected by high noise levels. This accident progression could be stopped by barrier 2—implementation of an RF/EMI-free zone around the detector instrumentation. If this barrier fails as well and the event resulted in a spurious trip of the system, barrier 3 is activated. Effective, timely troubleshooting could identify the cause of system malfunction and initiate the required repairs. On the other hand, lack of troubleshooting procedures, the inexperience of personnel, fatigue, confusing fast-changing information, and other adverse conditions (escalation factor 2) may lead to failure of this barrier. When barrier 3 fails, the accident will complete its progression, resulting in a reactor trip.

The effectiveness of control barriers can be determined by applying semi-quantitative measures to the evaluation of the frequency of potential incidents and the probability of failure. Based on the nature of the hazard, the barrier analysis can be used to lower the consequence and frequency of possible incidents to a tolerable risk level. The

risk can be established based on the probability of occurrence and consequences, both to plant equipment and life. Next, the probability of failure on demand can be calculated as:

$$PFD_{avg} = \frac{F_t}{F_{np}} \qquad \text{[Equation 3.50]}$$

where:

- F_t - is tolerable frequency;
- F_{np} - is Process Demand frequency

Next, consequences can be assessed based on the projected damage to plant equipment, human life and health, ecological and environmental impacts, losses to reputation, or financial losses. These can be done both qualitatively and quantitatively. Once the matrix of consequences and their weights is established, the acceptable risk level can be estimated using the proposed risk acceptance line, as shown below in Figure 3.21.

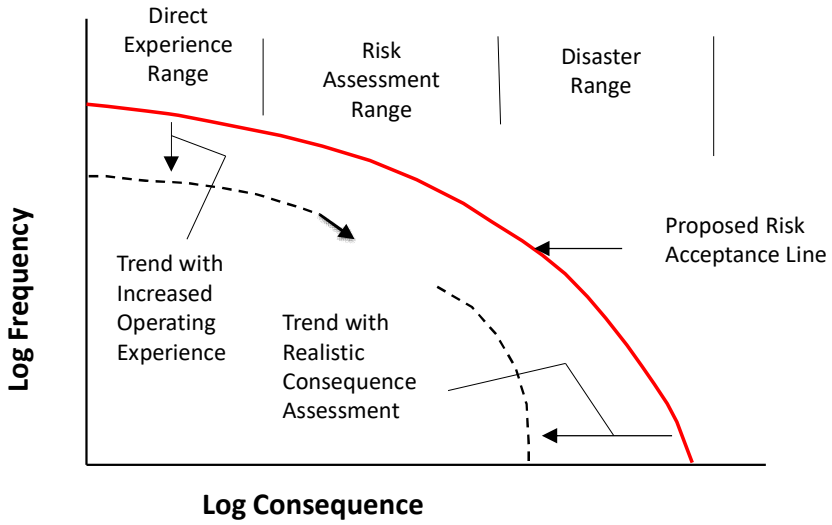

Figure 3.21: Projected risk is calculated as a product of the probability of occurrence, i.e. frequency, and consequences, adapted from [138].

This approach is similar to layers of protection analysis (LOPA) method in [138], where the adequacy of protection layers is assessed applying semi-quantitative measures. The

frequency of potential incidents and the probability of failure of the protection layers are evaluated based on [138, 139], a detailed description of the hazard scenario. This approach allows one to quantify the expected risk with a known specific amount. Each barrier is considered independent of all others, and the effect of a failure of a particular barrier is not considered. Thus, each control barrier must address all hazard and accident scenarios it is designed for without affecting the integrity of the next one. For example, as shown in Figure 3.21, if the absolute risk is greater than the risk acceptance line, additional control barriers are required. If an existing barrier does not provide enough protection against the projected risk, further mitigating actions or measurements are needed. Thus, the protection layer analysis can be used to drive the consequence and/or frequency of potential incidents to a tolerable risk level.

Rules are associated with each transition of the causation model within FSN, as shown in Figure 3.22. The rules can be defined either quantitatively (probabilistic) or qualitatively. If at least one characteristic or parameter of the system deviates from the acceptable condition, a fault is identified. For example, failures related to corrosion might be associated with rules such as:

IF (Structure.Material = (X or Y))
and (PV= Gas.Pressure)
and (Dev = Very-Low)
THEN (FM = failure.detector*)*

Formal language is proposed to represent process domain knowledge and safety control rules, as explained in [124, 125], to facilitate synthesis and validation of fault models within FSN. These rules are initially defined in a generic form based on domain knowledge, i.e., regardless of plant-specific knowledge, and are then further explained. A sample FSN is shown next for three (3) initiating causes as demonstrated in Figure 3.22.

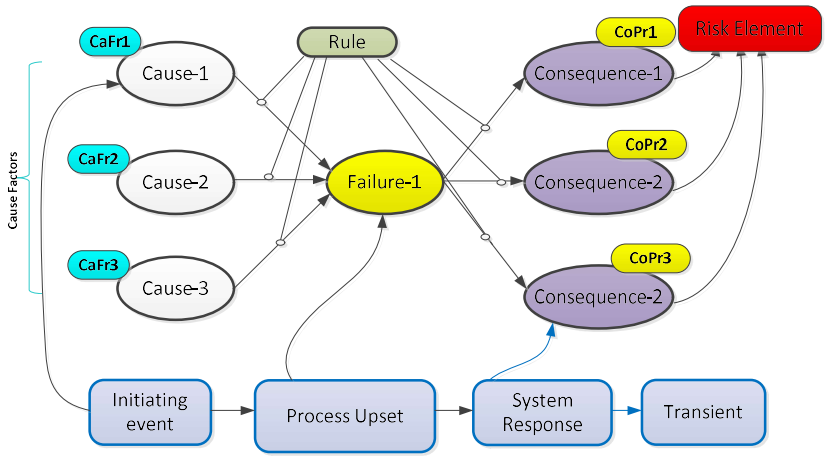

Figure 3.22: A sample FSN is shown for a case of three (3) initiating causes.

The proposed FSN consists of two layers for static (offline) and dynamic (online) modes. Real-time data are gathered for the selected case study and analyzed in MATLAB. The model shown in Figure 3.23 is developed within MS Visio to capture and structure process design models for process block diagrams (PBD), process flow diagrams (PFD), and piping and instrumentation diagram (P&ID), based on ISA-S95/88.

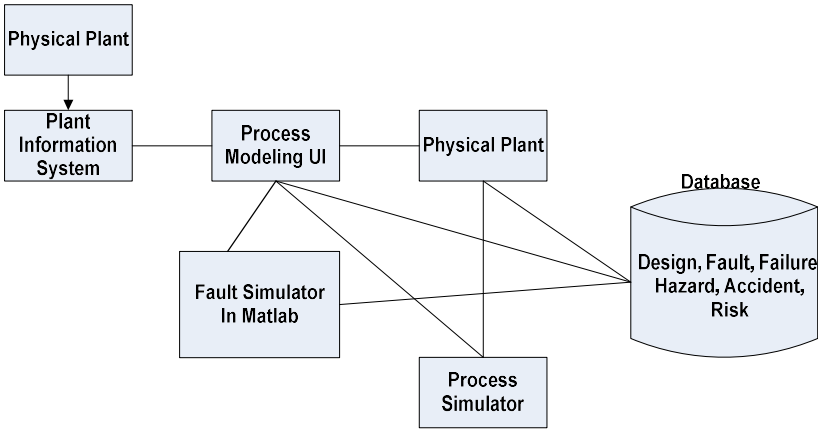

Figure 3.23: Proposed System Architecture for Failure, Fault, Hazard, and Accident Data Acquisition.

Static FSN:

Static FSN includes historical faults, failures, hazards, and accidents structured and linked in the form of causation models associated with process equipment. Implementation of fault modeling in static FSN starts with a collection of historical data, either from a real

process or simulation and observations for each process variable (PV) that is passed to the FSN. Using this historical data, the FSN interprets the results and calculates the probability of failures and the risks associated with each based on the predefined rules. This principle is schematically shown next in Figure 3.24:

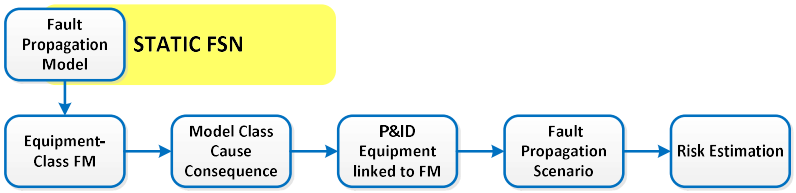

Figure 3.24: Fault modeling with static FSN.

Dynamic FSN:

A dynamic FSN, shown in Figure 3.25, is constructed using dynamic simulated or real-time data that can be obtained from operation, maintenance, safety, and control. After the knowledge base has been sufficiently expanded and the accuracy of the forecasting based on the historical data reaches a certain level, the system can be used for real-time forecasting fault propagation scenarios based on the real-time data.

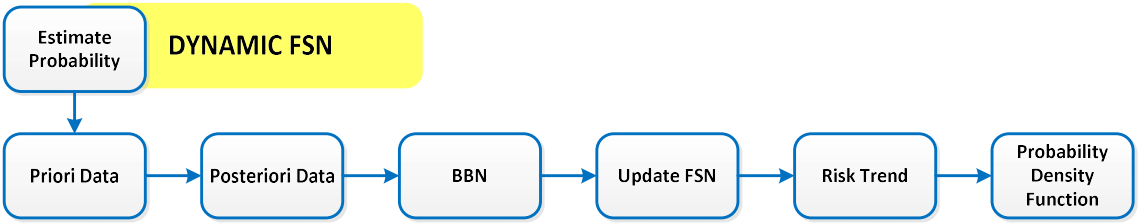

Figure 3.25: Dynamic FSN with risk estimation process.

New information can be sent to the FSN knowledge database and is used to futher train the network to optimize its performance and accuracy of results. It is possible to predict the consequences for the posteriori or predicted data for the future faults. Probabilistic methods, such as the Bayesian belief network (BBN), are proposed to account for potentially incomplete or missing data.

When considering any dynamic activity, it is reasonable to assume that the safety status of the whole system is always changing. Parameters of the current control barriers can be stored in the database to be taken into account when calculating the risk factor. For each fault propagation scenario, a link to control barriers/mitigating actions can be established, as shown below in Figure 3.26.

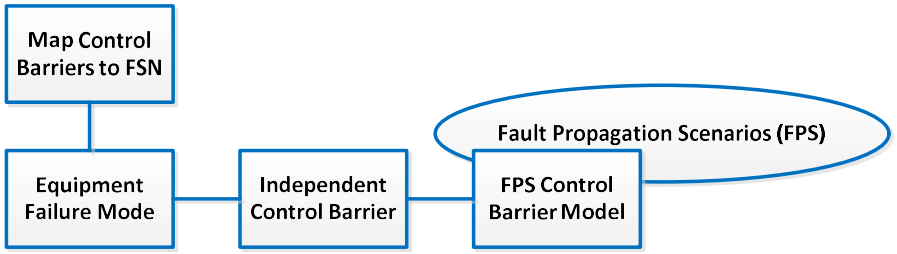

Figure 3.26: Mapping of the Control Barriers (mitigating actions) to FSN.

Estimation of risk to continuous operation of degraded detectors will be based on FSN methods. In the example shown below, there are three (3) possible risks associated with consequence-1, namely:

[a] cause-1, failure-1, consequence-1;
[b] cause-2, failure-1, consequence-1;
[c] cause-3, failure-1, consequence-1.

For independent events, total risk associated with consequence-1 is shown as:

$$R\ (Consequence\text{-}1) = [(CaFr1 + CaFr2 + CaFr3) * FPr1 * CoPr1] * CoIm1$$

[Equation 3.51]

where:

- Causal factor *CaFr1* is used to define the frequency of cause-1;
- Probability of failure *FPr1* is the probability that failure-1 will occur due to any cause;
- Probability of consequence *CoPr1* is the probability that consequence-1 will occur due to any cause and failure;
- *CoIm1* is the total impact of consequence-1.

The total risk of consequence-2 and consequence-3 can be computed in a similar way. For the case when events are codependent, the Bayesian theorem can be applied to determine the total risk based on dependencies for cause-1, cause-2, and cause-3.

$$P(X|A) = \frac{P(A|X)P(X)}{P(A)} \qquad \text{[Equation 3.52]}$$

The process of diagnosis for detector performance starts when the detector readings are obtained. These readings are synthesized with the prior (unconditional probability) of each root node, together with conditional probability distributions of each child node. The prior of each root node can be determined from the performance of the equipment (e.g., tendency to fault) or simply from historical data. The conditional probability distribution (the detector reading node) is built according to a noise distribution equation. The intermediate node (process node) is a function node, meaning that it is a function of its parent nodes only and completely determined by its parents. The joint distribution among the remaining six random variables can be established for:

- sensor bias;
- process input;
- process gain;
- noise variance;
- noise;
- sensor reading.

The Bayesian-based approach can be used for both the static and dynamic environments [136]. Also, the model of the static or dynamic system can be trained from examples if the model is not available in the analytical form [136]. Unlike neural network-based controllers, Bayesian algorithms could be used to train systems even in cases when some information is missing [136]. Through Bayes theorem, probabilistic inferences can be made, e.g., when, for a given time instance, there are two readings available.

Using this approach, detector response data can be collected daily and analyzed for risk factor trends using the event probability calculations shown below:
Dormant failure probability prior to mission (or an undetected failure):

$$P = \frac{\lambda_d}{1000}\left[\frac{T_i}{730} + \frac{T_a + T_r}{8760}\right] + \frac{T_t}{24T_i} \qquad \text{[Equation 3.53]}$$

Running failure probability prior to mission (or detected failure):

$$P = \lambda_r\left[\frac{T_a + T_r}{(8.76 * 10^6) + \lambda_r (T_a + T_r)}\right] \qquad \text{[Equation 3.54]}$$

Running failure probability during mission:

$$P = 1 - \exp\left[-\frac{\lambda_r * T_m}{8.76 * 10^6}\right] \qquad \text{[Equation 3.55]}$$

Probability of occurrence of event-oriented failure data or scheduled maintenance:

$$P = \frac{\lambda_d}{1000}\left[\frac{T_i}{730} + \frac{T_a + T_r}{8760}\right] + \frac{T_t}{24T_i} \qquad \text{[Equation 3.56]}$$

where:

- λ_d – dormant failure rate, failures per one thousand years;
- λ_r – running failure rate, failures per one thousand years;
- f_m – frequency of occurrence, occurrences per year;
- T_m – mission time in hours;
- T_r – mean time to repair, hours per failure;
- T_t – test duration where the component is unavailable during test, in hours;
- T_e – average duration of the event, in hours per occurrence;
- T_a – administration time in hours per failure;
- T_i – test interval in days;
- P – probability or unavailability, 0=P=1;
- $(T_a + T_r)$ – restoration time.

The values of λ_d, λ_r, and T_r are obtained from historical records of component failure data. The values of T_i and T_t are obtained from station testing practices, and those of f_m, T_e, and T_a are obtained from station maintenance practices. In some cases, the values of λ_d are not available; therefore, the λ_r value is used. Since λ_r is usually greater than λ_d this practice

tends to conservatively over-predict failure probabilities. Also, in some cases, T_a is much larger than T_r, which may then be ignored.

The mission time of a system is the time over which the system is required to function after the initiating event. One of the main factors that affects the mission time is the accessibility of the component in question of repair. For example, a neutron detector cable may not be accessible for a substantial period if there are high radiation fields in its vicinity. In this study, the mission time was selected to be seventy-two hours, which is a conservative value since this allows enough time to take the appropriate mitigating action to alter the course of an accident sequence.

A component/system failure rate and test interval can be assigned to the failure event to derive a failure-on-demand probability.

The front-end graphical user interface for the data collection can be set up using the existing application or tools already in use at the station, e.g., MS Excel. This operation mapping solution provides system designers, engineers, and operators with a single view of all detectors in a specific unit. All the station detectors are identified and connected to a plant information server for near real-time data collection. Next, the specific detectors of interest can be selected for analysis in any unit. While the detector data is being retrieved and saved, detector performance can be trended against the predefined parameters, e.g., the 3 and 5% MTT bounds.

Historical and real-time information about detector performance is then collected and compiled in the FSN knowledge base for analysis of the risk profile and the need for appropriate mitigating barriers and their magnitude.

3.8.1. FSN versus the PRA Approach

Once the system fault is detected, to determine whether it is acceptable to operate the plant in that particular configuration, a risk-based decision needs to be made by utility operators. If the potential consequences of an event are unacceptable, regardless of the improbability of occurrence, the risk should not be tolerated, and compensatory actions commensurate with the safety impact should be implemented.

However, assessing the nuclear safety risk of operating in a specific plant configuration expected to be in place for a limited period of time is typically not within the

scope of the existing station's probabilistic risk assessment (PRA) procedures and tools. As briefly discussed in Chapter 2's "Literature Review, critical limitation of the current PRA methods is due to the assumption that the probabilities of all failure modes of a particular component remain the same. The fault data collection is conducted throughout the current year and is used to update failure frequency tables on an annual basis. The applicable models (unavailability/risk) are evaluated after the failure rate update. The model is then rerun with the newly discovered knowledge, and the system unavailability analysis can be conducted.

Additionally, the accuracy of methods based on pure process history data is greatly affected by noisy or missing data and do not present a sound alternative on their own. Traditional model-based techniques use a mathematical model of the process and process measurement data to detect process faults or failures by comparison to a predefined threshold. The main limitation of this approach is the presence of false or nuisance alarms if the threshold is set up incorrectly in relation to the current state of the system, e.g., due to aging effects. On the other hand, qualitative model-based techniques are based on the causal relationship between the process variables and are not concerned with the actual values. This limitation does not provide a sound basis for risk-informed decision making, which is a critical feature in NPPs due to the nature of the industry and the possibility of catastrophic outcomes of wrong decisions.

PRA methods based on the FTA/ETA approach model propagation of accident sequences following initiating events and are commonly used for assessing probability, progression, and consequences of equipment failures at NPPs but are mostly static, i.e., it does not undergo frequent changes and updates. The proposed approach based on FSN methodology has a great advantage in the fact that the plant data can be continuously collected, expanded, and transferred as needed. It is possible that additional initiating events may be identified during operating experience review or as new research and knowledge becomes available. Parent-child relational structures of an FSN allow for ease of knowledge transfer and result in great savings in terms of time and resources required for knowledge-based maintenance. Fault probabilities calculated by an FSN can be dynamically updated as new knowledge becomes available and even in cases of missing or incomplete data. For example, a comparison of system unavailability statistics based on

the assumed component failure rates and actual component failure rates based on operating experience is critical for risk-informed and cost-effective safety-driven decisions. However, if due to a specific system configuration, a safety system is required to be placed in an unusual state for a short duration, risk evaluation can still be performed without waiting for the annual PRA model updates by using the instantaneous risk estimated from the FSN. FSN-based methodology can be used to incorporate the plant-specific observed failures with generic failure rates to determine the immediate instantaneous risk and compare it with the existing margin.

Using the proposed FSN approach, all collected data is initially stored in the database, where data is classified according to the rules described earlier, e.g., equipment data, class data, etc. All previous maintenance data, historical failure data, and expert knowledge are considered as well since they contain a valuable list of symptoms, diagnosis modules, remedies, and associated rules. A system performance assessment model in an FSN can be shown as a BBN directed graph together with a set of probability tables, as shown in Figure 3.27.

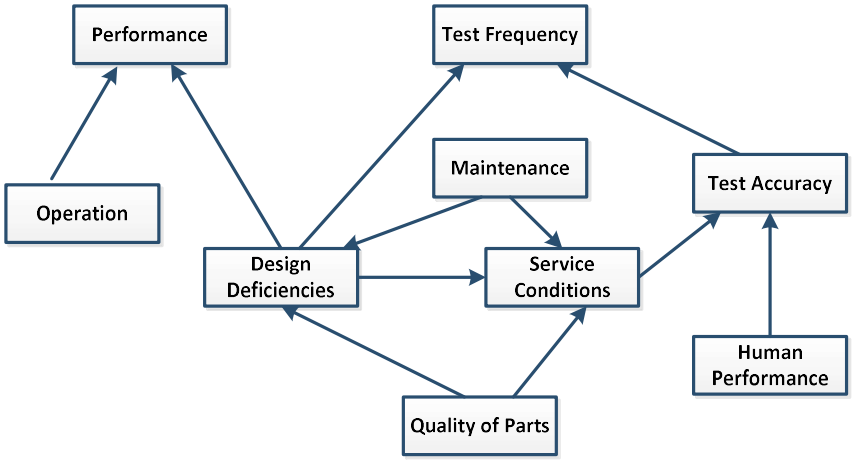

Figure 3.27: Performance Assessment Model using a BBN Directed Graph.

The graph consists of nodes and arcs, where the nodes represent variables, e.g., *test frequency*. In this case, it is discrete with values such as 0, 1, 2… The node "performance" is continuous, such as the probability of failure on demand. The directed arrows, or arcs, represent causal relationships between variables. For example, the number of faults in *test*

accuracy is influenced by the *human performance*, i.e., skill and experience of the test personnel, and the *service conditions* of the detectors. The node probability table (NPT) captures the conditional probabilities of a node given the state of its parent nodes. The incoming new information can then be sent to the FSN knowledge database and is used to further train the network to optimize its performance and accuracy of results, as illustrated in Figure 3.28.

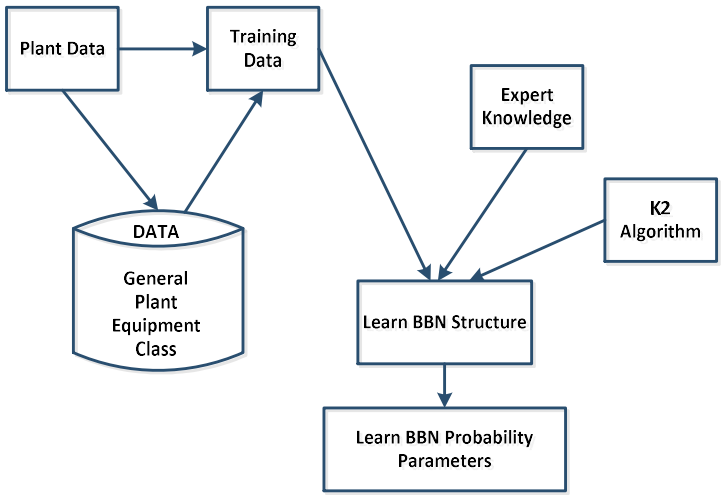

Figure 3.28: The process of learning BBN structure and probability parameters.

Probability parameters of BBN are conditional distributions relating random variables and their parents. Inference is the process of computing the probabilities of each variable based on evidence that has been specified, in this case based on observations of plant data. The inference process extends the knowledge base automatically and updates the network probabilities according to the evidence entered, as shown in Figure 3.29.

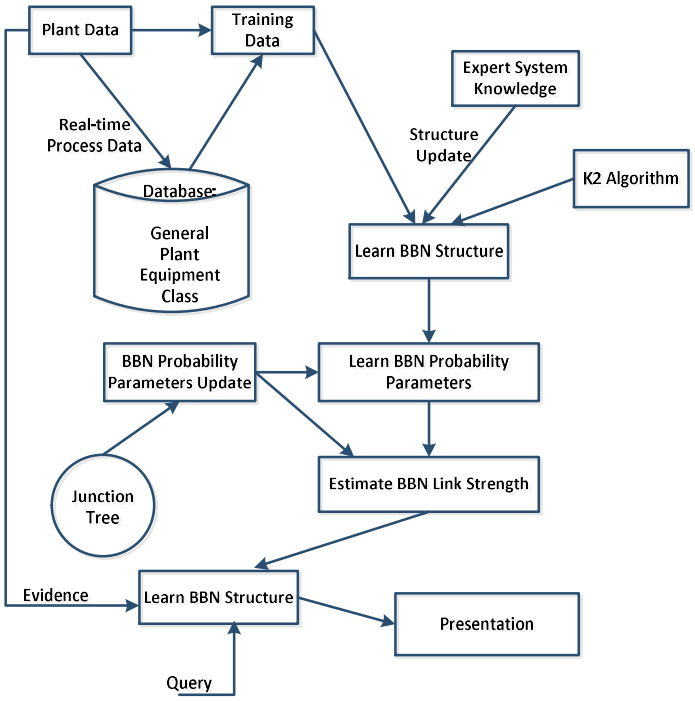

Figure 3.29: New data is dynamically incorporated into the BBN.

The failure rate trend analysis can be performed using the following meta-algorithm:

1. Identify the starting point for the failure rate trend analysis,
2. Identify the moving intervals for the trend analysis,
3. Extract data for the first interval,
4. Calculate the failure rate,
5. If the failure rates exhibit successive increasing value for each of the intervals, then the test identifies an increasing trend for the group failure mode, e.g.:

IF(L2>K2, IF(K2>J2, IF(J2>I2,"TRUE","FALSE"),"FALSE"))

where:

- I2 - is the failure rate in the first interval;
- J2 - is the failure rate in the second interval;
- K2 - is the failure rate in the third interval;
- L2 - is the failure rate in the fourth interval;
- TRUE - identifies an increasing trend;

- FALSE - identifies no increasing trend.

6. If the failure rates exhibit successive decreasing value for each of the intervals, then the test identifies a decreasing trend for the Group Failure Mode:

IF(I2>J2,IF(J2>K2,IF(K2>L2,"TRUE","FALSE"),"FALSE"))

where:

- I2 - is the failure rate in the first interval;
- J2 - is the failure rate in the second interval;
- K2 - is the failure rate in the third interval;
- L2 - the failure rate in the fourth interval;
- TRUE - identifies a decreasing trend;
- FALSE - identifies no decreasing trend.

7. If neither an increasing nor a decreasing trend is observed, then the failure rates exhibit no trend.
8. Calculate the component failure rate, RATE_NEW,
9. Compare the RATE_NEW against the fifth percentile and ninety-fifth percentile: If the RATE_NEW value is greater than the ninety-fifth percentile, then the failure rate is considered a statistically significant increase. If the RATE_NEW value is less that the fifth percentile, then the failure rate is considered a statistically significant decrease. If the RATE_NEW value is within the fifth and ninety-fifth percentile, then no statistically significant change in failure rate has been observed.
10. When a statistically significant increase in failure rate is observed, follow up with a calculation of the available margin and comparison to the limiting criterion.

In a risk assessment process, determination of the available margin and the need for immediate compensatory actions is a fundamental requirement. The available margin can be calculated as the difference between the applicable safety goal and the risk baseline frequency:

Margin = Safety Goal Limit – Baseline Frequency [Equation 3.57]

The risk of core-damage is expressed as a baseline frequency, which is normalized by dividing by a zero-maintenance state. The baseline is only subtracted if the baseline model is used in the calculation of risk that would occur if there are interdependencies between the new components and the baseline model.

If there are no interdependencies, then the calculation can be completed in isolation from the baseline model. In this case, the calculation is the risk increment (RI) above the baseline model. The RI can be shown as the increase in the baseline risk as the result of a risk activity. This can be shown as a difference between the instantaneous risk (IR) and the baseline risk (BR).

$$RI = IR - BR*\Delta T \qquad \text{[Equation 3.58]}$$

where:

- ΔT – duration of risk state.

Typically, the duration of risk state is calculated in hours; thus, the RI can be expressed as:

$$RI = IR - BR*\Delta T/8760hr \qquad \text{[Equation 3.59]}$$

Next, the need and the extent of the compensatory actions can be determined. For example, the magnitude of the acceptable RI can be limited to no more than 10% of the available margin, and the total risk due to all maintenance activities in the system can be limited to 25% of the available margin.

3.9. Summary

In this chapter, a methodology for new detector model development and set-up in Simulink is given. The models are created to represent behavior of aged in-core flux detectors while accurately modeling plant transient response during normal fueling operations and power ramp-up. The models are customized for three (3) typical transient cases where detector noise and signal oscillations are accounted for.

Additional methodology on denoising of plant data is discussed using LPF and WTA to minimize the noise impact on the plant transient scenarios. Methods for

dimensionality reduction and pattern recognition to work with both linear and nonlinear data were explored as well, particularly as they pertain to the detector signal oscillation phenomenon. These aspects are not the primary focus of this thesis but are considered important enhancements.

A GA is proposed as a heuristic technique for solving optimization and search problem for the optimal set of the DSC gain constants. It is expected that this heuristic approach can be useful to reduce the amount of computational effort required to find an acceptable solution to a problem while still satisfying the main performance criteria of ≤1% of impact to the MTT.

To assess whether the risk to continuous operation due to this detector degradation is acceptable, this study proposes using FSN methods as the means to justify the proposed life extension. The main advantage of the FSN methodology is that it provides a qualitative-quantitative approach to fault identification and is both model-based as well as process-history based. Thus, in addition to reliance on personnel judgment and subjective opinions, this method provides a qualitative model where the causal relationship between the process variables is established and mapped using associations between PVs and information about hazards, faults, and failures from previous historical accidents.

Chapter 4: Case Studies

This chapter describes the selected case studies to demonstrate various aspects of detector aging where the proposed research methods will be applied. The main purpose of this chapter is to demonstrate how the proposed methodology can be used to provide a range of tools that may be drawn from to facilitate detector life extension. There are three (3) main cases examined: noise reduction, detector signal oscillations, and detector dynamic response degradation, as shown in Table 4.1. Each study is presented in the format of an operational challenge and proposed solution.

Table 4.1: Case studies summary table.

Case Study	Challenge	Impact	Proposed Methodology
1	Noise Reduction	Potential complications due to detector noise, particularly during fueling operations.	LPF and WTA
2	Detector Signal Oscillations	Potential complications due to detector signal oscillations	PCA, wPCA, and NLPCA
3	Decrease in Detector Dynamic Response (PF)	The detector response, including PF and delayed components, is understood for nominal detectors but is less known for aged detectors.	Develop aged detector models for typical plant transients (MATLAB/Simulink) and optimize PF values with GA

4.1. Case Study One: Operational Challenges and Proposed Solutions for Noise Reduction

4.1.1. Operational Challenge—Increasing Noise Factor

The existing PF management methodology does not account for potential complications due to detector noise, particularly during fueling operations. However, basic noise analysis techniques, such as plotting detector response versus time, show that the overall noise factor for in-core neutron detectors is continuing to increase in severity. In this analysis, noise factor refers to the magnitude of variation in the time-series signal compared to the mean (or baseline) for that channel. Some detectors are affected more than others, e.g., in the trend in Figure 4.1, detector AF3H shows substantially worse performance than detector AF10E. This adverse trend is expected to continue into the future, consistent with detector aging and component wear and tear.

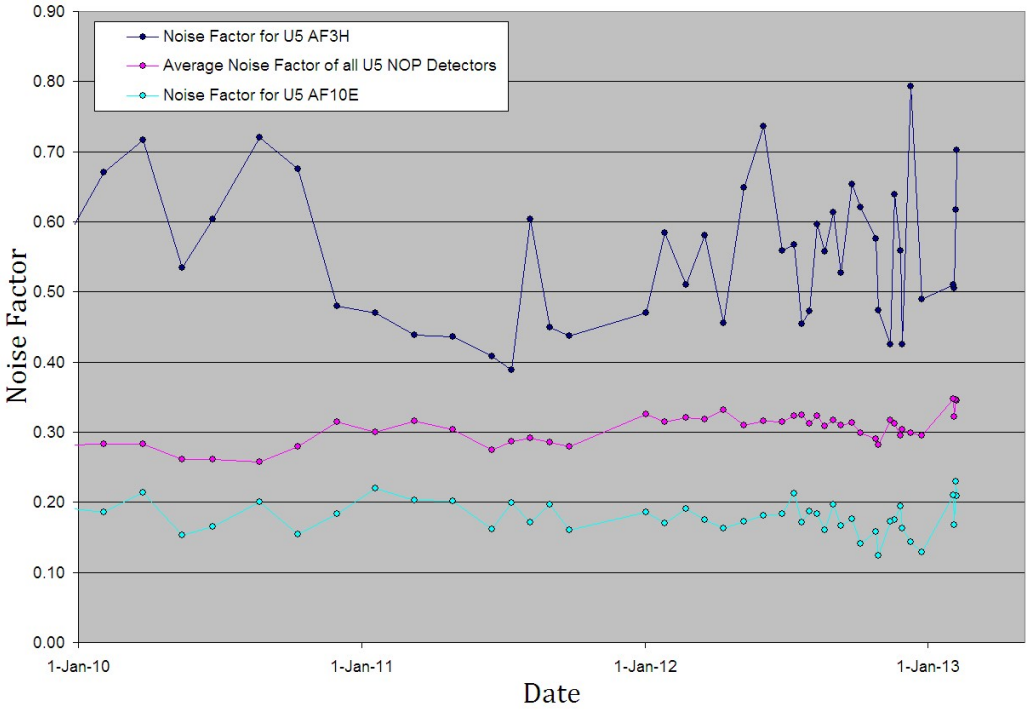

Figure 4.1: Noise factor trends for two detectors. AF3H (dark-blue trend) is substantially more affected than AF10E (light-blue trend).

A particularly noisy neutron detector, designated here as AF10F, was selected for this case study. This detector has been out of service for some years due to erratic response. The AF10F signal was observed to be noisy in January 2011, February 2011, and April 2014, as shown below in Figure 4.2. The detector signal appears contaminated with random spikes, both positive and negative, shown in blue. A control detector, designated as AF11F, is shown in red and performs steadily as expected.

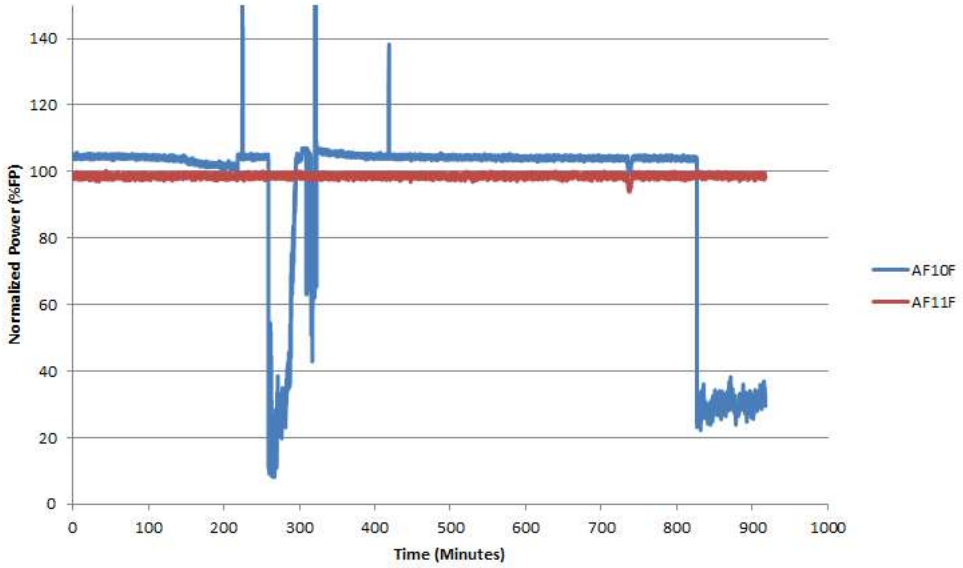

Figure 4.2: Data trend of AF10F (blue) and AF11F (red) performance on April 18, 2014.

Analysis of the sampled AF10F detector signal showed that perturbations of the digital switching (about 14 kHz) were superimposed upon the 115-60 Hz waveform and coupled into the wiring of the system. Even though best efforts are made to improve cable connections and shielding to minimize or eliminate the introduction of noise, these sources are still strong contributors and result in a large amount of corrupted, incomplete, or noisy data. Periodic, short-lived transients (spikes) due to the inverter switching circuitry are also still prominent in the amplifier signals. A newer model of amplifiers resolved the 14 kHz spike problem but showed an unanticipated pulse (50 mV ripple) at a frequency of about 1 MHz.

To obtain data for this case study, a Yokogawa DL750 data logger was connected to the detector amplifier and used to capture detector signal. A portion of the AF10F signal with three distinct peaks was selected as shown in Figure 4.3:

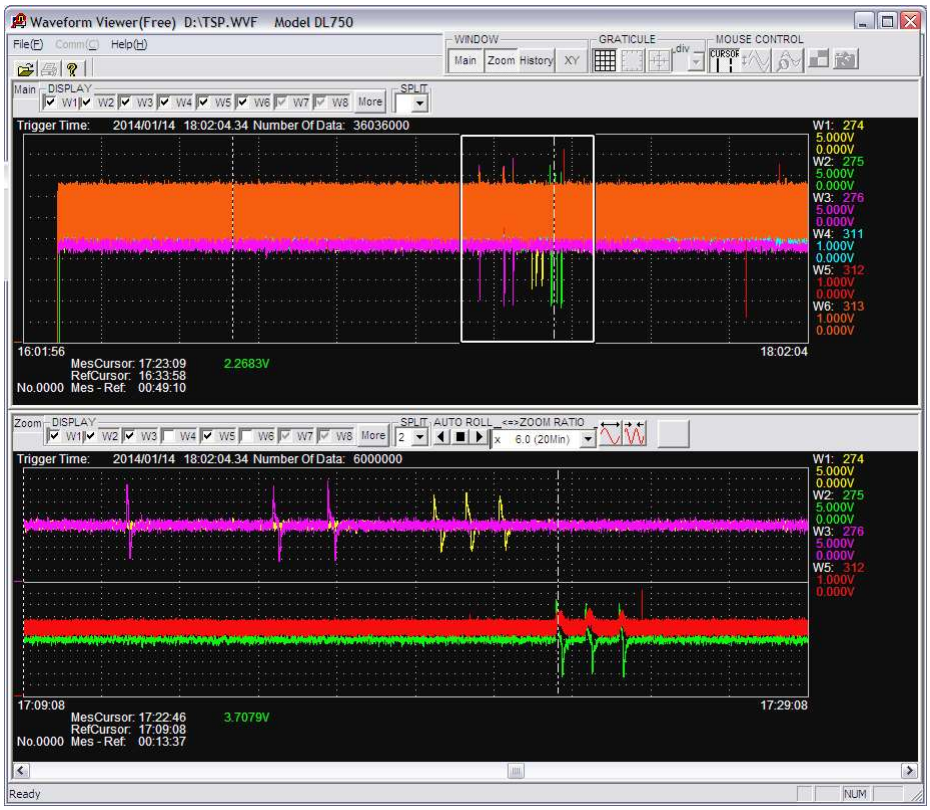

Figure 4.3: The signal appears to be visibly contaminated with random noise.

The true signal waveform is unclear due to the presence of noise, but several irregularities can be noted. First, at the beginning of the trend, there is a large negative signal spike of approximately ~2.5V. Second, during the test interval, there is a visible disturbance with three large signal spikes in both positive and negative direction ranging in the magnitude of 0.25V to 0.4V. These voltage spikes have a very short duration (~0.003 to ~0.08 seconds). Lastly, there are two large spikes at the end of the test interval. Yokogawa data-logger DL750 data was imported into MATLAB software, and the portion of the detector signal of interest was reconstructed as shown in Figure 4.4 and Figure 4.5:

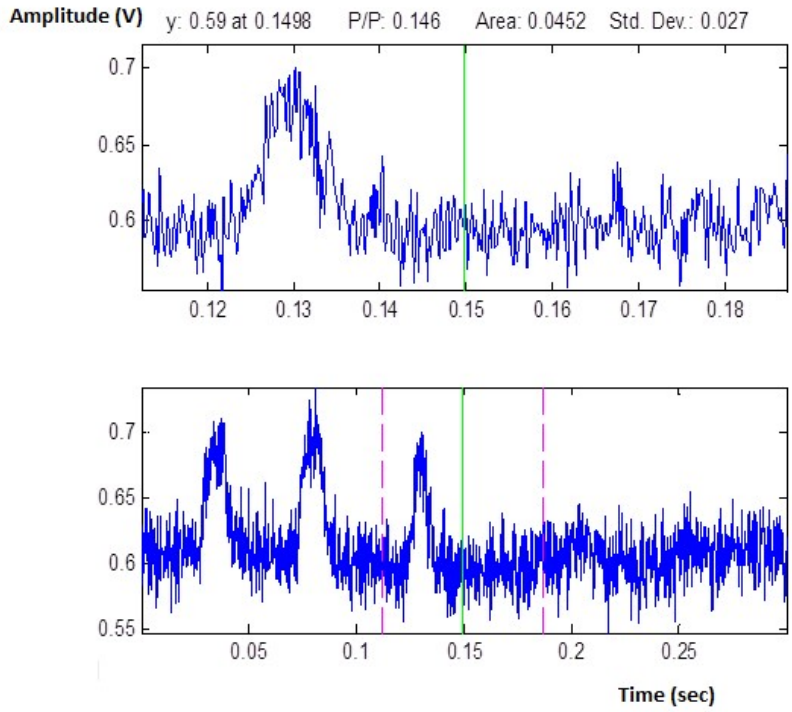

Figure 4.4: Portion of the original noisy signal selected for analysis is shown in two pink discriminator lines.

The original noisy signal is shown in the lower graph, while the upper graph shows a zoomed-in area of interest. Several peaks of different amplitudes were detected in this portion of the data set by observation, and the signal waveform appears near Gaussian.

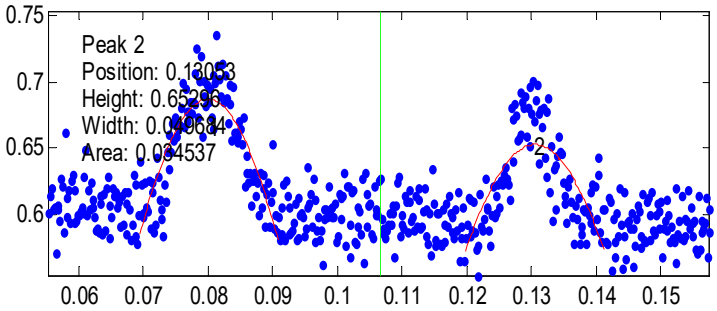

Figure 4.5: Curve fitting of the identified peaks. The waveform appears near-Gaussian.

4.1.2. Proposed Methodology for Noise Mitigation

Plant data, in this case, appears to be contaminated with random signal spikes, both positive and negative, lasting for very brief time intervals. Two methods (namely LPF and

WT) will be used to denoise data. Theoretical predictions will be compared to the experimental results for the LPF method. Additionally, it is proposed to evaluate whether a hardware modification (a long-term permanent physical implementation of a causal and stable low-pass filtering feature) can be used to increase the input impedance of the amplifier to reduce the input noise current.

4.2. Case Study Two: Operational Challenges and Proposed Solutions for Detector Signal Oscillations

In this thesis, the term "oscillation" is used to describe unexpected variations in detector signals during seemingly normal operation.

4.2.1. Operational Challenge—Signal Oscillations Phenomenon

The existing PF management methodology does not consider potential complications due to detector signal oscillations, particularly when combined with noise, during fueling operations. From the operational perspective, of greatest concern is the resultant potential for a reduced MTT. An example of signal oscillations is shown below in Figure 4.6. In this case, the signal variations occur simultaneously in zones 6 and 7, located on the northeast (NE) side of the reactor, but in the opposite direction of zones 8 and 9, on the northwest (NW) side. This behavior is unexpected because the in-core detector signals and liquid zone controller levels are not synchronized with the corresponding reactor-regulating system signals.

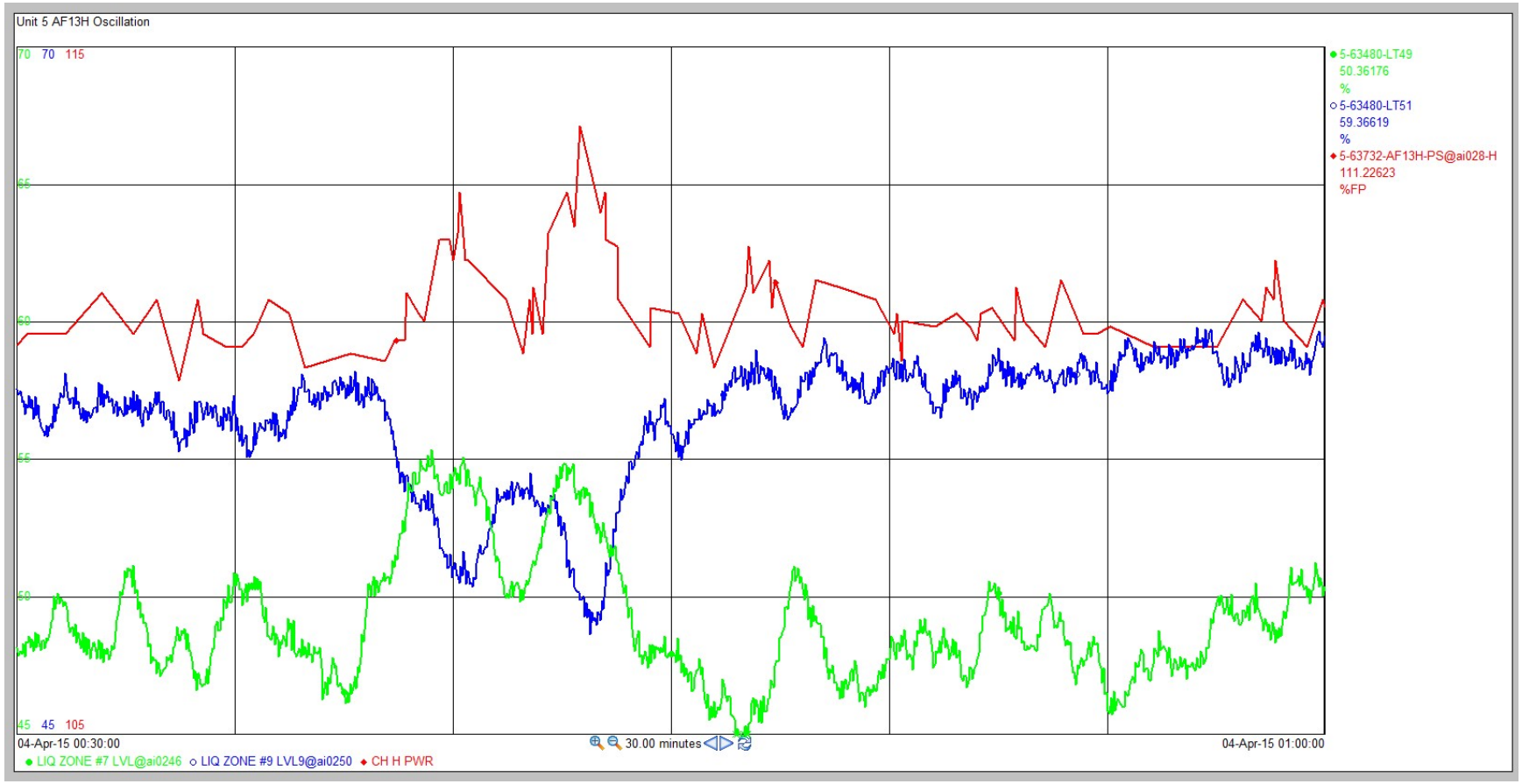

Figure 4.6: Trends of in-core neutron detector AF13H (red), reactor-regulating system detector signals, and liquid zone control levels (green and blue).

Previously performed engineering analysis confirmed that the detector loops and zone controllers operated correctly in every case where signal oscillations were present but failed to identify the root cause of unexpected system performance due to a high number of potential suspects, i.e., potential variables that could affect detector output.

A similar phenomenon (shown below in Figure 4.7) was noted at several NPPs in Canada. For example, from 1999 to 2003, a detector (designated here as detector 4F) was showing steady performance with relatively little noise present. At midyear point in 2003, an unexplained adverse change in the detector signal occurred. A high rate of signal variations persisted until January 2010, when the detector signal returned to its previous performance with minimum disturbances.

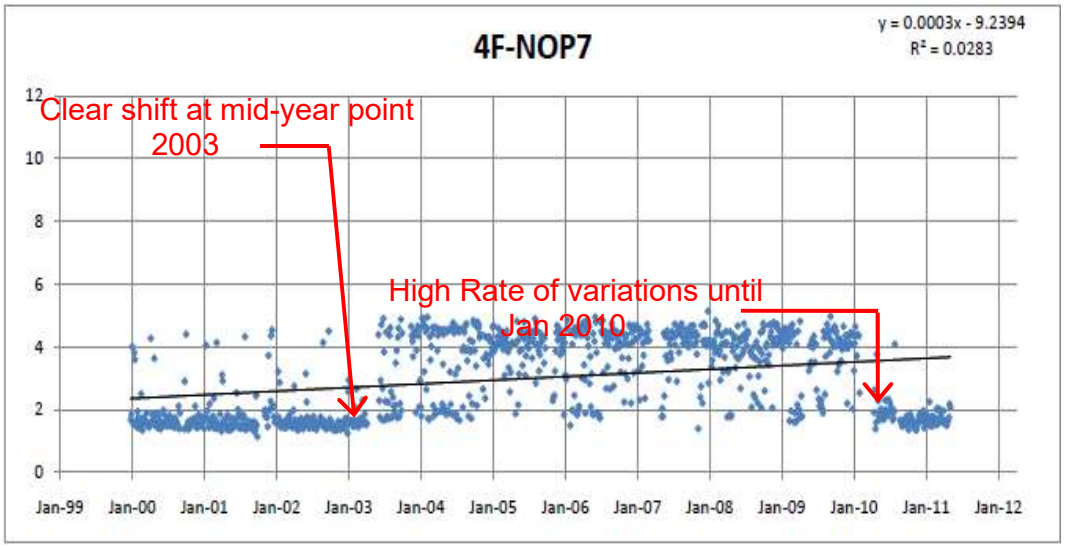

Figure 4.7: Detector performance trend example for January 1999 – January 2011.

The main concern, in this case, is the impact on MTT, both during normal operation and particularly during refueling. A trend of typical margin at normal full power operation sampled every five (5) minutes across four reactor units is shown in Figure 4.8.

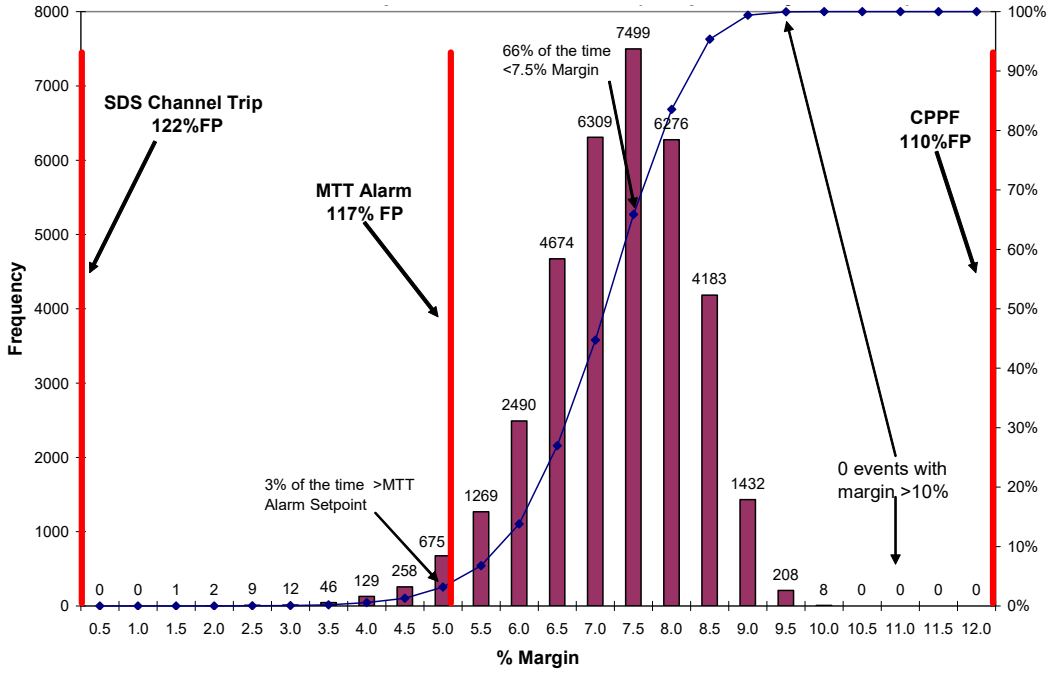

Figure 4.8: A typical margin for Shutdown System detectors at full power.

Analysis of plant data shows that during a typical high-power operation, 66% of the time there was less than 7.5% margin available, and there were no events where margin exceeded 10%. Thus, to maintain the required margin, reactor power de-rates were required. Cases where the available margin drops even further due to poor neutron detector performance add to the existing burden for operators and challenge both production and safety.

In an ideal case, e.g., with 105 detectors randomly distributed with two-out-of-three trip logic, the required detector setting can be shown as:

$$RDS = CPPF \times Pwr = 110\% \qquad \text{[Equation 4.1]}$$

where:

- CPPF – is the minimum issued channel power peaking factor = 1.10,
- trip setpoint = 122%,
- all units operating at 100% FP.

Thus, the maximum achievable margin is 12% when a reactor is operating at 100%.

The impact of margin reduction due to signal oscillation can be seen by comparing trends shown in Figures 4.9 and 4.10 below, where the margin was reduced by 2% on average due to signal variation.

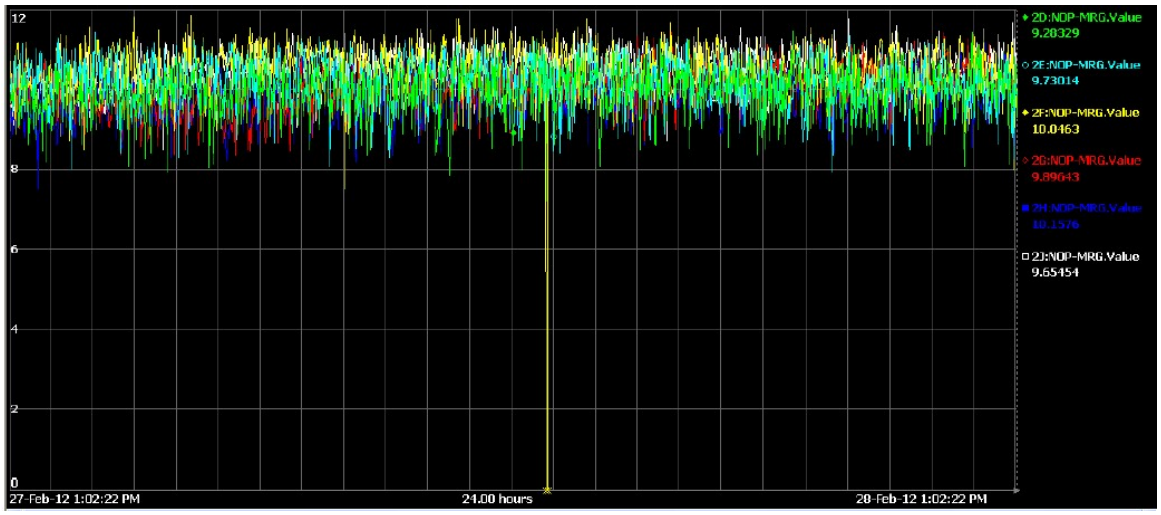

Figure 4.9: Margin in the absence of signal variations, February 20, 2012.

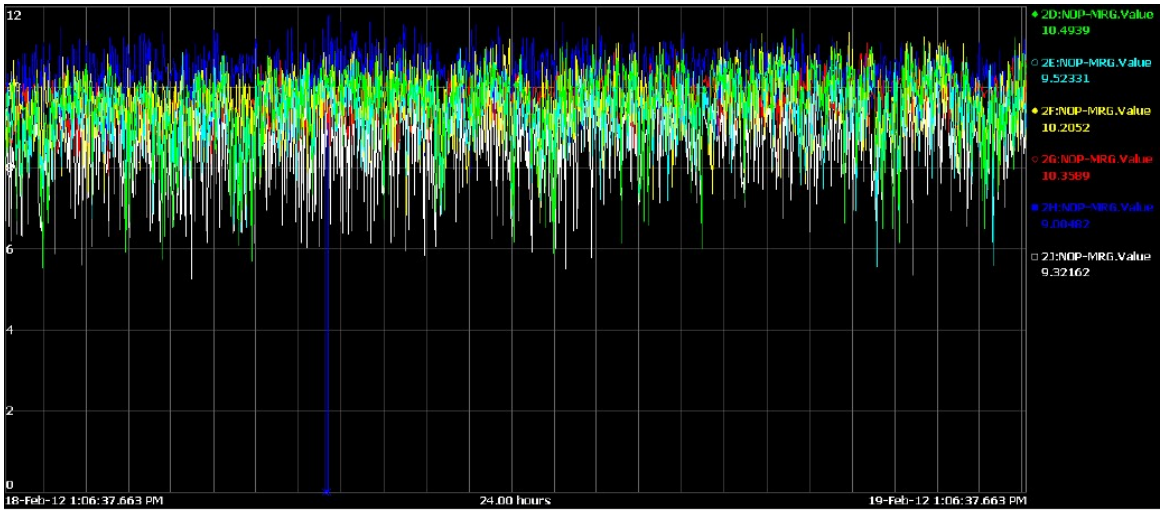

Figure 4.10: Impact on margin when signal variations are present, February 19, 2012.

The unexplained detector signal behavior is always present during high power operation at greater than 86% FP and typically results in a 2 to 3% decrease in margin. The specific concern for this study is that random onsets of variations in detector signals can result in an increased number of parameter trips. Subsequently, they can reduce the

effective operational margin to a reactor trip, challenging the assumptions used in the safety analysis.

4.2.2. Proposed Solution—Dimensionality Reduction with PCA, wPCA, and NLPCA with ANN

There appear to be multiple fast-changing process variables that must be analyzed simultaneously to establish the main contributing factors of system faults. Plant data dimensionality reduction is important in this case. It is necessary to identify the cause of related process variation to identify the cause of detector signal oscillations. The PCA and wPCA algorithms will be used for dimensionality reduction and modified to work with both linear and nonlinear data to support cases where linearity is not known in advance using NLPCA with the ANN.

4.3. Case Study Three: Operational Concerns and Solutions for Decrease in Detector Dynamic Response (PF)

The detector response, including PF and delayed components, is understood for nominal detectors but is less known for aged detectors. Measurements of detector performance at NPPs focus on assessing detector prompt fraction and replacement of detectors that are no longer considered fit for duty.

4.3.1. Operational Challenge—Management of Degrading PFs with Noise and Signal Oscillations for Transient Scenarios

As discussed in the previous two sections, the existing PF management methodology does not account for potential complications due to degraded PFs of the neutron detectors, signal oscillations, and noise, during fueling operations. Certain neutron detectors tend to exhibit an unusually high response to fueling operations of nearby channels. As reactor units age, to extend the service life of pressure tubes, it is necessary to use depleted fuel bundles or selectively defuel some channels in the core. Therefore, detector responses to fueling increase over time, and certain channels are considered high-risk actors based on the magnitude of change. In the example in Figure 4.11, the upper red trend delineates a 5% MTT and the upper dotted line 3% MTT. Examination of the trend

suggests that the response of detector H3 (dark red) is significantly greater than G12 (purple) and often challenges both MTT limits.

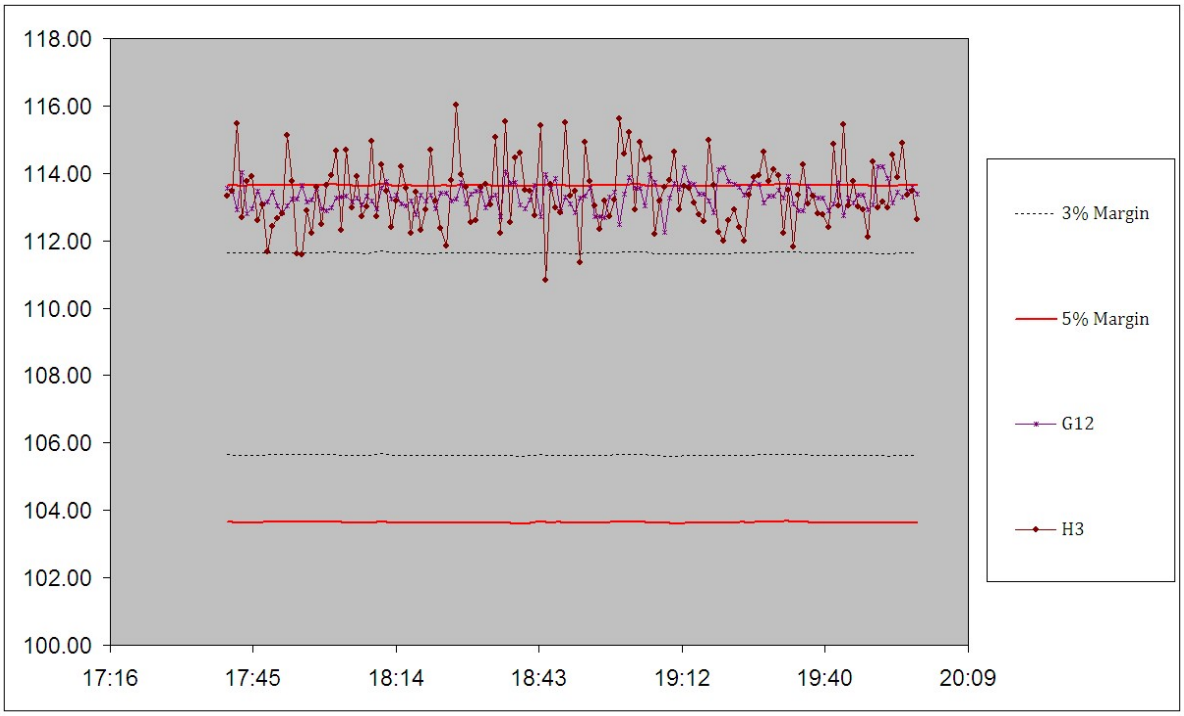

Figure 4.11: High response of detector H3 versus a steadier performance of detector G12.

This trend is expected to continue with detector aging and PF degradation, and may present significant challenges from a nuclear safety as well as operational point of view.

4.3.2. Proposed Solution—Extension of Methodology for Assessing Impact of DSC Amplifier Gain Change

The existing detector gain setting methodology does not consider potential complications discussed earlier, namely, aging, noisy detectors with high response to fueling, oscillations, or reactor power maneuvers following a prolonged outage. This thesis proposes to extend a detector gain setting methodology to address these gaps. In this thesis, it is proposed to develop an aged detector model assuming a proportional increase of all delayed components. Thus, only the fastest delayed components are impacted by aging effects and will be included in the new detector models for analysis. This approach will maximize the operational impact from the perspective of reductions in MTT of changes in

detector PF. When certain neutron detectors exhibit an unusually high response to fueling coincidental with a signal oscillation, the impact on MTT may be even more significant. This scenario seems never to have been evaluated before, and no simulations of aged detector response to fueling superimposed on a signal oscillation were found to exist in open literature or proprietary sources. Similarly, some detectors tend to exhibit an unusually high response to reactor power maneuvers, particularly during startups. Thus, the proposed detector models will have to account for these transient scenarios. The focus will be on developing new detector models for particular cases of interest in MATLAB/Simulink. The models will be used along with plant data to confirm the impact of gain changes on the MTT assumptions in the safety analysis.

4.4. Risk Estimation

Currently, NPP operators cannot monitor instantaneous risk nor have a graphical representation of neutron detector risk status in real time. Similarly, the existing PRA tools do not enable plant users to perform risk assessments for what-if scenarios prior to entering a particular new plant configuration. For example, if a certain detector exhibits noisy response, there are no tools or operator aids to determine the risk to continuous operation if the condition persists for a certain time period, e.g., two weeks. A decision to replace a suspected faulty detector often results in penalties and reductions to the MTT. Since detector replacements involve complex tradeoffs among safety, plant economics, and equipment availability, it is desirable to have an additional tool for making more accurate risk-informed decisions for monitoring the health status of the detector systems.

This thesis proposes an FSN-based solution to address this gap and to complement the existing PRA tools. The instantaneous risk estimation in an FSN can be used to review the impact of scheduled maintenance activities on risk, evaluate the magnitude of the detector system impairments due to noise or signal oscillations, and provide operators with the appropriate mitigating actions to minimize the level and the duration of high-risk activities, e.g., fueling near a noisy detector.

Chapter 5: Results Analysis

In this chapter, results of testing new detector models, denoising and dimensionality reduction, PF optimization, and risk estimation results are given. The study is summarized in a table at the end of the chapter, where execution, main performance criteria, and results relevant to each case are given.

Table 5.1: Case studies summary table.

Case	Description	Execution	Performance Criteria
5.1.1	Model Validation	Detector responses to fueling and oscillations assumed to be 10% of full power and 6% respectively.	Detector response to the power ramp of 16% in ten (10) seconds.
5.1.2	DSC Difference	16% Ramp/10 sec for aged detectors	MTT loss ≤1%
5.2.1	Denoising and Smoothing of Data	LPF	SNR ≥110/1
5.2.2	Denoising and Smoothing of Data with WTA	MWT	SNR ≥110/1
5.3.1	Dimensionality Reduction	PCA	95% of the total variance.
5.3.2	Dimensionality Reduction	wPCA	95% of the total variance.
5.3.3	Dimensionality Reduction for Non-linear Data	NLPCA	Check for non-linear behavior based on pattern recognition in a 3D PC space.

Table 5.1: Case studies summary table (continued).

Case	Description	Execution	Performance Criteria
5.4.	DSC Model for Transient Scenarios	Application of the new gains	Residual DSC error ≤1%
5.5	Optimization of DSC gain coefficients	GA solver in MATLAB	Residual DSC error ≤1%
5.6	Risk Estimation	FSN	Qualitative/quantitative

5.1 Model Validation—Old versus New DSC Gain Settings and Comparison to FUELPIN Predictions

A detector model is developed using mathematical/electrical circuit models with an MATLAB/Simulink software package, as discussed in Chapter 3. The assumptions on the detector signal are that the response of all detectors to the neutron flux are linear and composed of a prompt response and a linear combination of delayed fractions. The PF has the largest gain and is a direct component (i.e., no delay, dominating for the limiting accident).

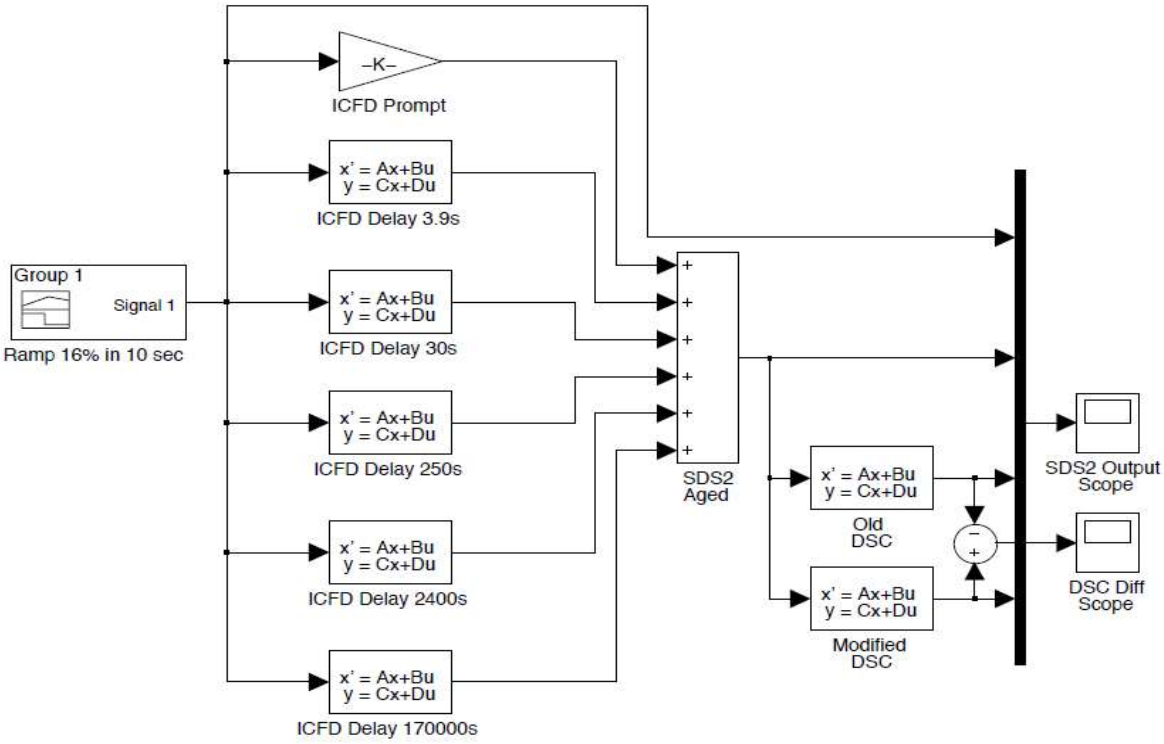

Figure 5.1: A detector model showing the prompt and the delayed groups.

Figure 5.1 shows a Simulink model of an aged in-core detector response to the power ramp of 16% in ten (10) seconds. In this model, the nominal values for the delayed components are shown, e.g., at time constants of 3.9 seconds, 30 seconds, etc. The model has four (4) constant matrices: A, B, C, and D. Values for constants and parameters in the Simulink models are obtained from the original design documentation. The initial value for the neutron flux is assumed to be 1.0 n/cm^{2}·s for stylized cases. For the cases where measured data is preprocessed, the initial conditions will be set to the initial sample value, and an inverse of the transform is applied to reconstruct the signal at the detector. The new gains are then applied to the reconstructed signal. The response of the model is compared to the plant data for a stylized case in FUELPIN to validate the model output. This case considers the impact of the gain factor change on a fueling transient coincidental with a detector signal oscillation. New proposed gains are implemented in this model along with the old gain values to compare with the FUELPIN code predictions. The assumptions for the magnitude of the signal oscillations are as as follows:

- Based on historical observations, detector responses to fueling are conservatively assumed to be 10% of FP,
- The magnitude of the signal oscillation is assumed to be 6%, based on historical trends.

The simulation results are shown below in Figure 5.2. The results suggest that the simulated ramp rate with the maximum DSC gain constants is conservative (i.e., faster) compared to actual fuelling and oscillation rates.

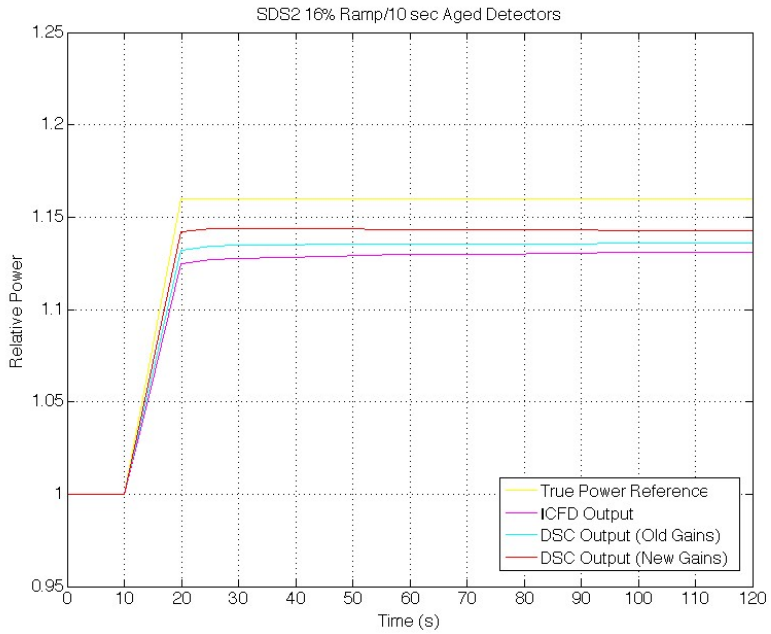

Figure 5.2: 16% ramp/10 sec for aged in-core flux detectors. The simulated ramp rate with the new DSC gain constants is shown in red.

It can be observed that the response is under-prompt, which is as expected. The compensated signal with new gains better matches the input power. The maximum MTT loss due to the gain change was 1.0%, as shown in shown in Figure 5.3 below. The results are consistent with the FUELPIN predictions discussed in Chapter 3.

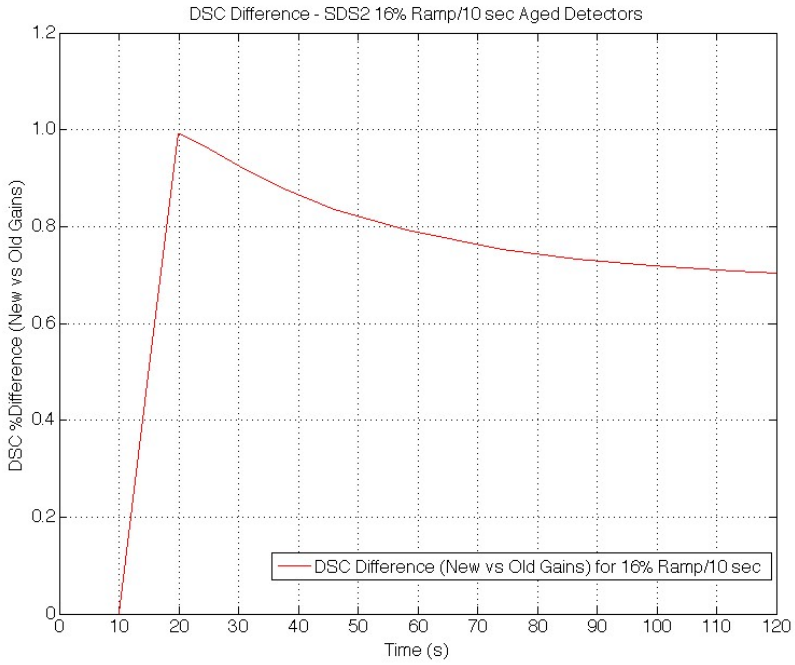

Figure 5.3: DSC difference—16% ramp/10 sec for aged detectors.

Next, it is important to confirm that the proposed optimized gains will not result in the unacceptable reduction in MTT following transients such as those observed from fueling operations. Prior to adjusting the DSC gains to determine the potential operational impact, the plant data is denoised and reduced in dimensionality so that the model can be validated with a large historical dataset for the typical plant transients such as those observed from fueling operations near noisy detectors and oscillations of the detector signals impacting the MTT.

5.2 Denoising and Smoothing of Data

The peak data was acquired using flat baseline correction and threshold criteria shown below:

- Slope threshold (SlopeT) = 0.00017778
- Smooth width (SmoothW) = 25 points
- Fit width (FitW) = 107 points
- Window span: 0.1024

Peak Summary Statistics are shown below in Table 5.2. The peak analysis results and histograms of the peak data are shown in Table 5.3 and Figure 5.4.

Table 5.2: The peak summary statistics.

Peak#	Position	Height	Width	Area
1	0.6872	0.04421	0.04421	0.03235
2	0.13057	0.65297	0.04965	0.03452

Table 5.3: Summary of the peak analysis results.

	Interval	Height	Width	Area
Maximum	0.050553	0.6872	0.04965	0.03452
Minimum	0.050553	0.65297	0.04421	0.03235
Mean	0.050553	0.67009	0.04693	0.03343
% STD	0	3.6113	8.1978	4.5933

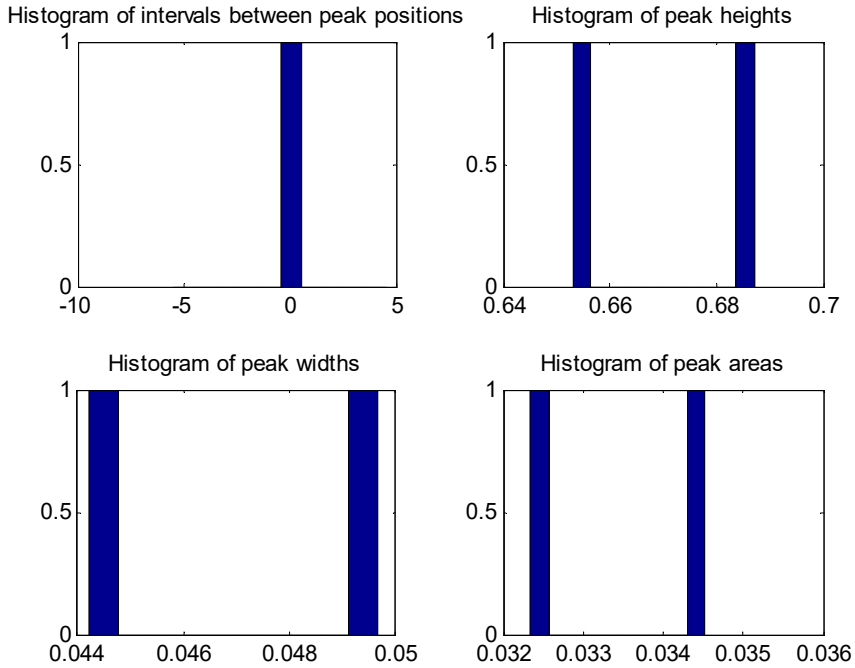

Figure 5.4: Histograms of the peak data.

Next, to determine the closest waveform of the peaks, several iterations of curve fitting of the selected peaks were performed, alternating among Gaussian, Lorentzian, logistic, Pearson, exponential pulse, alpha function, and Voigt profile. The Gaussian waveform produced the closest fit with the least error as shown in Figure 5.5 and summarized in Table 5.4:

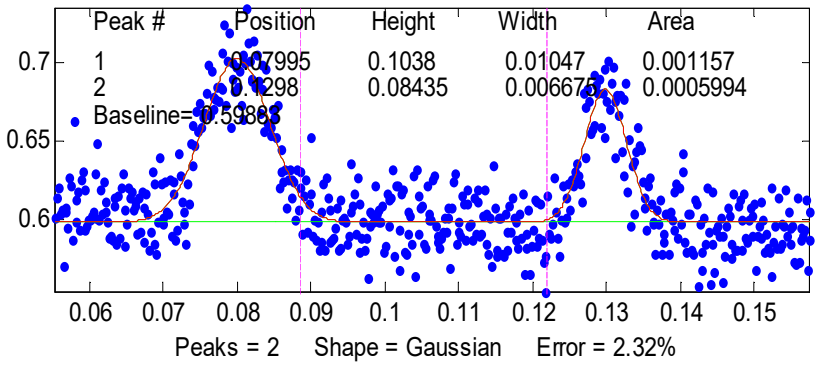

Figure 5.5: Gaussian—the closest curve fitting results with the highest accuracy.

Table 5.4: Signal statistics for unprocessed original signal.

1,500 total points from x= 0 to 0.2998
Interval between points = 0.0002 to 0.0002
min/max Y = 0.547/0.7352
No baseline correction
Smooth: = 3 point No, Ends = 0
Selected range: 375 points from x=0.1124 to 0.1872
Peak-to-peak Y: 0.1207
Standard deviation: 0.0232
Area: 0.04521

5.2.1 Signal Processing with LPF—Results

Next, the signal smoothing was performed using rectangular, triangular, Gaussian, and Savitsky-Golay approaches. The summary of signal statistics for each method is shown

in Table 5.5. Of greatest interest is the resultant SNR as compared to the typical SNR of 110/1 for these detectors.

Table 5.5: Comparison of signal de-noised results using the four proposed methods. Of most interest is the filter performance in terms of the obtained SNR.

	Tri	**Rec**	**Gaussian**	**Savitzky-Golay**
Position	0.15053	0.15058	0.15052	0.15055
Height	0.59489	0.59491	0.59482	0.59493
Width	0.11125	0.11045	0.11414	0.10952
Gaussian area	0.07045	0.069949	0.072273	0.069362
Total area	0.045211	0.045211	0.045212	0.045211
R2	0.19606	0.12588	0.22719	0.12843
SNR	122.9	92.5	142.1	92.5

5.2.2 Signal De-Noising with WTA – Results

Denoising using WTA of a one-dimensional signal was performed with the assumption that the sample signal is a general 1-D function with random Gaussian distributed variables. Following the approach described in the methodology sections, the data was transformed into the wavelet domain, thresholds were selected for the wavelet coefficients, and the transform was inverted. Various threshold options were applied to determine the optimal denoise approach. Stein's Unbiased Risk Estimate (SURE) is based on the quadratic loss function and a combination of a fixed-form threshold equal to sqrt(2*log(length(y)). The SURE threshold produced the most conservative results. Similar to the SURE method, the threshold based on the minimax [28] principle was also successful at reducing noise, particularly when small details of the signal lie in the noise range. Signal decomposition was used for the assumption that nonwhite noise might be present in the signal. Comparison of the denoising metrics for each approach is compiled in Table 5.6 below. Notably, the WTA approach did not produce the desired SNR of ≥110/1.

Table 5.6: Evaluation of the denoising metrics for each approach.

	level5sym8	softSURE	stddev
mean squared error	0.000278	0.000278	0.000278
mean absolute error	0.013279	0.013268	0.013279
SNR (dB)	31.308271	31.316610	31.308271
peak SNR (dB)	32.886957	32.895296	32.886957
cross correlation	0.809729	0.810137	0.809729

5.2.3 Comparison of Results and Selection of the Method for Implementation

Two (2) methods, namely LPF and WTA, were used to obtain theoretical predictions of noise reduction efficiency. Overall, LPFs used in this study performed better than the WTA for reducing the high-frequency components of a signal while retaining the low-frequency components. Smoothing methods were useful for removal of sharp spikes of not normally distributed random noise. The results show that the most considerable noise reduction was obtained from the pseudo-Gaussian method along with the highest improvement in SNR (≥110). The Savitsky-Golay smoothing algorithm yielded the smallest reduction in peak height but offered the least reduction in noise amplitude.

Application of wavelet analysis techniques combined with smoothing of derivatives produced less desirable results in terms of an acceptable SNR and loss of signal amplitude. This method showed better capabilities to eliminate the high frequency components of noise, where most of the white noise energy is concentrated, but did not demonstrate the desired SNR improvement. One characteristic of the wavelets is that they account for the nonstationarity of the data. Thus, intuitively, the MWT approach should perform better or, as a minimum, produce results similar to the standard LPF filtering. However, one of the challenges in the wavelet filtering may be due to the choice of the wavelets for this study. The basis function needs to be selected such that it closely matches input signal. Then, using the level of decomposition, it is possible to control the frequency bands that are classified as useful data or noise. The scaling function is the low pass component, and the wavelets are subsequent bands of higher and higher frequency. Therefore, further work is

required for the choice of wavelet method, filter, and length to determine their implications for the expected signal denoising results with the optimal SNR values.

The results of this study show that the greatest noise reduction was obtained from the pseudo-Gaussian method along with the highest improvement in SNR compared to the WTA approach. Therefore, the LPF approach was selected for experimental validation at the plant.

5.2.4 Implementation and Validation with Plant Data

The LPF approach was used to validate the theoretical response using plant data for one of the detectors in the case study. None of the interfacing devices, such as cables and connectors, is included within the scope of this study. A digital LPF was applied as a temporary design change to a noisy neutron detector, designated as AF10F. This detector loop has been out of service for some years due to the erratic response observed from the associated in-core flux detector. The initial signal was decomposed into its frequency components, and the high frequency components were suppressed. Next, detector signal cable was reconnected to the amplifier AF10F while remaining disconnected from the safety system trip circuit. Plant data from July 15, 2016, to August 1, 2016, was downloaded and analyzed to check the detector response. The original unfiltered signal and the filtered signal are shown in Figures 5.6 and 5.7, respectively.

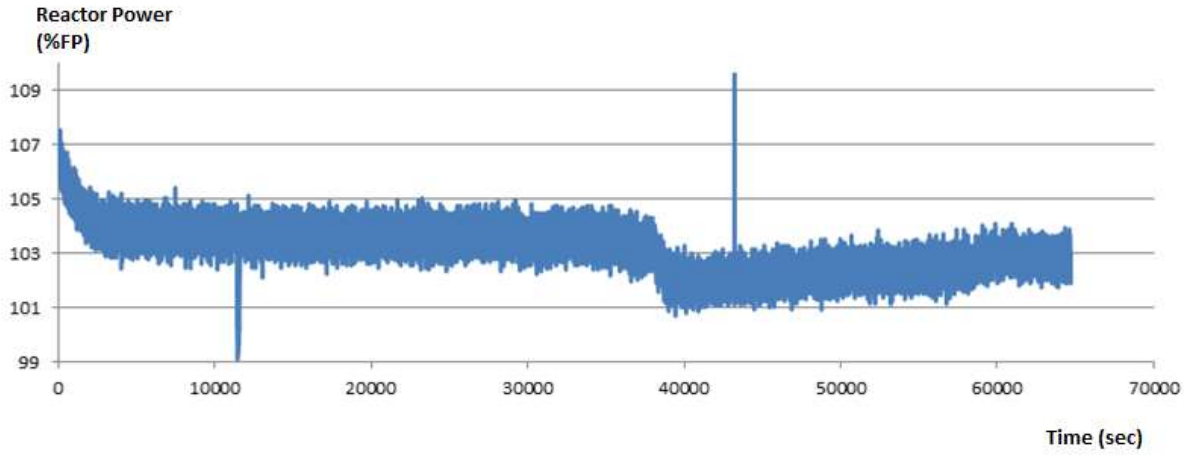

Figure 5.6: AF10F response—unfiltered signal with random noise spikes

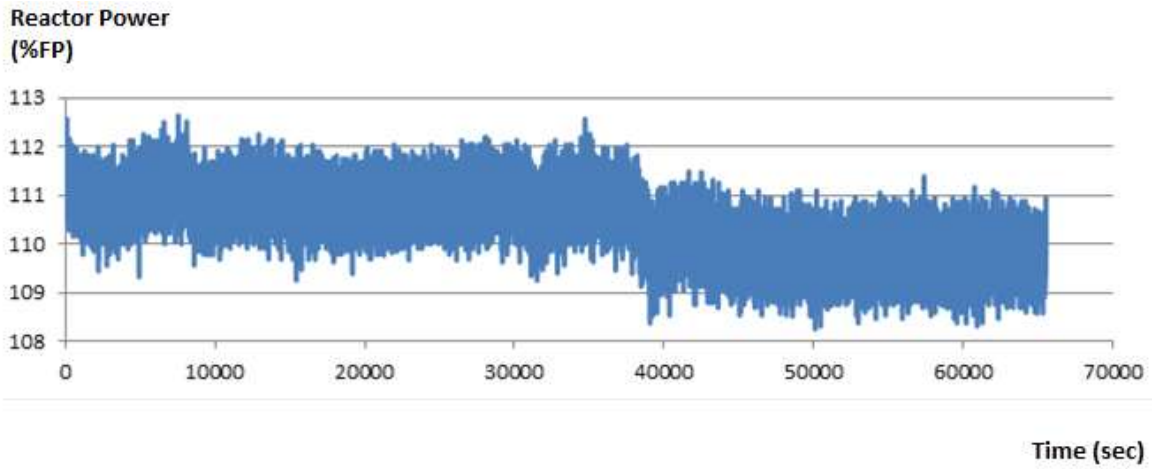

Figure 5.7: AF10F response—filtered signal with random spikes visibly removed.

Several additional cases were analyzed to validate the detector response (post-filter) against introduced transients, and the results are shown below in Figures 5.8, Figure 5.9, Figure 5.10, Figure 5.11, and Figure 5.12. Both the steady state and transient conditions were carefully selected to correspond to specific operating conditions at the plant, namely:

- A controlled power maneuver,
- Steady-state operation,
- Fueling near the AF10F detector,
- Comparison with a control and an adjacent detector.

Case 1: Response to a Controlled Power Maneuver Test.

AF10F response (shown in blue in Figure 5.8) was recorded during a system test along with a number of nearby detectors that typically exhibit optimal response.

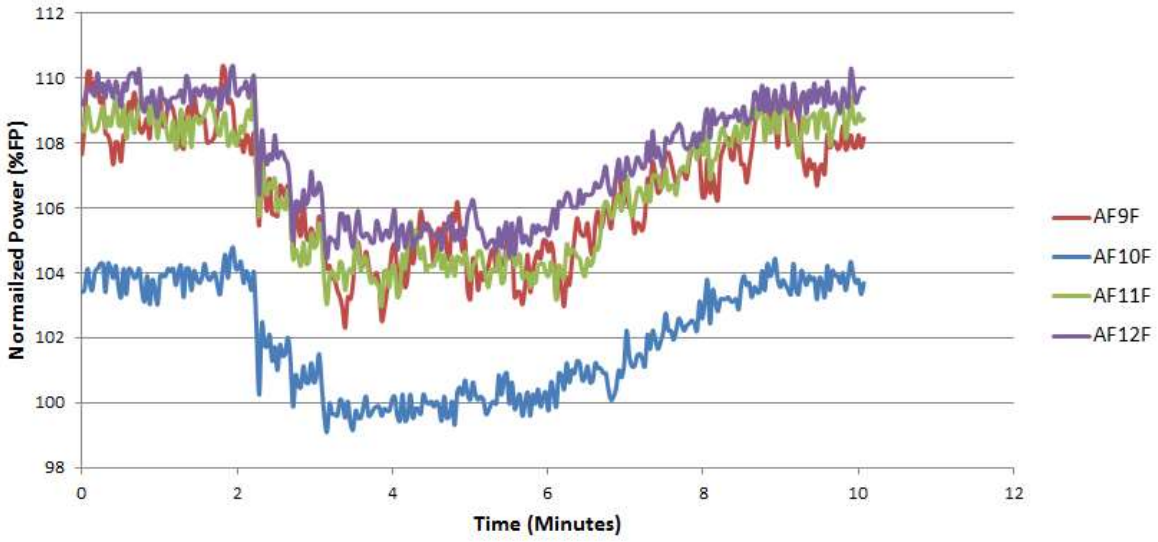

Figure 5.8: Testing AF10F response to a system test compared to some nearby detectors.

In this trend, plant data is captured at a sample rate of 0.5Hz with minimal filtering. The analysis shows that AF10F closely followed changes in power with other nearby detectors (designated here as AF9F, AF11F, and AF12F). The gain to normalize AF10F in line with other amplifiers was not adjusted at the time the test was performed, and as such, AF10F appears with an offset.

Case 2: Response during Steady-State Operation

A steady-state response was monitored and analyzed for the data collection period, as can be seen below in Figure 5.9. Examination of this trend shows that from July 15, 2016, to August 1, 2016, no erratic indication, high noise, or signal drift was observed. Both the detector and the loop behaved in line with other detectors during the seventeen-day monitoring period.

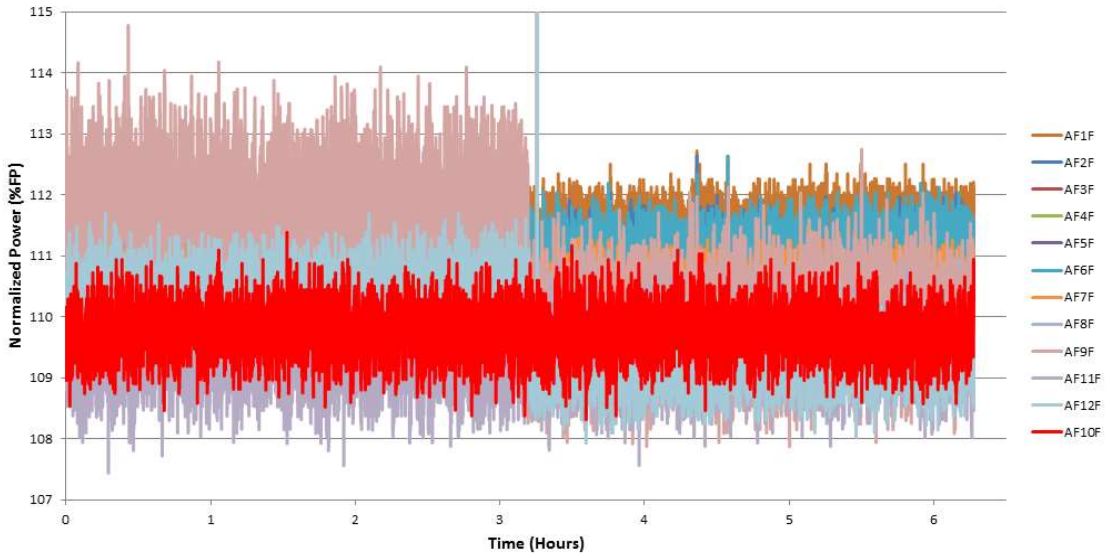

Figure 5.9: Response to steady-state conditions is shown in the left-side portion of the graph; AF10F is shown in red.

Case 3: Response to Fueling

Due to the physical location of detector AF10F, it was expected that fueling of fuel channel X10 would result in a visible level of localized changes in flux. Fueling of channel X10 occurred on July 29, 2016, and the response of AF10F can be seen below in Figure 5.10.

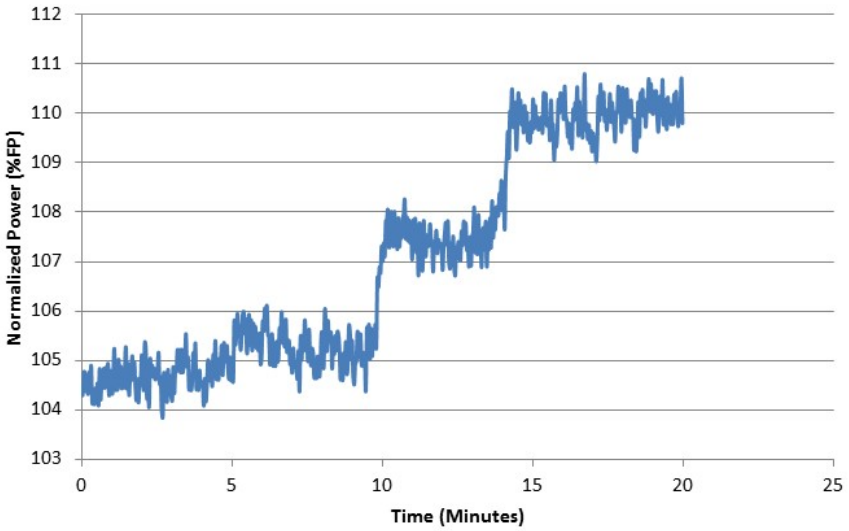

Figure 5.10: AF10F response during fueling of channel X10.

The equivalent fueling runs in another reactor unit were investigated to interpret this response. The AF10F detector in the case study response closely followed the comparable

trends of equivalent fueling runs, as seen next. The response of a modified AF10F appears to be consistent with the expected behavior shown in Figure 5.11.

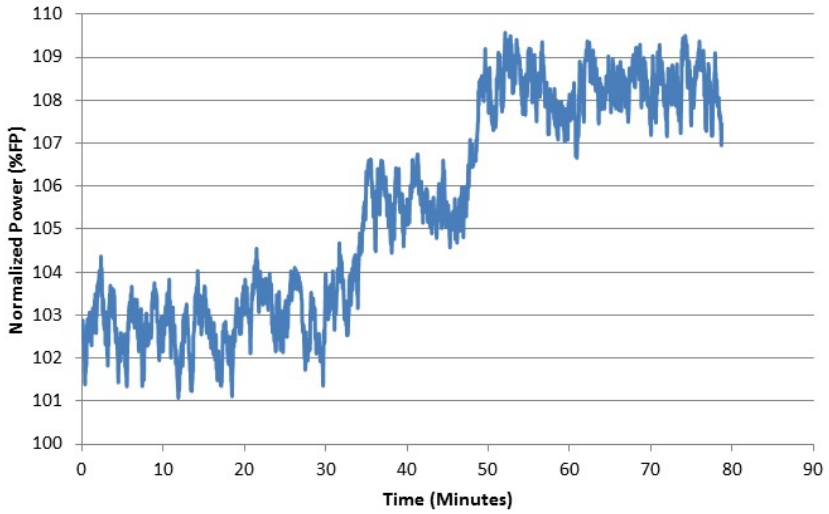

Figure 5.11: Response of another AF10F detector at a different unit during fueling (for baseline comparison).

Case 4: Comparison of AF11F (Control Detector) and AF12F (Adjacent Detector)

Finally, detector AF10F performance was trended against the control detector AF11F, as shown in Figure 5.12. AF11F detector was designated because of its location in the same instrumentation channel and acceptable performance over time. Detector AF12F is a nearby detector in the same channel and was used to compare with an AF10F response.

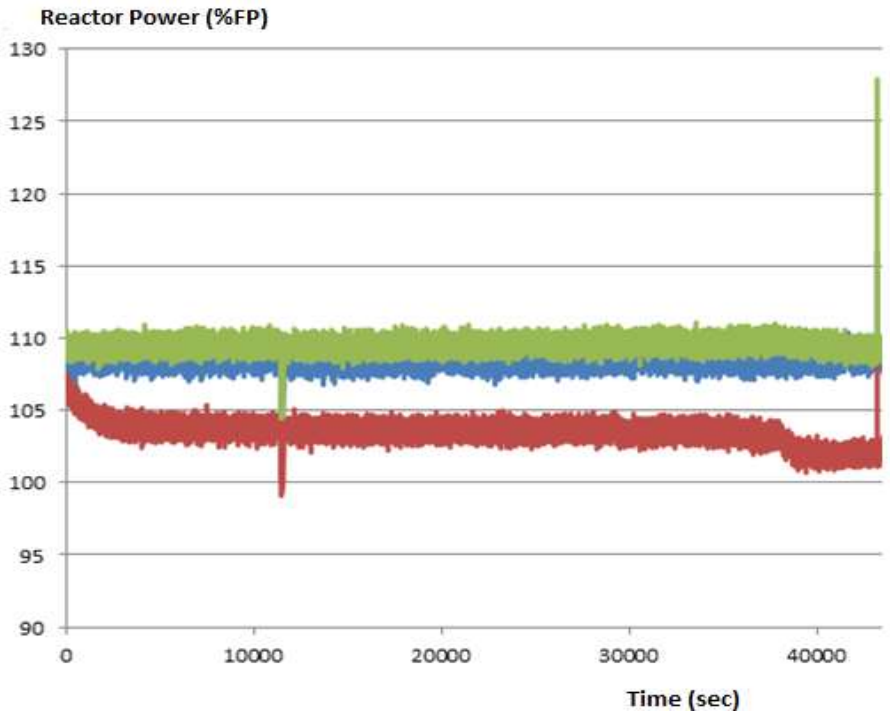

Figure 5.12: AF10F detector response post modification (shown in red) versus the control detector, AF11F (shown in blue), and another nearby detector in the same channel, AF12F.

In this case, the data was collected from July 15, 2016, to August 1, 2016. The first significant spike (in the negative direction) occurs during a scheduled control power reduction and is expected. The last spike in the graph below occurs when the data logger was disconnected and is expected. Overall, the AF10F detector signal appears consistent with the control detector AF11F as well as AF12F (another nearby detector in the same channel).

5.2.5 Performance Acceptance—Criteria and Results

In addition to the SNR requirements, the performance acceptance criterial for the detector outfitted with an LPF includes evaluation of inherent noise in power measurement signal during normal online operation. As discussed in the previous section, based on the four (4) case studies, the results are deemed acceptable. No increase in inherent output noise is observed. While no tolerance can be provided as to what the acceptable noise-to-

signal ratio is, engineering judgment can be used when comparing signal quality before and after the installation (for the same detector). The comparison is limited to the interval where the corresponding detector with LPF is trended against control and adjacent detectors in the same channel.

Another performance acceptance criterion for the affected detector is to track changes in reactor power, either during power maneuvers or fueling. Responses of the detector with LPF are identical to the trends of the detectors to which they were compared. There will be offsets in power levels being indicated (due to normalization and CPPF values or CPPF penalties). Hence, the evaluation will be limited to observing the degree of agreement between the affected and the adjacent detectors. It is expected that all of them will be registering an increase in power—or a decrease in power should a power maneuver occur. The complete ramp-down/ramp-up in reactor power is not part of the criterion of the filter credibility because the detector was already tested on all power levels during bench calibration. There is very little to be gained by observing a ramp-down/ramp-up. The tests shown in this section demonstrate that the results in all cases are positive.

5.3 Dimensionality Reduction with PCA and wPCA

Plant data for the selected case study was arranged into a 108x2200 dataset, and a 108x2200 data matrix was created and exported from Excel datasheet into MATLAB for analysis in PCA, wPCA, and NLPCA.

5.3.1 Results—PCA

For the first iteration of a PCA algorithm for 108x2200 matrix, the sample data was converted into a 108x108 principal component space, as shown in Figure 5.13.

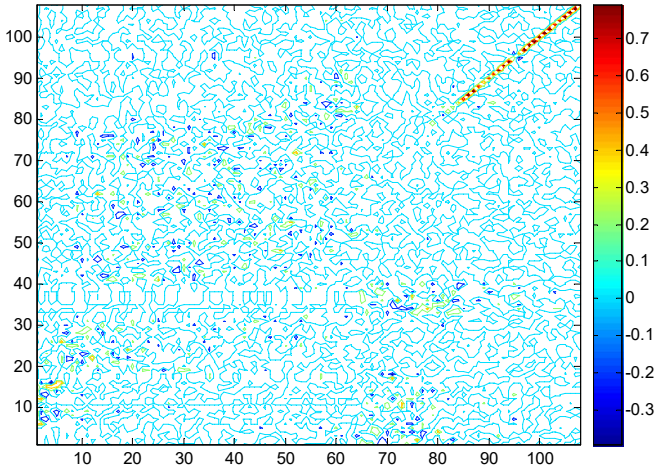

Figure 5.13: 108x108 principal component space after first PCA rendition of the sample dataset. Due to a large number of variables, it is difficult to interpret the results.

This identified a challenge with traditional PCA analysis. In cases with more than three (3) variables, it is difficult to visualize their relationships. The graph does show principal component space, but due to the number of variables, it is also difficult to determine which specific component has the most weight. Next, the following assumption was made: each principal component is a linear combination of the original variables and all the principal components are orthogonal to each other, so there is no redundant information. Thus, there should be no need for redundant information in the process data.

Following this assumption, all channelized measurements were removed from the historical sample of data, thus reducing the number of PVs to fourteen. Also, the focus time interval was shortened to one (1) hour. The sampling frequency was increased to ten (10) seconds. The second iteration of the PCA analysis was repeated on the restricted dataset. The results are given in Figure 5.14 below, where the principle components are shown as a single axis.

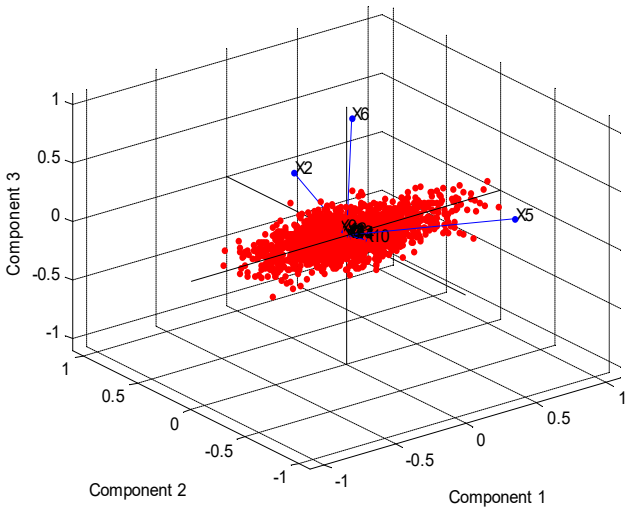

Figure 5.14: PCA analysis results showing the multivariate distance of each observation from the center of the dataset, with the most prominent vectors corresponding to X2, X6, and X5 variables.

Each observation of data is projected on the axis so that the resulting values form a new variable. Variability of this parameter is of particular interest; it is the maximum among all possible choices. The process is repeated for the second and third principal components to obtain the variance of this variable among all possible choices of the second axis. All fourteen variables are represented by blue vectors in Figure 5.14. Direction and length of each vector show how each variable contributes to the principal components.

In this case, the algorithm generated a new set of variables (principal components). Each principal component is a linear combination of the original variables. The original variables—in our case, instances of PVs—are represented by a point, and their locations indicate the score of each measurement for the two (2) factors. Coordinates of each point indicate the score of each observation for the principal components in the plot. The points are scaled to fit within the unit square, so only their relative locations can be determined from the plot. Process variables are represented in this plot by blue vectors, and the direction and length indicate how each variable depends on the underlying factors, e.g., X2, X6, and X5 are the most prominent PVs. In this iteration, the most prominent vectors correspond to X2, X6, and X5 variables, although only X2 and X6 are positive, while X5 is negative.

To determine the percent variability explained by each principal component, and ultimately find the most extreme points in the data, Hotelling's T-square was calculated and is shown in Figure 5.15:

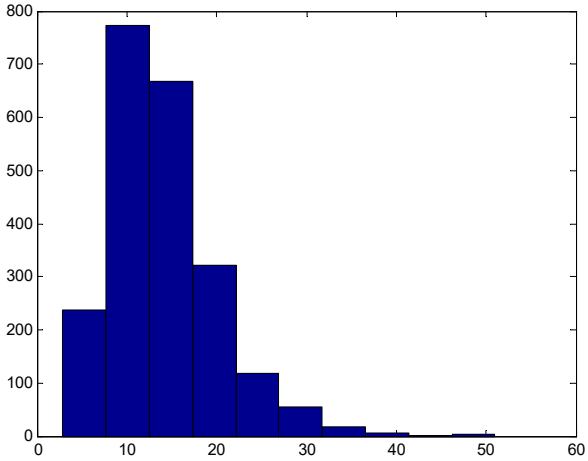

Figure 5.15: Hotelling's T-square statistic, showing the percent variability explained by each principal component.

Based on these findings, the PCA algorithm suggests that process variables X2 and X6 **(**corresponding to moderator temperature and calandria inlet pressure) have the strongest effect on signal oscillations.

5.3.2 Results—wPCA

While PCA algorithm has shown promising results, it is known to be less than optimal for large sets of data where data clusters and outliers are not identified in advance or their existence is unknown. Weighted PCA (wPCA) was performed on the selected data set by using the inverse variances of the ratings as weights to improve the robustness of the algorithm. The same general approach is used as in the PCA method. In this case, however, the data is standardized by assigning weights to the mean and the outer products that form the covariance matrix. This puts a weight on every point in the training data and makes identification of extreme points easier. The scores for each principal component were calculated by transforming the original data into the space of the principal components. The original data matrix is the same 14x2200 dataset used in the previous analysis. The principal components define these original data (in the new coordinate system). The scaled

and rated data is projected onto the first two principal components. Data points farthest away from the center of the cluster are outliers, i.e., more extreme than the rest of the data, as presented in Figure 5.16:

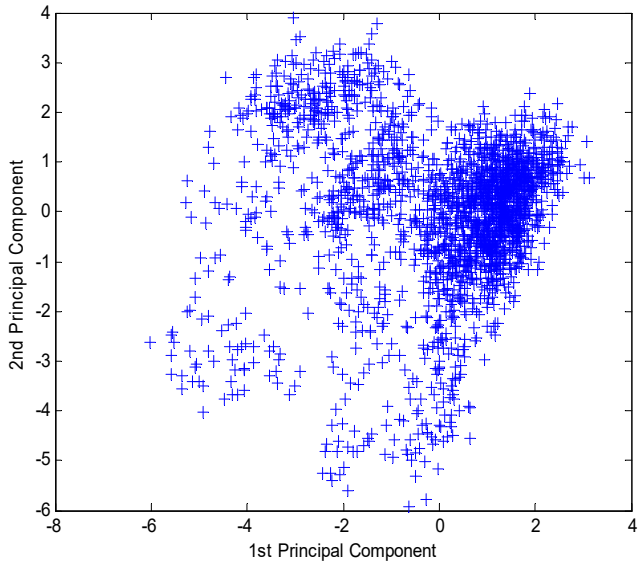

Figure 5.16: Principal component space for sample data processed with wPCA algorithm.

Weighted coefficients are determined first. Since the coefficient matrix was not orthogonal it had to be transformed. Next, all fourteen variables were plotted in the graph shown in Figure 5.17:

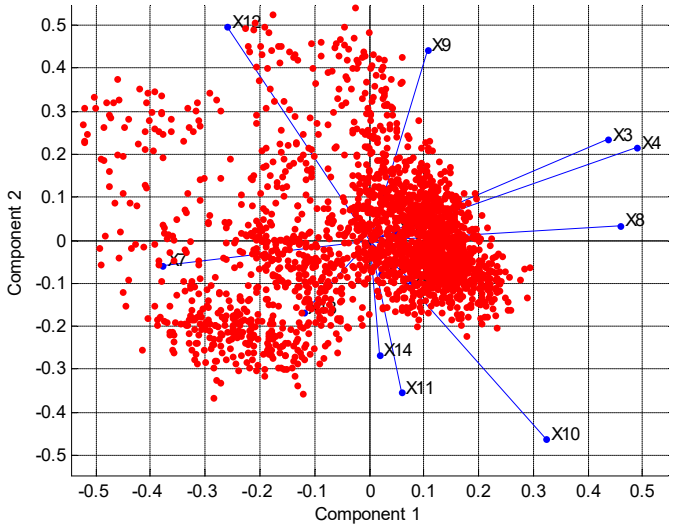

Figure 5.17: Results of wPCA analysis—blue vectors correspond to process variables that have the primary effect.

Each variable is represented by a blue vector, where its length and direction indicated how much each variable impacts the principal components. For example, on the horizontal axis of component 1, variables X3, X4, X8, and X9 have positive coefficients (in the upper right side of the plot). Variables X3 and X4 have the largest coefficients and will be selected for fault reconstruction scenario. Process variables with negative coefficients will not be considered in the follow-up analysis. Thus, weighted PCA identified X3, X4, X8, and X9 vectors as requiring further attention. In the data model of this study, X3 and X4 correspond to moderator pump-bearing temperature for Pump 1 and Pump 2, respectively. X8 corresponds to the average liquid zone level (AZL) measurement and X9 to zone 6 level. Next, the eigenvalues of a correlation matrix were sorted in descending order of magnitude and plotted as shown below to determine the fraction of total variance in the data as represented by each principal component.

It can be noted that there is a significant amount of variance between the first and second components, and together they explain roughly two-thirds of the total variability in the standardized ratings, as shown in Figure 5.18.

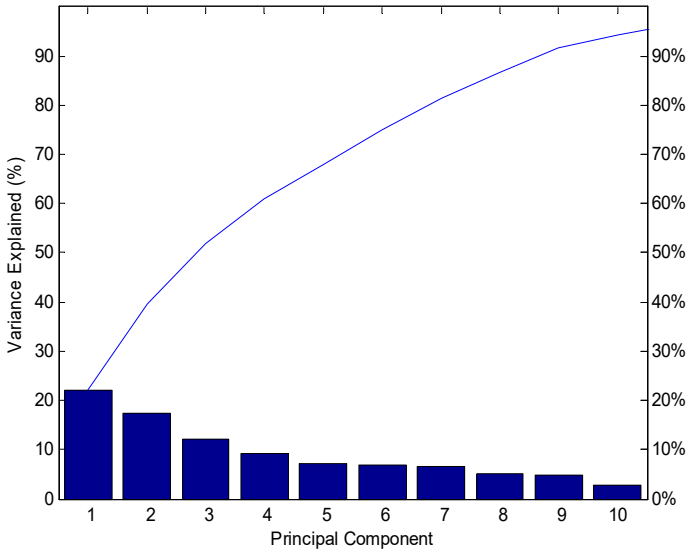

Figure 5.18: Pareto plot of variance distribution shows components that explain 95% of the total variance.

The two cases, one based on PCA and the other based on wPCA, produced slightly inconsistent results. Application of the PCA to the 108x108 parameter matrix with 2,200 instances identified X2 and X6 factors corresponding to moderator temperature and

calandria inlet pressure, while the weighted PCA determined two (2) variables with the most covariance, namely X3, X4, corresponding to pump-bearing temperature for Pump 1 and Pump 2, as summarized in Table 5.7.

Table 5.7: Results of PCA and wPCA analysis. X3 and X4 correspond to the moderator pump bearing temperature change during the pump duty swap. X8 and X9 are the LZC level transient and the signal oscillation for the axial zone pair 6/8.

Method	Moderator				Calandria		Power	Liquid Zone			Neutron Detector		RRS	
	Temp		PUMP 1/2 Temp		Level	Inlet Pressure	RRS PLIN	AZL	Zone 6	Zone 8	Zone 6	Zone 8	Zone 6	Zone 8
PCA	X1	X2	X3	X4	X5	X6	X7	X8	X9	X10	X11	X12	X13	X14
wPCA	X1	X2	X3	X4	X5	X6	X7	X8	X9	X10	X11	X12	X13	X14

Cross-Validation Case 1: Normal Operation

Since the unsupervised models are used in this study, standard techniques for cross-validation do not perform well. However, the results can still be looked at in relation to the previous engineering analysis and other studies on the moderator pump properties and temperature distributions. Such validation was performed using field data collected for the moderator pump-bearing temperature during normal operation and referenced with the detector response, as shown below in Figure 5.19.

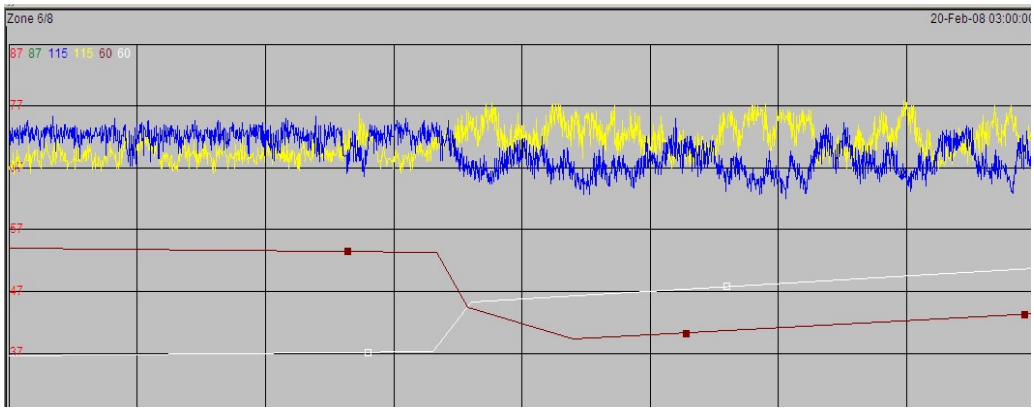

Figure 5.19: Neutron detector signals (yellow and blue) plotted against moderator pump bearing temperature. Pump1 shown in white, Pump2 shown in red.

Examination of this trend suggests that activation of Pump 2 is indicated by the increase in the pump-bearing temperature (shown in white). The Pump 1 temperature drop (shown in brown) indicates that the pump was swapped out of duty. The onset of noticeable detector signal variations is coincidental with the pump duty swap timestamp. This observation suggests that changes in moderator parameters (coincidental or causational with main moderator duty pump swap) are intimately related to the cause of signal oscillations, in line with the PCA/wPCA predictions. This leads to the formulation of the following hypothesis: the pump duty swap event causes the onset of significant detector signal variations (oscillations). To validate this hypothesis, fault diagnosis and reconstruction of fault propagation scenario was conducted next. A high number of potential causes of disturbance was reduced from 108 to only two: changes in the temperature and pressure due to a pump swap operation, as shown in Figures 5.20 and 5.21

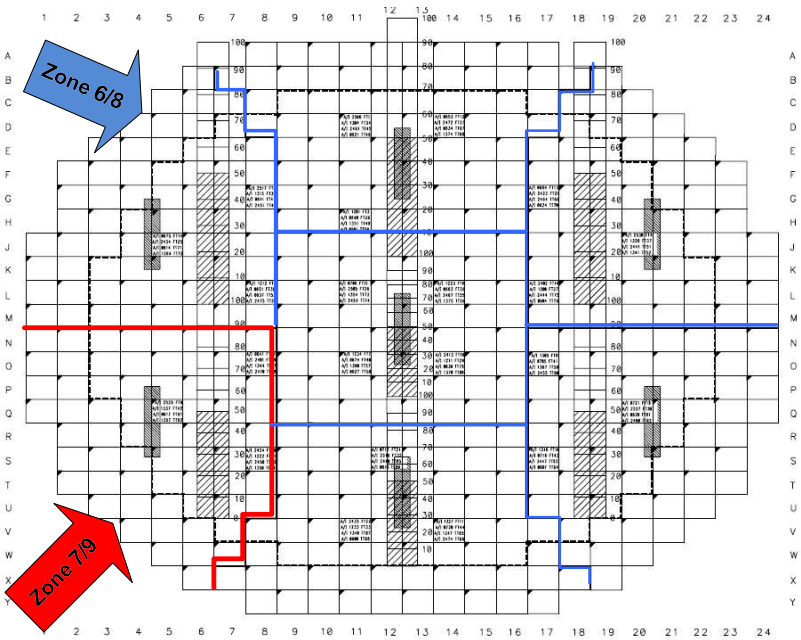

Figure 5.20: Location of LZ units and in-core detectors in zones 6/8 and 7/9.

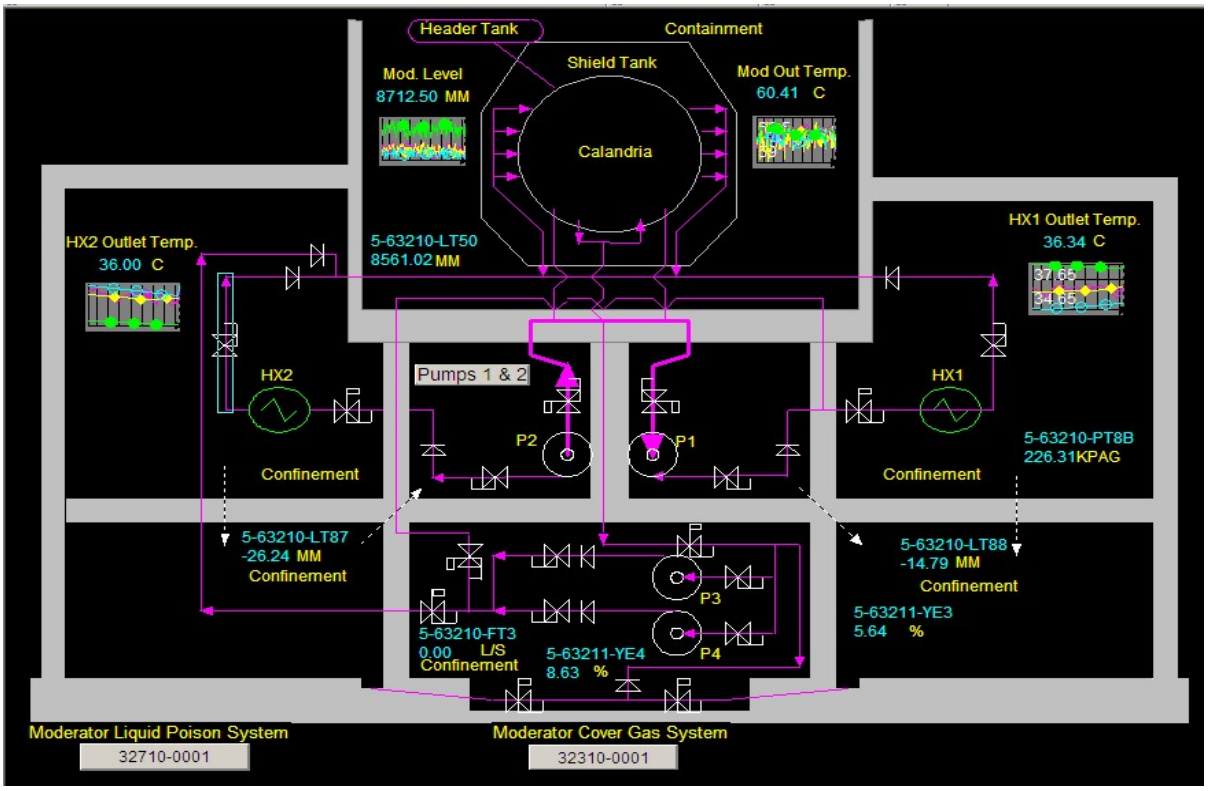

Figure 5.21: Plant process mapping. Moderator pump system (P1 and P2) and pump circuit are shown in relation to the calandria.

This process schematic can be simplified to focus on the moderator pumps P1 and P2 and their impact on the calandria inlet temperature and pressure, particularly in the axial zone pair 6/8 and 7/9. This is shown in Figure 5.22, where the fault can be reconstructed due to the effects of Pump 1 duty swap.

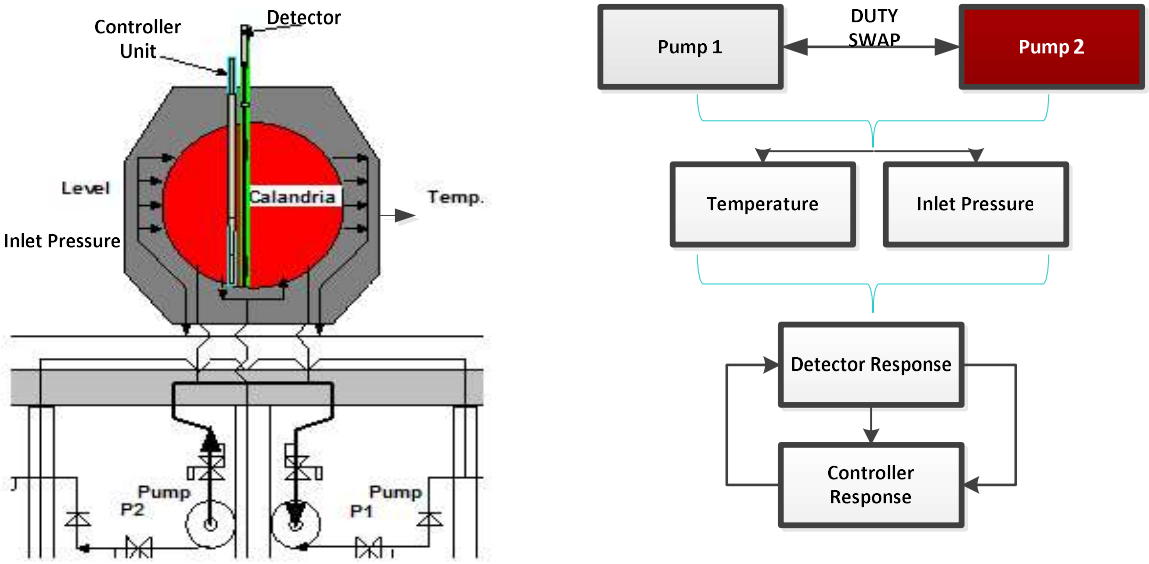

Figure 5.22: Fault propagation scenario based on wPCA results.

Two case studies were selected for validation exercise; one corresponds to normal operation of the plant, while the other represents a transient condition.

Cross Validation Case 2: Reverse Operation

A period when pump duty swap was reversed was examined to determine if the reversal of changes in pump-bearing temperature will result in reversal of signal variations. Two consecutive pump swap events (indicated by the changes in pump-bearing temperature in Figure 5.23) were identified and trended versus the detector response.

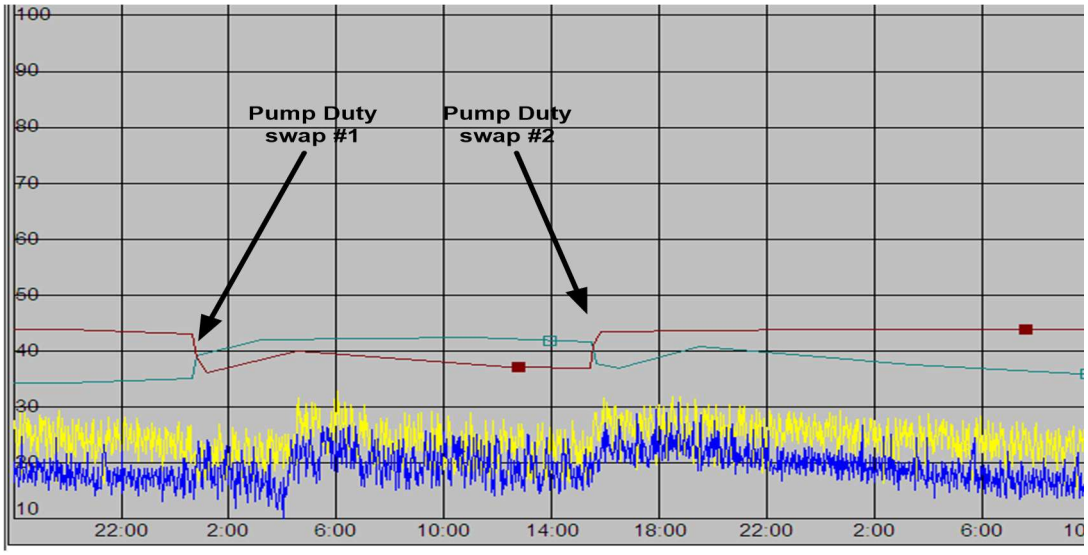

Figure 5.23: Two consecutive pump swaps indicated by the changes in pump bearing temperature for Pump 1 (shown in brown) and Pump 2 (shown in teal blue) are plotted along with the detector response (shown in blue and yellow).

It can be noted that, before, the first pump swap detector signals were relatively steady. After the pumps had been swapped, detector signals experienced a high rate of variation. After the second pump swap had occurred, the signals returned to steady operation.

Cross-Validation Case 3: Transient Conditions

A transient condition case was selected next. In this instance, both pumps were simultaneously running for twenty minutes, which is highly unusual. Pump 1 (shown in dark navy blue in Figure 5.24) was in service and was supposed to shut down at eleven-thirty but failed due to a circuit breaker malfunction. Pump 2 (shown in light blue in Figure 5.24) was in standby mode before eleven-thirty and was put on duty once Pump 1 was shut down. This resulted in the approximately twenty-minute interval when both pumps were running at the same time. Similar to previous trends, detector signals are shown in yellow and blue, and corresponding control responses are shown in red and blue. Variations in detector signals and controller levels are quite noticeable before the dual-run period but diminish to negligible values during the two-pump run.

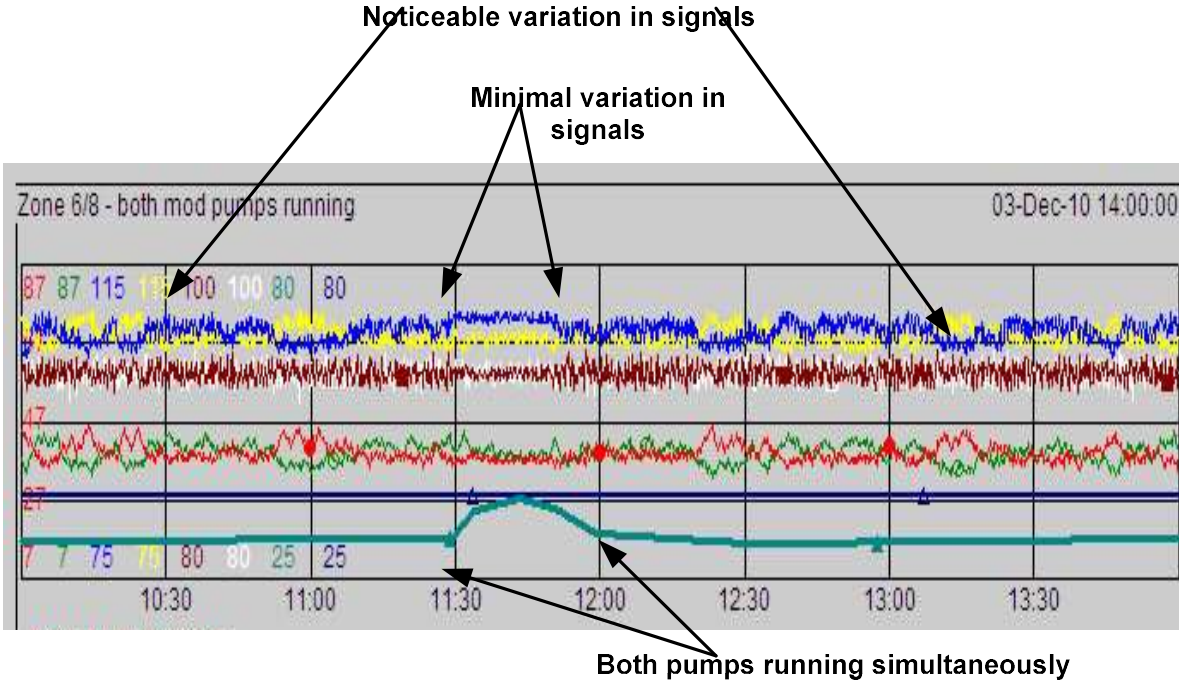

Figure 5.24: Both pumps running in parallel resulted in a steady period with minimal signal variations.

The results of this study suggest that pump duty swap is likely the cause of signal variations. In this unusual case of two moderator pumps running in parallel, detector signal variations disappear during the simultaneous dual run.

5.3.3 Results—NLPCA

In the previous analysis, an assumption was made to overlook the fact that the application of linear PCA to nonlinear data may be inadequate. To make the proposed PCA methods suitable for a wide range of field applications, compression, reconstruction, and denoising in nonlinear data must be addressed. Experimental, nonlinear extension of PCA algorithm was developed in the open research. The algorithm was tested and optimized for use in this thesis using MATLAB software package.

Whenever a high-frequency oscillation occurs, the resultant behavior will permeate throughout the entire system. Since high-frequency oscillations cause nonlinear system response, a simple way of detecting the oscillating signals is to check for nonlinear behavior. An NLPCA model was built based on pattern recognition and feature extraction by the algorithm in a 3-D principal component space. Process data from the field, shown as blue dots, were processed and mapped into an NLPCA space, as shown below. Initially, the network is trained with 14x1100 PV instances, representing a ten-minute interval of plant data. The algorithm starts with PCA preprocessing and linear weight initialization to begin NLPCA with the linear solution of a PCA. The dimensionality is still fourteen and is not reduced here, but the data space is rotated by the PCA. The data space of the first three (3) principal components is plotted, but if there are nonlinear components identified by the algorithm, they will be originally located in the full fourteen-dimensional space. The results of the initial network set up with 1,200 iterations are shown below:

```
# version: 0.90
# network  type: bottleneck
# training mode: hierarchic
# hierarchic layer: 3
# hierarchic coefficients: 1    1    1 0.01
# number of components: 3
# network architecture: [14-8-3-8-14]
# weight decay: ON,  coefficient = 0.01
# PCA pre-processing by 'pre_pca'
#  using first 14 of 14 PCA components
# data scaling, set max std to 0.1 (scal=0.0114)
# initializing weights using: set_weights_linear.m
# network training

# sorting components at iteration 1 - done
  # sorting components at iteration 3 - done
  # sorting components at iteration 23 - done
  # sorting components at iteration 55 - done
  # sorting components at iteration 1198 - done
```

sorting components at iteration 1199 - done

sorting components at iteration 1200 - done

network training - finished

Explained variance (see: net.variance)

nonlinear PC 1: 76.58%

nonlinear PC 2: 10.03%

nonlinear PC 3: 6.57%

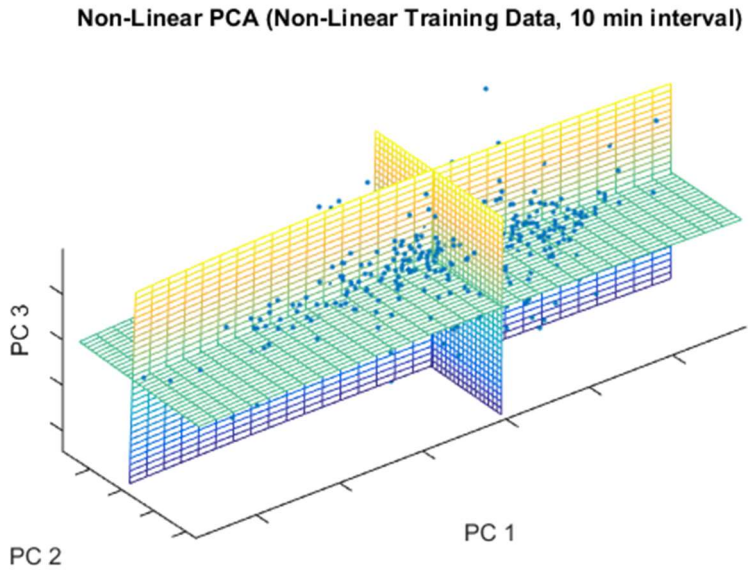

Figure 5.25: Results of NLPCA shown in the case study.

In Figure 5.25, the first three (3) components of NLPCA are shown by grids. Each grid represents the two-dimensional subspace given by two components, while the third one is set to zero. This can also be described as the new coordinate system of the transformation. For this training case, the training and test errors are:

trainerror =0.4857

testerror = 0.8493

Next, the network is run with 14x2200 PV instances which represent a twenty-minute plant data interval for further training:

```
# version: 0.90
# network  type: bottleneck
# training mode: hierarchic
# hierarchic layer: 3
# hierarchic coefficients: 1    1    1 0.01
# number of components: 3
# network architecture: [14-8-3-8-14]
# weight decay: ON,  coefficient = 0.01
# PCA pre-processing by 'pre_pca'
#  using first 14 of 14 PCA components
# data scaling, set max std to 0.1 (scal=0.0114)
# initializing weights using: set_weights_linear.m
# network training
# ...

  # sorting components at iteration 1 - done
  # sorting components at iteration 11 - done
  # sorting components at iteration 23 - done
  # sorting components at iteration 55 - done
  # sorting components at iteration 1198 - done
  # sorting components at iteration 1199 - done
  # sorting components at iteration 1200 - done

# network training - finished

# Explained variance (see: net.variance)
  # nonlinear PC 1: 75.53%
  # nonlinear PC 2: 10.38%
```

nonlinear PC 3: 6.23%

trainerror = 0.6246

testerror = 0.7171

The variance ratio of the first principal components is high enough in comparison to the others, and the gap between training error and validation error (testerror) gets smaller as the training process is repeated. The training error decreases sharply when the number of iterations increases and reaches a level of 0.6246 at 1,200 iteration. Also, the training error comes closer to the validation error, even though both are being increased as expected. The results of network training with twenty minutes of plant data is shown in Figure 5.26:

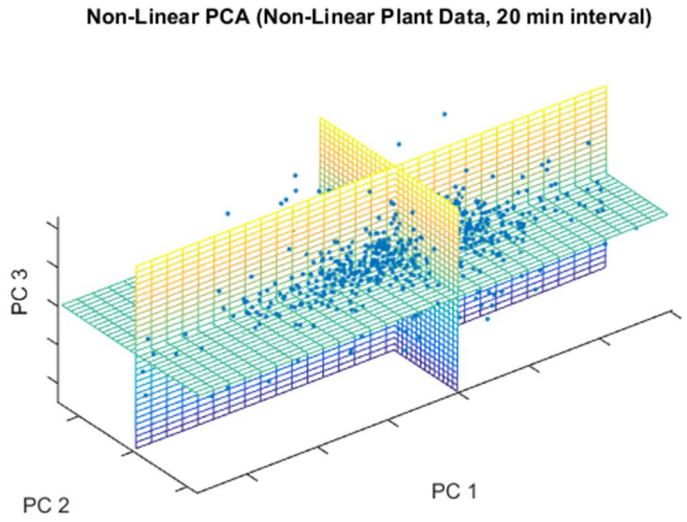

Figure 5.26: Results of network training with twenty-minute plant data, 14x2200 PVs

The hypothesis in this study is that if nonlinear system performance is identified, the onset of oscillations can be expected. The system in Figure 5.26 shows a linear behavior. Thus, the absence of oscillations in detector signal/LZC response can be confirmed. The training can stop at this time since the validation error (testerror) is minimized and is bigger than the training error (trainerror); thus, the network can generalize to unseen data.

Next, a set of nonlinear data was used to validate the algorithm, as shown below in Figure 5.27. Unlike the linear PCA used earlier, the NLPCA produced a nonlinear (curved) description of the data, as shown next in Figure 5.27.

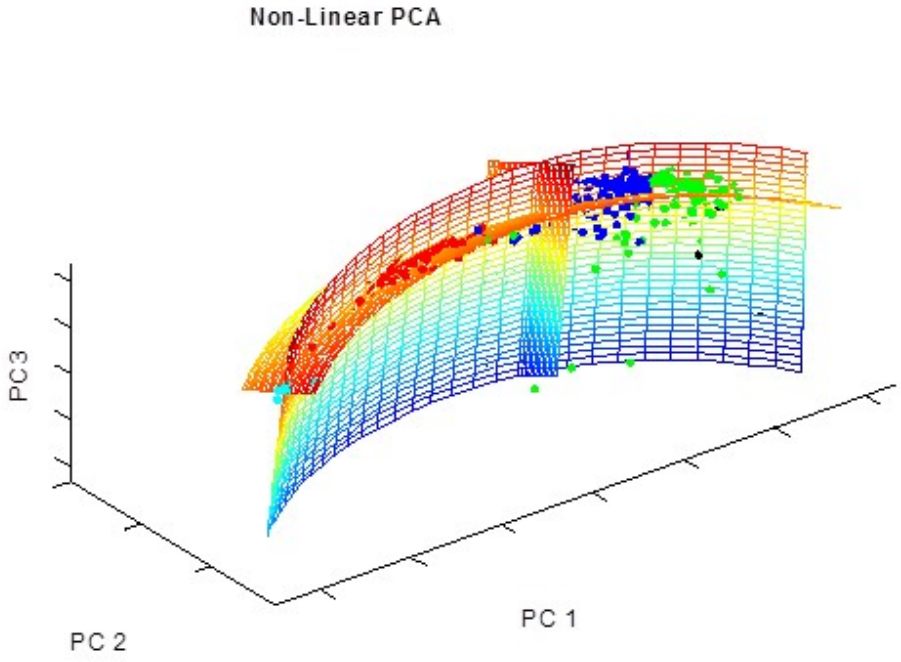

Figure 5.27: Results of NLPCA algorithm validated using nonlinear data.

Typically, the test error of ANNs decreases monotonically as a function of the iteration number, while the training error also continuously decreases; however, such behavior may not occur in systems where the input data is corrupted by noise. The network training adjusts the internal weights of the network to minimize a predefined error measure. The magnitude of error describes the deviation of predicted outcomes from the observed ones where a large deviation suggests a poorly fitted model. For typical regression problems, the most commonly used error function is the mean square error (MSE). However, depending on the application, it is possible to train the network on different error functions to achieve optimal performance for specific performance criteria. In this study the computational speed is a critical parameter since the approach is suggested for large nonlinear numerical models in near real-time applications. Further network training results in minimizing a predefined error function.

Next, the network performance is measured using test error validation. The “testerror” is calculated in the same way as the training error but on a different data set not used for network

training. The desired component values, or scores, are computed at the bottleneck layer where a reduction of the dimension of the data is performed. This portion of the work is not shown here but can be further developed in the future.

5.3.4 NLPCA Cross-Validation of Results

Since the unsupervised models are used in this study, standard techniques for cross-validation do not perform well. However, the results can still be looked at in relation to the previous engineering analysis and other studies on the moderator pump properties and temperature distributions.

Previous engineering analysis confirmed that the detector loops and zone controllers operated correctly in every case where signal oscillations were present. Moderator poison data and distribution patterns in the calandria were also examined to ensure that the zone level oscillation was not due to some local reactivity perturbation. Although the actual cause was not identified at the time, it was believed that the signal perturbations were caused by a change in moderator flow characteristics on the side of calandria corresponding to Pump 2, i.e., zones 6, 7, 8, and 9.

Cross-Validation Study for NLPCA Results:

Figure 5.28 shows results of a study on moderator temperature and flow distribution. This study modeled moderator inlet jets and internal heating in the calandria-like cylindrical vessel to represent the characteristics of a typical PHWR reactor. Recirculating jet-induced flow, heating of the water by volumetric heat generation, and a matrix of horizontal tubes parallel to the cylindrical axis were mapped to determine the major parameters affecting the flow patterns.

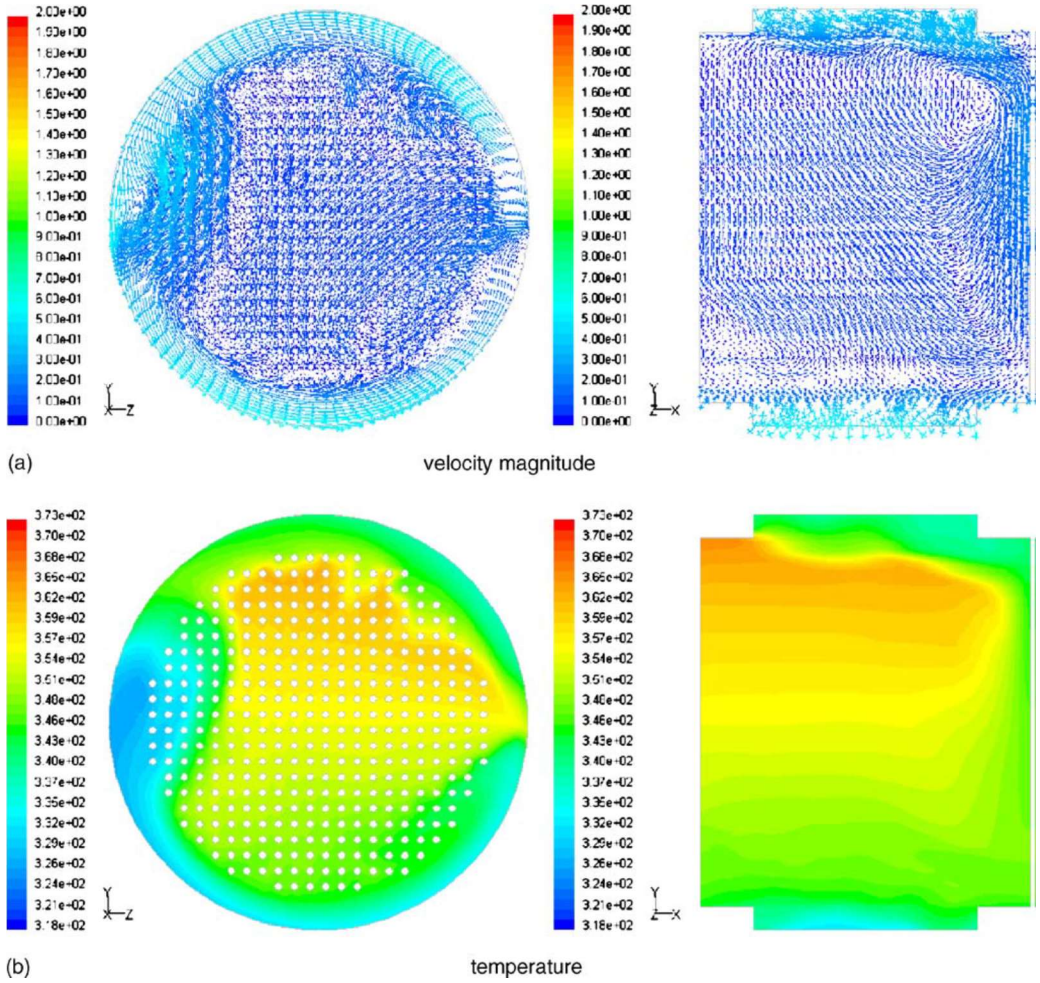

Figure 5.28: Flow velocity and temperature during normal operating conditions [140].

The results shown in Figure 5.28 indicate that the inlet flow rate and heat load to the fluid differ noticeably between the east and west sides of the calandria, i.e., the split between the Pump 1 and Pump 2 injection nozzles is not even. The two main moderator pumps are both 100% duty pumps, and in terms of design there should be very few differences. During the manufacturing process, the effort is made to ensure that the hydraulic components, namely the impeller, are consistent between both pump assemblies. It is expected that the inlet header produced for each pump is slightly different due to trivial differences in manufacturing, servicing, etc. However, due to the site design requirements for placing the pump heat exchangers in two (2) separate rooms, the flow split is approximately 55% and 45%, which is likely to cause less flow on one side of the calandria than the other.

Another significant issue for pump duty swaps is that for a very brief period, both pumps are online at the same time, which may cause some extra flow. This increase in feed to two pumps during that period can potentially introduce some turbulence in the piping. In the case study in this thesis, assuming moderator temperature coefficient is 0.067mk/degree C at 60^{o}C and the reactivity worth of all fourteen zones is 6mk, then a typical increase of 6% zone level during an oscillation event corresponds to:

$$2*0.06*6/14 = 0.05 \text{ mk or slightly higher than } 1^{o}C \qquad \text{[Equation 5.1]}$$

This is in a reasonable agreement with the assumption that slight localized changes in moderator temperature, approximately 1^{o}C, may lead to zone level increase in the affected zones. Since the zones 6/8 and 7/9 are closest to moderator Pump 2 injection nozzles, it is possible that moderator temperature is slightly different when produced by this pump.

Thus, both linear and nonlinear PCA algorithms suggest that moderator circulation at the calandria nozzles is varied, which produces local variations of the moderator temperature. These artificially induced perturbations lead to variations in localized detector measurements. The resolution of this phenomenon is outside the scope of this thesis.

5.4 Model Validation with Residual Noise, Oscillation, and Transient Data

To validate the detector model with noise and oscillation transient data, it was further tuned for the three additional cases, thus extending the existing detector modeling methodology to be applicable to operational transients. The analysis consists of three test case simulations. In each case, trends of the DSC output with the old and new gains are presented for comparison, followed by a single trend of the difference in DSC output due to the gain change. This last trend represents the MTT loss.

Case 1: Residual Detector Noise

The model for detector AF8G, shown in Figure 5.29 below, represents a modified detector model to accurately show the noisy detector's response to fueling of a nearby channel. Plant data is used as an input into the model signal building block.

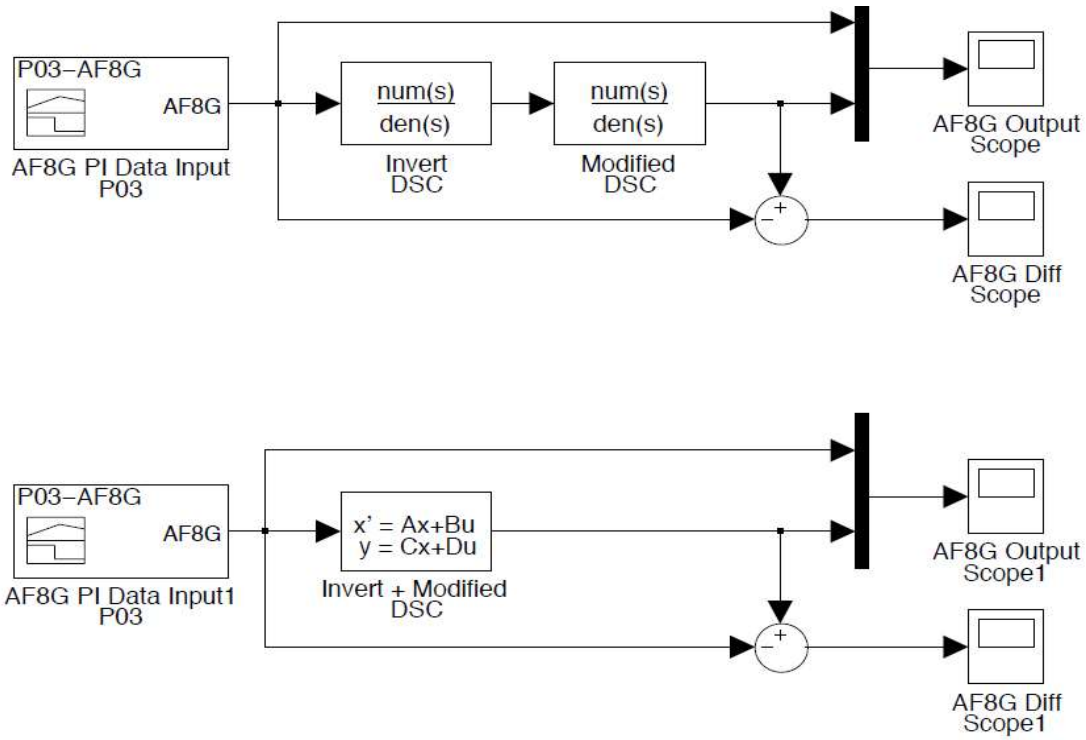

Figure 5.29: AF8G detector developed for this thesis to model noise during a fueling operation.

This case analyzed the impact of the gain factor change on the MTT during refueling of fuel channel P03, using plant data. Fuel channel P03 was selected for two reasons. Firstly, it is known to cause a high response—about 8% in this case. It is normal for certain four-bundle region channels and eight-bundle region channels refueled near detectors to show a high response. Eight-bundle region channels can have a high detector response because replacing eight bundles with fresh fuel will cause a localized power increase. In certain four-bundle and eight-bundle region channels, the bundles pushed from positions 2 and 3 are generally near their *Pu* peak and are, therefore, relatively high-power bundles when pushed through the channel. Therefore, due to either Xenon-free fresh fuel or high reactivity bundles near their *Pu* peak, a high response may be observed while fueling specific channels. Secondly, it is located in zone 7/9, which is prone to significant detector oscillations. The historical oscillation data was input into the detector AF8G model to determine its response to fueling conditions. The simulation was run for both old and new gain settings. The DSC difference (new versus old gains) is shown below in Figures 5.30 and 5.31. The yellow trace in Figure 5.30 represents the as-is configuration, the purple trace represents the result of the application of the new gains, and the residual DSC error is shown in red.

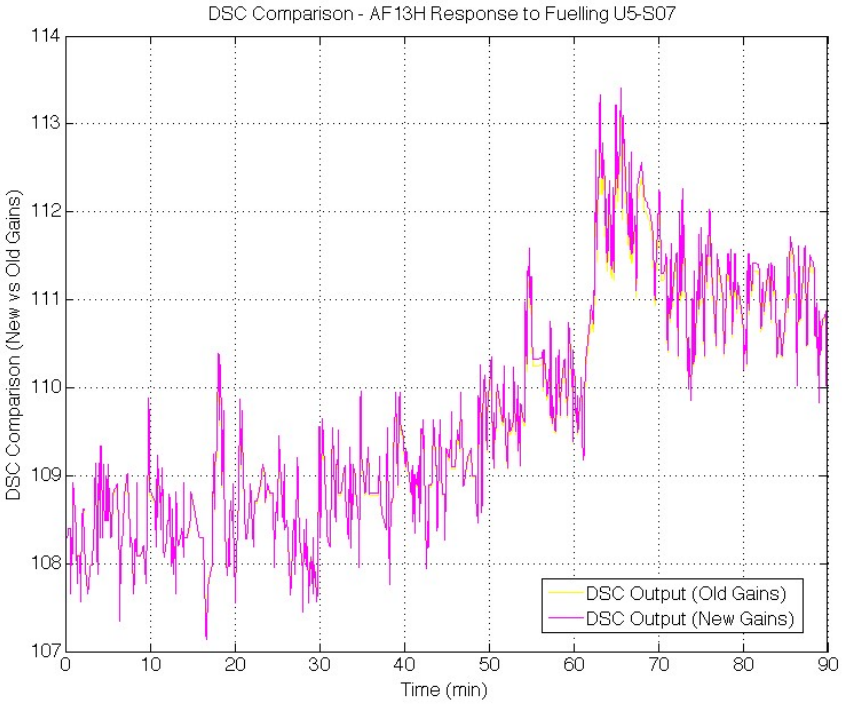

Figure 5.30: DSC comparison—AF8G response to fueling U5-P03.

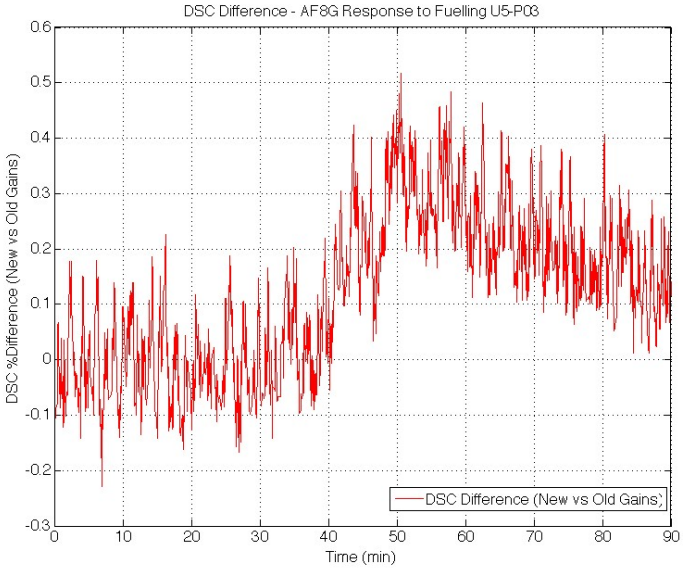

Figure 5.31: DSC difference—AF8G response to fueling channel P03; the maximum MTT loss is ≤0.5%.

The difference between the two traces in Figure 5.31 indicates the maximum MTT loss of 0.5%. These results are consistent with the theoretical predictions and are within the bounding refueling cases discussed earlier.

Case 2: Detector Signal Oscillation

The model for the detector (designated as AF13H) was developed to accurately depict the noisy detector's response to fueling of a nearby fuel channel, S07. The detector signal with oscillations is used as an input into the model signal building block. A circuit for processing plant data is added to the model to enable comparison of the predicted response with the actual plant data, as shown in Figure 5.32.

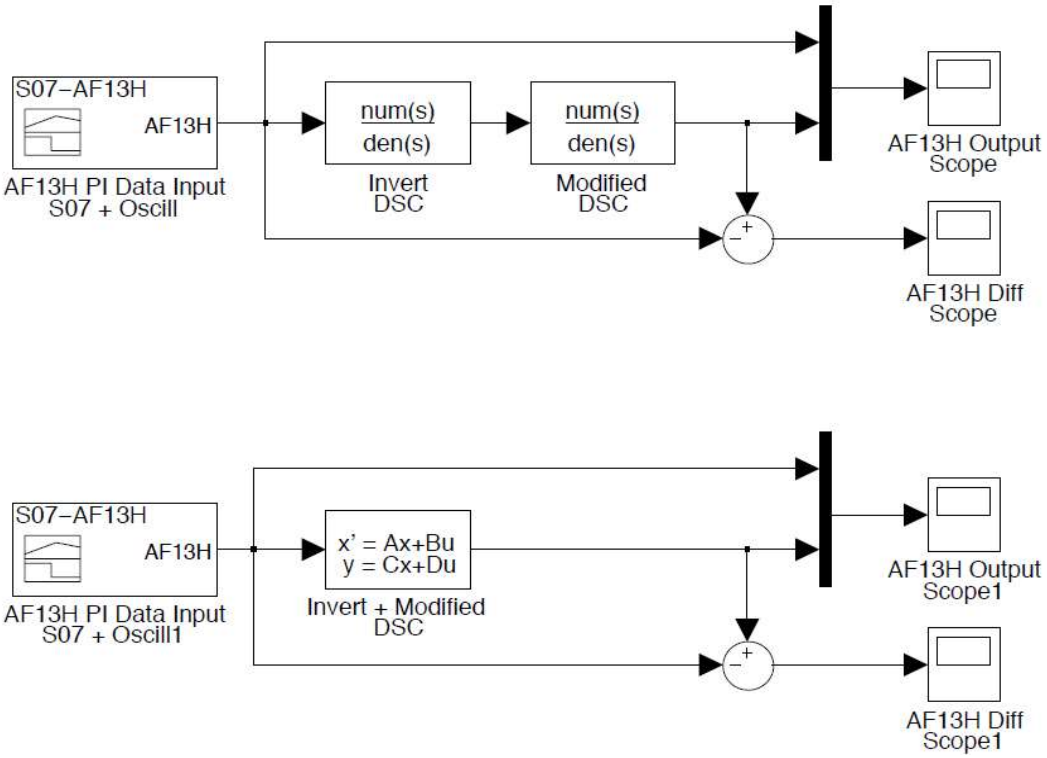

Figure 5.32: A detector model for detector AF13H. This model represents detector response during fueling coincidental with signal oscillations.

This case analyzed the impact of the gain factor change on MTT during refueling of channel S07 using plant data. Channel S07 was selected for analysis because of the signal oscillations, which are observed to occur shortly after the completion of fueling. The results of the DSC comparison are shown in Figure 5.33, where the yellow trace represents the as-is configuration, and the purple trace represents the result of the application of the new gains.

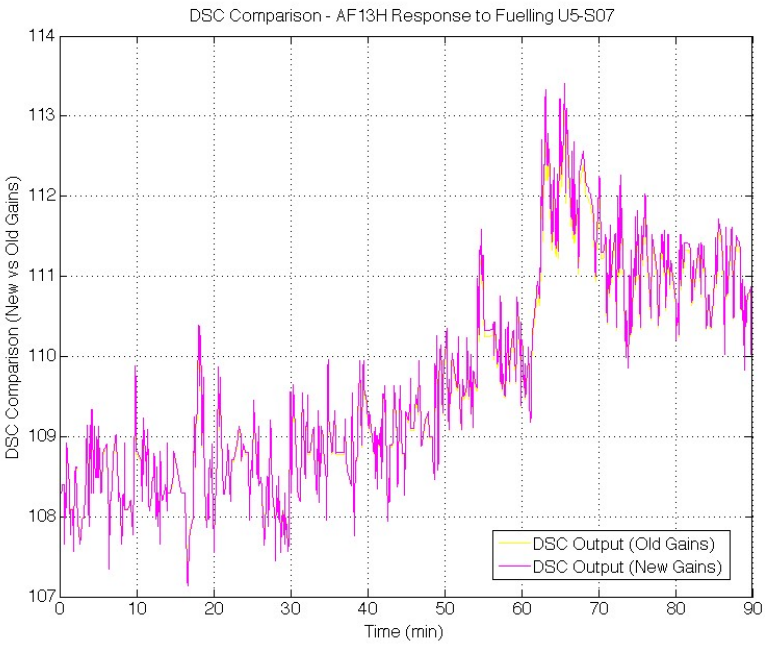

Figure 5.33: DSC comparison—detector AF13H response to fueling channel S07.

The difference between the two traces in Figure 5.34 indicates that the maximum MTT loss occurs during the noted variations and has a magnitude of 0.25%. These results are consistent with the theoretical predictions and are within the bounding refueling cases discussed earlier.

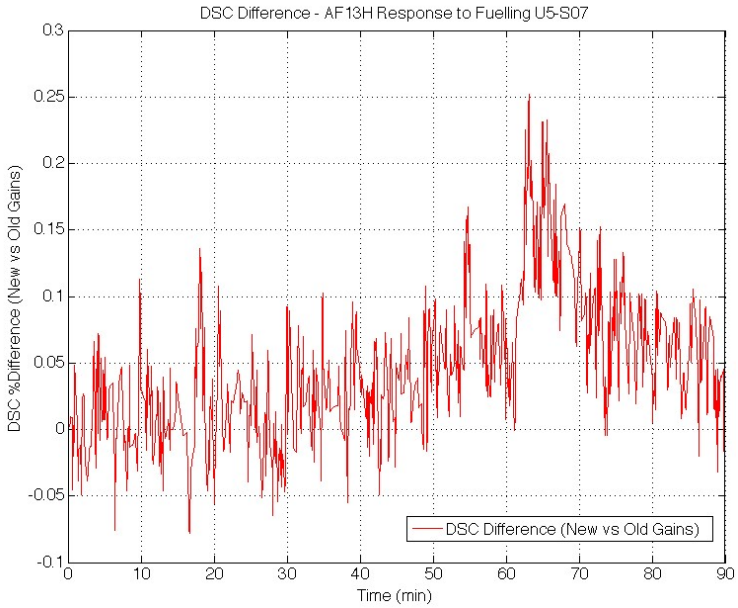

Figure 5.34: DSC difference—detector AF13H response to fueling channel S07; the maximum MTT loss is ≤0.25%.

Case 3: Power Ramp-Up—Transient Data

This transient condition case was selected next to test the model response over the full range of power spectrum using historical power ramp-up data. A detector (designated as AF3H) was chosen to represent response during the reactor unit start-up, particularly in terms of the model dynamic changes in reactor power. Plant data is used as input into the model signal building block, as shown in Figure 5.35.

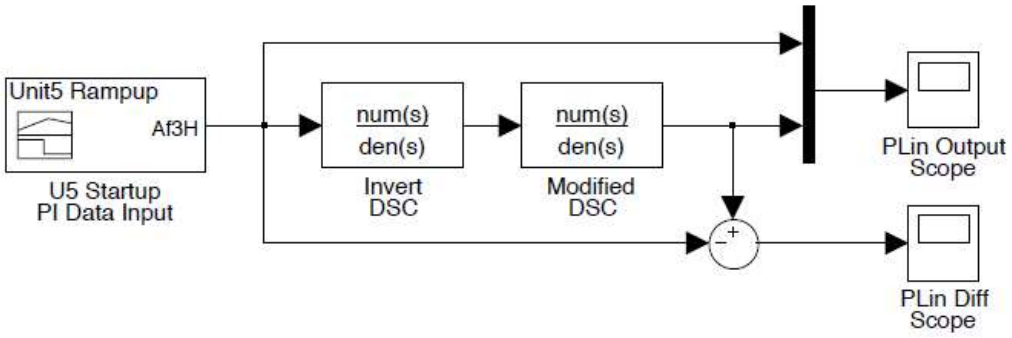

Figure 5.35: A detector model developed for detector AF3H to represent a power increase and dynamic response during reactor unit start-up.

This final case considers the impact of the proposed gain factor change on the power raise profile after an outage. Power changes during start-up may be significantly greater than those caused by fueling. This was the primary reason this case was chosen for scrutiny. Data for analysis was collected for detector AF3H reactor start-up in May 2015. The results are shown below in Figure 5.36, where the yellow trace represents the as-is configuration, and the purple trace represents the result of the application of the new gains.

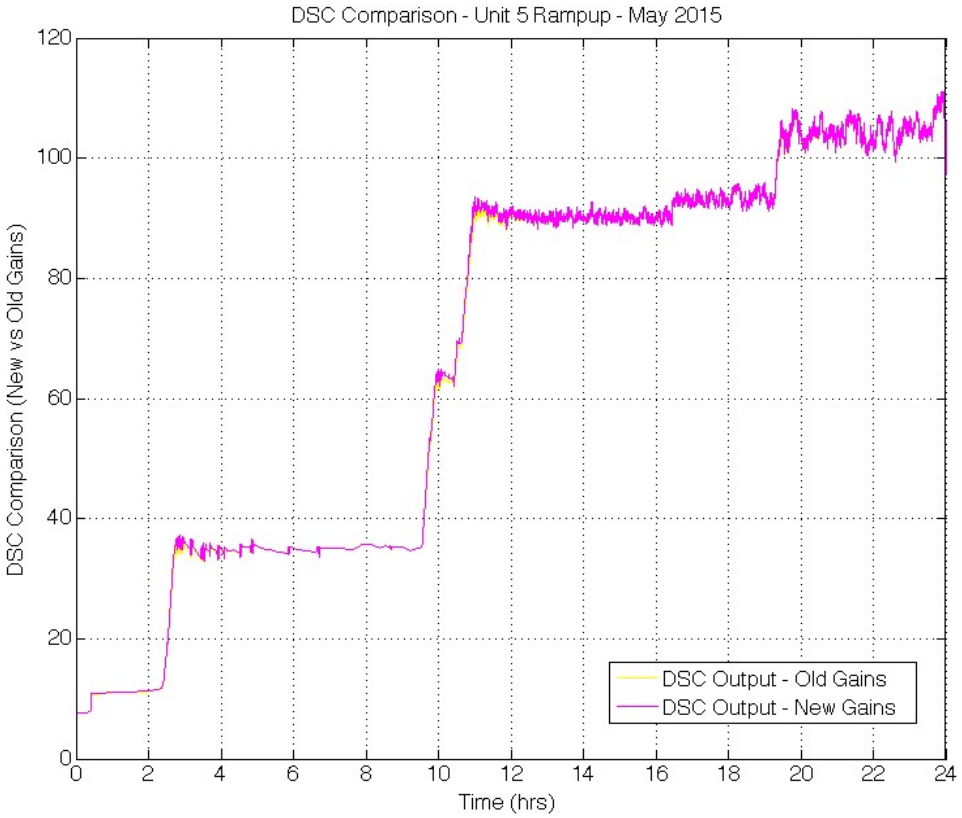

Figure 5.36: Reactor power ramp-up profile, May 2015.

The difference between the two traces in Figure 5.37 indicates the maximum the maximum MTT loss of 1.4%.

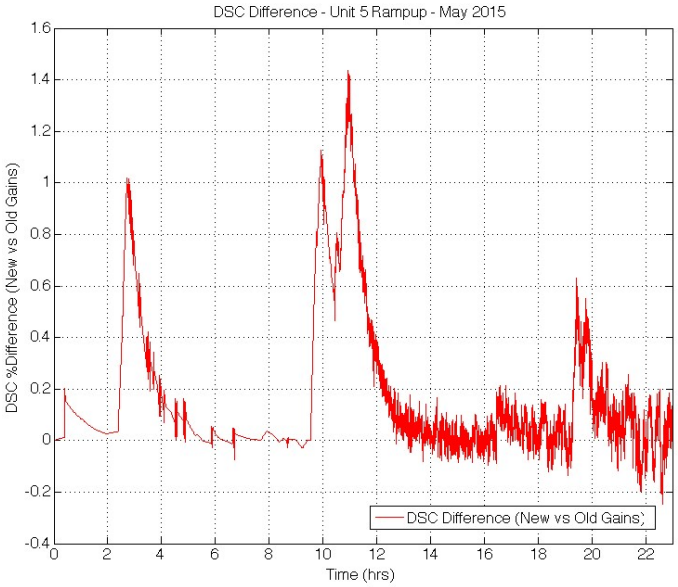

Figure 5.37: DSC difference—power ramp-up, May 2015; the maximum MTT loss is >1.4 %.

Throughout the ramp-up, the MTT remained greater than 10% FP with the revised gains. However, the impact of each step in power change on the MTT can be distinctly observed in the spikes in figure 5.37. The maximum MTT loss is 1.4% and occurs after the power raise from 63 to 90%. The effect on a step change in power is then calculated to a first order as follows:

$$\Delta MTT = \Delta Power\ (New\ Static\ Gain/Old\ Static\ Gain\ -1) \qquad [Equation\ 5.2]$$

The result of this calculation is:

$$(90 - 63) * \left(\frac{1.15}{1.066} - 1\right) = 2.1\%.$$

This exceeds the stylized ramp case in the FUELPIN prediction.

5.5 DSC Gain Optimization with GA

The solution to the DSC case study problem where the MTT loss exceeded the boundary condition of 1.0%, discussed in the previous section, was obtained using the genetic algorithm solver in MATLAB. The initial results for the optimized DSC gain solution are: [K_1, K_2, K_3] = [1.105, -0.035, -0.070]. The following Simulink DSC model, shown in Figure 5.38, was developed to visualize the solution, and represents a breakdown of the DSC state space model into a form that explicitly shows the gain parameters.

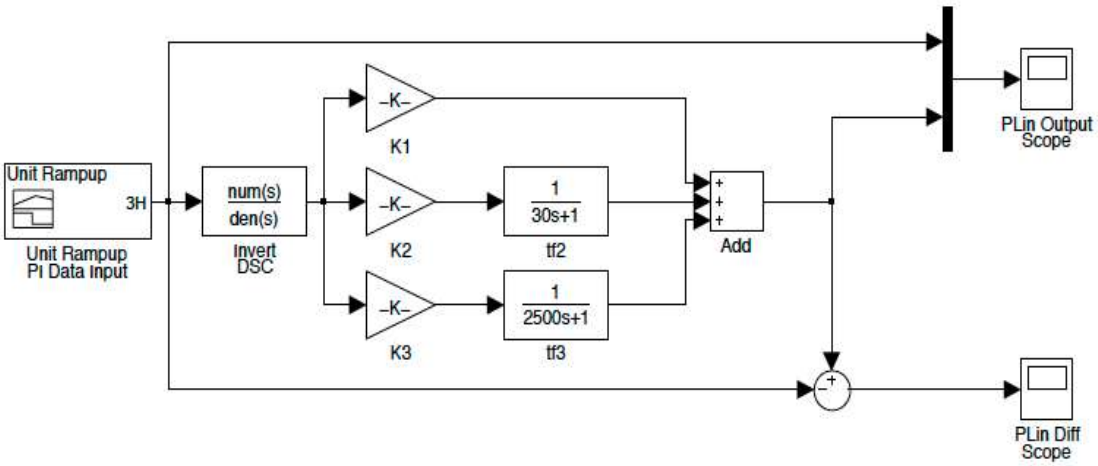

Figure 5.38: The breakdown of the DSC state space model to show the gain parameters.

The impact of the GA DSC gains on the MTT for the reactor power ramp-up case study is shown in the trend in Figure 5.39 below:

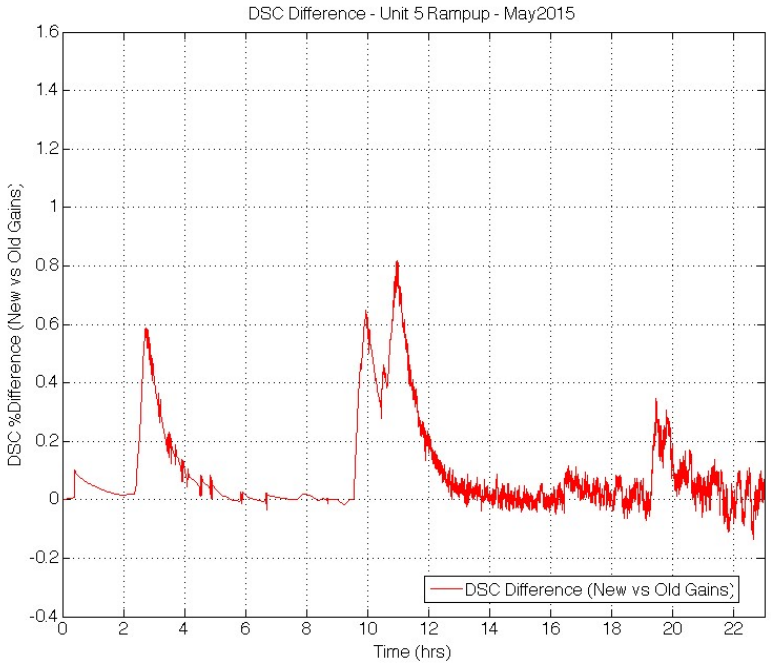

Figure 5.39: The MTT loss with the GA-optimized gains is shown for the ramp-up case.

Similar to the ramp-up case, the required safety analysis PF improvement target of 3% was met. The margin loss during the reactor power ramp-up with the new GA gains is 0.88%. This is contrasted against the design gain case, where the margin loss is 1.4%.

Additional Tuning:

With subsequent model tuning (shown in Figure 5.40) and additional iterations of the algorithm, the results of the GA run (including diagnostic, and iteration data) were further tuned and the solution is: $[K_1, K_2, K_3] = [1.1090, -0.0373, -0.0717]$.

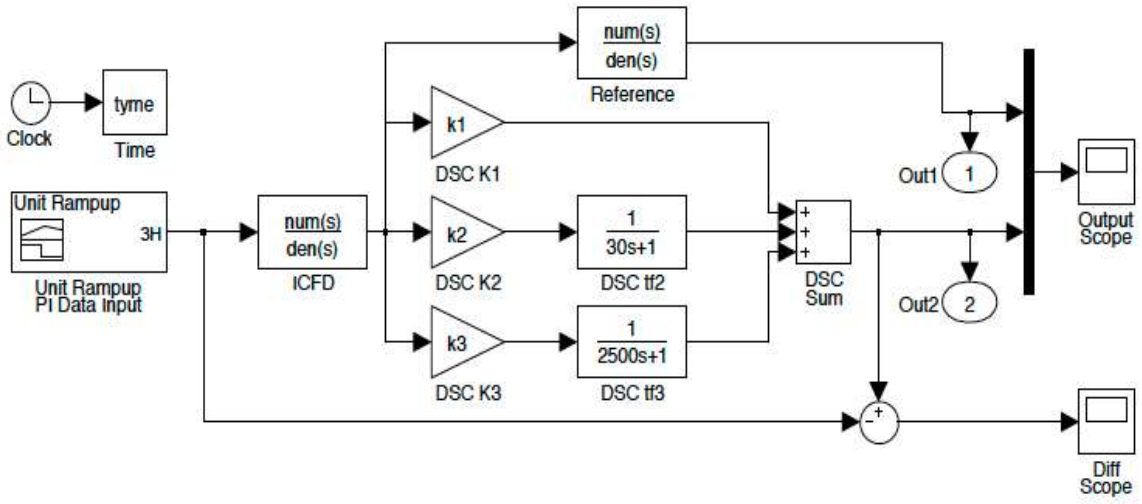

Figure 5.40: The final Simulink model with the breakdown of the DSC state space model to show the gain parameters.

The margin loss during the reactor power ramp-up with the GA gains is 0.8%. This is contrasted against the design limit case, where the margin loss is 1.4%. The impact of the GA DSC gains on the MTT for the reactor power ramp-up case is shown in Figure 5.41:

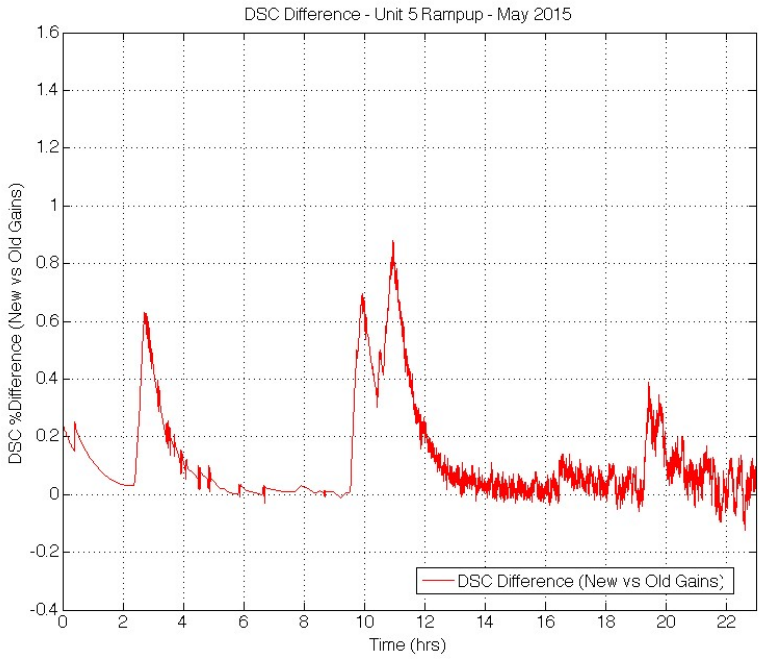

Figure 5.41: The MTT loss with the final GA-optimized gains is shown for the ramp-up case.

Thus, it can be concluded that the GA gains are an improvement over the design limit solution, meeting safety requirements and leaving a margin for further improvement in the future. It is importance to note that the obtained optimized results may not represent the best possible solution for DSC gains. There is no guarantee that a solution will be found or that a solution will be optimal. New generations of solutions are iteratively produced and evaluated until a termination condition is reached, e.g., if the desired fitness level has been attained. Using the GA method, it is possible to obtain efficiency improvements, which is shown in the thesis.

In this case, the margin loss during the reactor power ramp-up with the GA gains is 0.88%. This is contrasted against the design limit case, where the margin loss is 1.4%. With subsequent iterations, it is possible to achieve further improvement to 0.8%. Thus, with the use of the proposed methods, the GA gains are an improvement over the design limit solution. Further gains can be made if boundary conditions are tightened during subsequent GA runs based on past solution results. This, for example, can be done to ensure the solution will meet DSC hardware limitations.

5.6 Risk Estimation with FSN—Results

In this section, the result of an FSN/Bayesian-based approach for risk estimation (discussed in Chapter 3) is demonstrated considering the impact of detector noise and signal oscillations. The historical plant data was used to determine the acceptability of the risk increment. In this case, the process is subject to the change of gain, change of input signal, detector bias, and change of variance in the measurement disturbance. Therefore, the detector can be shown as follows:

$$y = Ku + f + e \qquad \text{[Equation 5.3]}$$

$$e \approx N(0, \sigma^2) \qquad \text{[Equation 5.4]}$$

where:

- y – sensor reading,
- K – process gain, K = [1, 0] corresponding to normal and abnormal operation,
- u – input, u = [-1, 0, and 1],
- f – sensor bias, f= [0 ,1] for bias and non-bias,
- e – noise,
- σ^2 – variance, σ^2 = [1,2] for normal and abnormal sensor noise.

Next, the conditional probability distribution (the detector reading node) is built according to noise distribution equation. The joint distribution among the remaining six (6) random variables can be established for:

- sensor bias,
- process input,
- process gain,
- noise variance,
- noise,
- sensor reading,

Through Bayes's theorem, probabilistic inferences are made, e.g., for a given time instance, there are two readings available, namely the input reading and detector output reading: u =1, y = 0.7. Next, the following posterior (probabilities conditioned on the measurements) can be calculated as:

- $P(Sensor = Bias|E) = 97\%$,
- $P(\mathrm{Pr}ocesGain = Abnormal|E) = 98.7\%$,
- $P(NoiseVariance = normal|E) = 74.1\%$, where E represents all evidence (measurements) available.

Based on the results of the Bayesian calculation, it can be concluded, with at least 97% probability, that the detector in question had bias, and process gain is abnormal. Also, the results show that noise variance is likely to be normal with 74.1% probability. Once noise is confirmed, a decision to continue operation of the system for a short period of time (e.g., one (1) week or one (1) month), must be made.

Case 1: Detector Noise

In this example, this neutron detector is assumed to be in a particular configuration (detector noise identified based on the noisy sensor analysis) for one (1) month. The detector in this case belongs to the equipment class of NOP_Det_01 with a failure mode (FM) of noise or NS_01. The

consequence of this FM (FM_Conseq = PS_01) is the inability to continue system operation, as shown in Table 5.8.

Table 5. 8: System equipment, FM, and consequence table for the detector in this case study. The detector belongs to the equipment class of NOP_Det_01 with an FM of noise, or NS_01.

Equipment	Equipment ID (Eq_ID)	Function	Failure Mode (FM)	FM_ID	Failure Cause (FM_Cause)	FM_Cause_ID	Consequence (FM_Conseq)	FM_Conseq _ID
Guide Tube	GT_01	Housing for detectors	Not fitting into the VP opening	Mech_01	Wrong size or concentricity during fabrication	FB_01	Unable to proceed with detector install	IN_01
Junction Box	JB_01	Holds cable conductor terminations and splices	Failure to protect terminations and splices	TR-01	Moisture	HM_01	Loss of power control	PS_01
			Line to Line insulation failure	IN_01			Loss of signal circuits	SG_01
Connector	CC_01	Connects cables	Line to ground insulation failure	GR_01	Exposure to high temp	TM_01	Signal/Current distortion	DS_01
			Line to line insulation failure	LL_01	Exposure to radiation	RD_01	Voltage collapse	VC_01
					Humidity	HM_02	Cross failure fail shot	SH_01
Cable	CB_01	Current/Voltage Conductor	Line to ground insulation failure	GR_01	Exposure to high temp	TM_01	Signal/Current distortion	DS_02
			Line to line insulation failure	LL_01	Exposure to radiation	RD_01	Voltage collapse	PS_02
					Humidity	HM_02	Cross failure fail shot	SH_02
Detector	NOP_Det_01	Neutron detection	Failure to respond	FF_00	Manufacturing defects	FB_01	Functional Failure - Unable to operate the system	FF_01
			Sensitivity too high	PF_01	Wrong type or model	MD_01		
			Sensitivity too low	PF_02	Ageing	MD_02		
			Noisy signal	NS_01	Reduction in high voltage supply values could result in a failed signal.	PS_04		
NimBin Electronics	NB_01	Signal processing and conversion	Signal distortion	SD_01	Component failure	CF_01	Signal/Current distortion	SD_01
			Loss of signal	LS_01	Power supply failure	PS_01	Loss of signal circuits	SC_01
Amplifier Assembly	AF_01	Converts detector current and shapes pulses	Drift	DR_01	Reduction in high voltage supply values could result in a failed signal.	PS_01	Channel trip	CT_01
			HV Bi-stable set-point	HV_01				
			Noisy signal	NS_01				
Power Supply	PS-01	Power supply for system components	Fuse failure	FS_01	Overload	OV_01	Loss of power control	PC_01
			A/C ripple out of spec	AC_01	Loose connections	LC_01	Loss of signal circuits	SC_02
					Humidity	HM_01		
					EM pickup	EM_01		
					Failure of cooling fan	FN_01		

The following sample failure data was collected and processed using an FSN, as shown in Table 5.9:

Table 5.9: Failure data for Case 1—equipment class is neutron detectors, and the failure mode is "functional failure—noise."

Equipment Class Eq_Class_ID	Failure Mode FM_ID	Highest Failure Rate (f/1000 yrs)
NOP_Det	FF_001 (noise_HIGH)	0.9
NOP_Det	FF_001 (noise_LOW)	0.1

Next, it is necessary to decide whether there will be a significant safety impact if the system remains in service. Per the collected data, the failure rates can be determined as shown in in Table 5.10:

Table 5.10: Breakdown of failure data for Case 1—equipment class is neutron detectors, and the failure mode is "functional failure—noise."

Failure Rate FR (f/1000y)	FM_ID	Rate	
Highest	NOP_Det_FF-001	0.9	
Lowest	NOP_Det_FF-002	0.1	
Discarded	None		
Geometric mean	-	0.3	
Selected FR	NOP_Det_FF-001	0.9	
MTTR for the selected FR	NOP_Det_FF-001	12	2.0E-04
FR for the required FM	FF_001	0.9	(f/m/h)

The instantaneous risk is calculated as $2*10^{-4}$/year. The sum of all risks of all maintenance activities (ΣRmtce) is $5*10^{-6}$/year, while the current risk baseline frequency is $2*10^{-5}$/year. The available margin can be calculated as:

$$2*10^{-4}\text{/year} - 2*10^{-5}\text{/year} = 18*10^{-5}\text{/year}$$

If the instantaneous risk is $2*10^{-4}$/year , the Risk Increment can be calculated as follows:

$$RI=(IR_i - BR)* \Delta T/8760hr = ((IR_i - BR)* 0.0821 = 1.482*10^{-5} = 1.5*10^{-5}\text{/year}$$

In this case, the magnitude of the acceptable risk increment (RI), including all other maintenance activities, must be limited to 10% of the available margin:

$$(RI + \Sigma R_{mtce}*4) = (1.5*10^{-5} + 5*10^{-6})*4 = 20^{-6}*4 = 8*10^{-5}\text{/year}$$

This is significantly above the $0.2*10^{-5}$/year limit stipulated above. Therefore, an immediate compensatory action is required for this detector.

Case 2: Signal Oscillations

In this example, a neutron detector is assumed to be in a particular configuration (frequent signal oscillations) for two (2) weeks. It is necessary to determine whether there will be a significant safety impact if the system remains in service. Historical failure data was collected for this case, as shown in Table 5.11 and 5.12 below.

Table 5.11: Failure data for Case 2—equipment class is neutron detectors, and the failure mode is "functional failure—oscillation."

Equipment Class Eq_Class_ID	Failure Mode FM_ID	Highest Failure Rate (f/1000 yrs)
NOP_Det	FF_003 (osc_TRUE)	11.9

Table 5.12: Breakdown of failure data for Case 2—equipment class is detectors, and the failure mode is "functional failure—oscillation."

Failure Rate FR (f/1000y)	FM_ID	Rate	
Highest	NOP_Det_FF-003	11.9	
Lowest	NOP_Det_FF-003	11.9	
Discarded	None		
Geometeric mean		11.9	
Selected FR	NOP_Det_FF-001	11.9	
MTTR for the selected FR	NOP_Det_FF-001	3	
FR for the required FM	FF_003	0.9	1.5E-04 (f/m/h)

The instantaneous risk is calculated as $1.5*10^{-4}$/year. The sum of all risks of all maintenance activities (ΣR_{mtce}) is $8*10^{-6}$/year while the current risk baseline frequency is $2*10^{-5}$/year. In this case, the available margin can be calculated as:

$$1*10^{-4}\text{/year} - 2*10^{-5}\text{/year} = 8*10^{-5}\text{/year}$$

Thus, for the risk activity of two (2) weeks that introduces an instantaneous risk of $1.5*10^{-4}$/year, the RI can be calculated as follows:

$$RI=(IR_i - BR)* 336/8760 =(1.5*10^{-4}-0.2*10^{-4})*336/8760=(5.0*10^{-6})\text{/year}$$

This risk activity meets the limiting criterion since the associated RI is 6.2% (i.e., less than 10%) of the available margin of $8*10^{-5}$/year. Therefore, immediate compensatory action is not required for this detector.

Case 3: Aggregate Risk—Coincidental Noise and Signal Oscillations

A component/system failure rate and test interval can be assigned to the basic failure event to derive a failure-on-demand probability. For example, for a particular neutron detector, a

failure rate and test interval are assigned to the component to derive a failure-on-demand probability, as shown in Table 5.13.

Table 5.13: Various failure rates for neutron detectors obtained using historical data.

Highest Failure Rate (f/1000y)	0.1
Lowest Failure Rate (f/1000y)	0.0045
Discarded failure rate (f/1000y)	0
Mean of failure rates (f/1000y)	0.021213203
Selected failure rate (f/1000y)	0.1
MTTR for selected failure rate (hours)	40

Next, the three (3) most prominent failure mode IDs are selected for analysis as shown in Table 5.14 below:

Table 5.14: Sample failure rates for three (3) separate failure modes affecting the detector.

FM Class ID	Highest failure rate (f/m/1000 years)
FM_1	0.1
FM_2	0
FM_3	0.0045

The failure rate for selected failure modes is then calculated as follows in Table 5.15:

Table 5.15: Calculated failure modes for the selected FM_IDs.

(f/m/1000 years)	(f/m/h)
0.1	1.14E-08

The aggregate risk due to both types of degradation in the system can be calculated as: $*10^{-6}$ $+5*10^{-6}=13*10^{-6}$/year. If the acceptable risk due to all degradation is defined as 25% of the available margin, then the aggregate risk of $13*10^{-6}$/year can be expressed as 16.2%. This is still below the limiting criterion, and immediate detector replacement is not required as shown in Figure 5.42. The risk increment of $5*10^{-6}$ /year, shown in blue is less than the 10% of the available margin of $8*10^{-5}$/year.

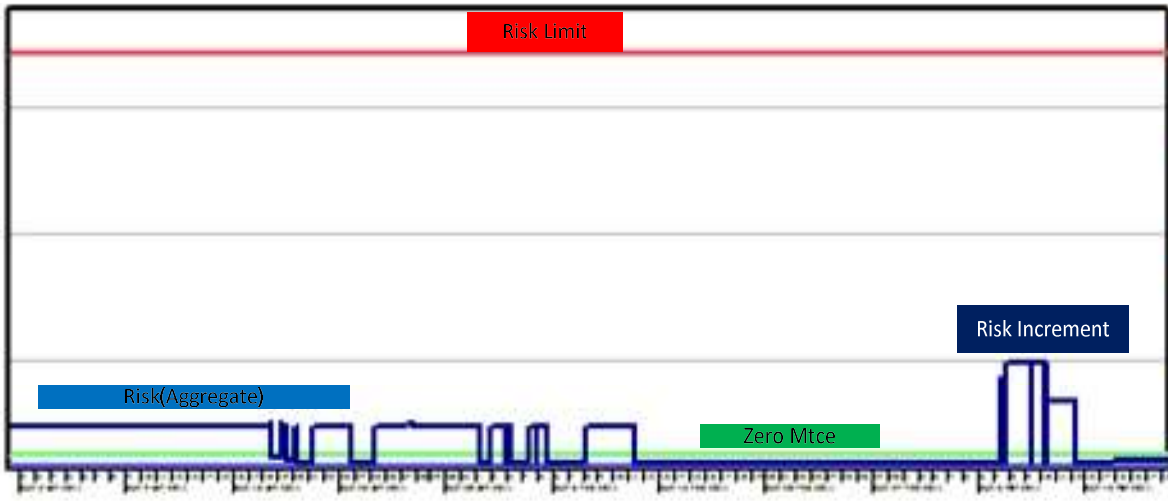

Figure 5.42: Updated risk profile, where risk increment changes over time due to system configuration, e.g., detector noise.

Based on the above discussion, an immediate detector replacement is not required, and delaying detector replacement can be justified. However, some mitigating actions are needed since there is a significant safety impact if the system is allowed to remain in service in its current state.

The risk due to the detector behavior is defined by two (2) quantities: the magnitude (severity) of the possible adverse consequences and the likelihood (probability) of occurrence of each consequence. The consequences can be expressed numerically, and their likelihoods of occurrence can be expressed as probabilities or frequencies (i.e., the number of occurrences or the probability of occurrence per unit time). The total risk is the sum of the products of the consequences multiplied by their probabilities. The magnitude of risk defines the risk category of the channel, e.g., the highest risk factor of "2" is assigned

based on the probability of a complete shutdown system trip due to the detector response. This is summarized in Table 5.16 below.

Initially it was assumed that all channels would fall into one of two categories, risk category 1 or risk category 2, since there was not enough current operating experience on how these channels respond. In this study, it was conservatively assumed that under abnormal circumstances (low zone levels, high burnup, and low MTT) there is a low risk of channel or completed trips. Subsequently, category 1 was further divided into two (2) subcategories, 1A and 1B, based on the projected magnitude of risk. Category 1A contains low-risk channels that could result in single-channel or full trips. Category 1B risk channels contain a high risk of single-channel trips, but there is no risk of completed system trips. Although the production risk is low for these channels, all neutron detector trips are reportable to the federal regulator and should be avoided.

Table 5.16: Risk categorization matrix. The highest risk value is assigned to a complete shutdown system trip.

Risk Value	Definition
2	High risk of a complete shutdown system trip
1B	Single-channel trip
1A	Low risk but potential for trip

Category-2 risk contains high-risk channels where completed trips could occur, based on detector location and operating experience. Risk category information for all reactor channels is analyzed next. Initially, no channels are categorized in relation to risk estimated for fueling operation near in-core detectors. With the static FSN, the locations of high-risk channels are mapped with their respective risk categories, as shown in Table 5.17.

Table 5.17: Categorization of all eight-bundle channels according to the risk matrix.

Risk Cat 2	Risk Cat 1B	Risk Cat 1A
D05	J02	G02
D20	J23	G23
E04	K01	H02
E21	K24	H23
F03	P01	R02
F22	P24	R23
S02	Q02	U04
S23	Q23	U21
T03		V05
T22		V20
Y12		X11
Y13		X14

Based on the risk category, a set of mitigating actions can be developed for each risk factor as shown in Table 5.18 below:

Table 5.18: Actions for each risk category.

Risk Value	Definition	Actions prior to Fueling
2	High risk of a complete shutdown system trip	• Ensure at least 12% MTT prior to fueling • Ensure no channels are rejected during fueling
1B	Single-channel trip	• Ensure at least 10% MTT prior to fueling • Ensure no channels are rejected during fueling
1A	Low risk but potential for trip	• Ensure at least 8% MTT prior to fueling • Ensure no channels are rejected during fueling

Based on this guidance, the appropriate action is taken in accordance with the risk categorization, as shown in Figure 5.43.

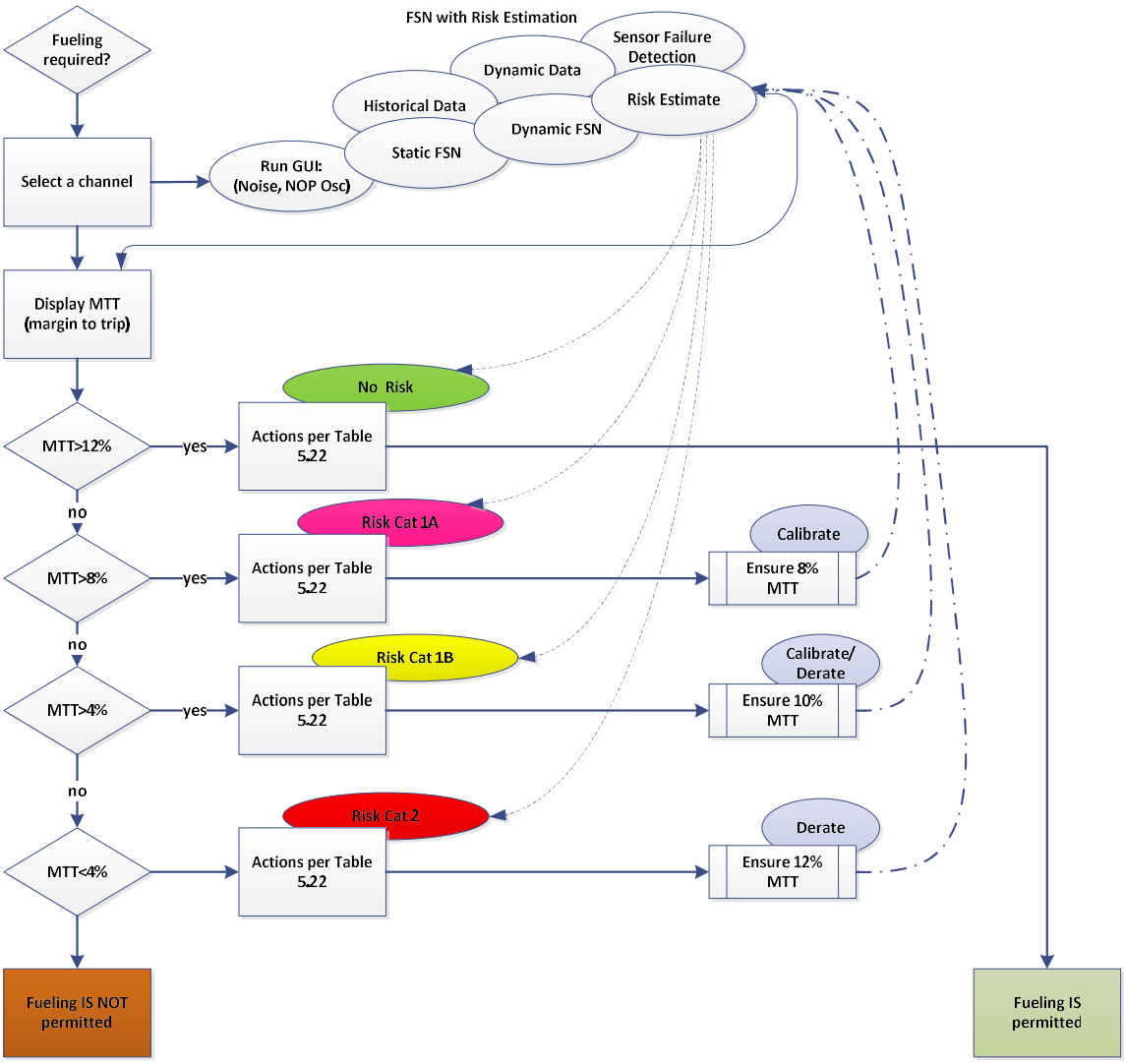

Figure 5.43: Flowchart for action response in case of the detector noise/malfunction challenging MTT prior to fueling.

The detector H3 shows high response during steady-state operation and presents a potential risk for fueling, as shown in Chapter 4. Noise on detector H3 is significantly higher than on the adjacent detector G12 and often challenges both MTT limits. Based on the risk

mitigation matrix, the reactor power was de-rated at 23:02 to bring the detector signal back into the allowable MTT. The resultant impact on MTT is shown below in Figure 5.44.

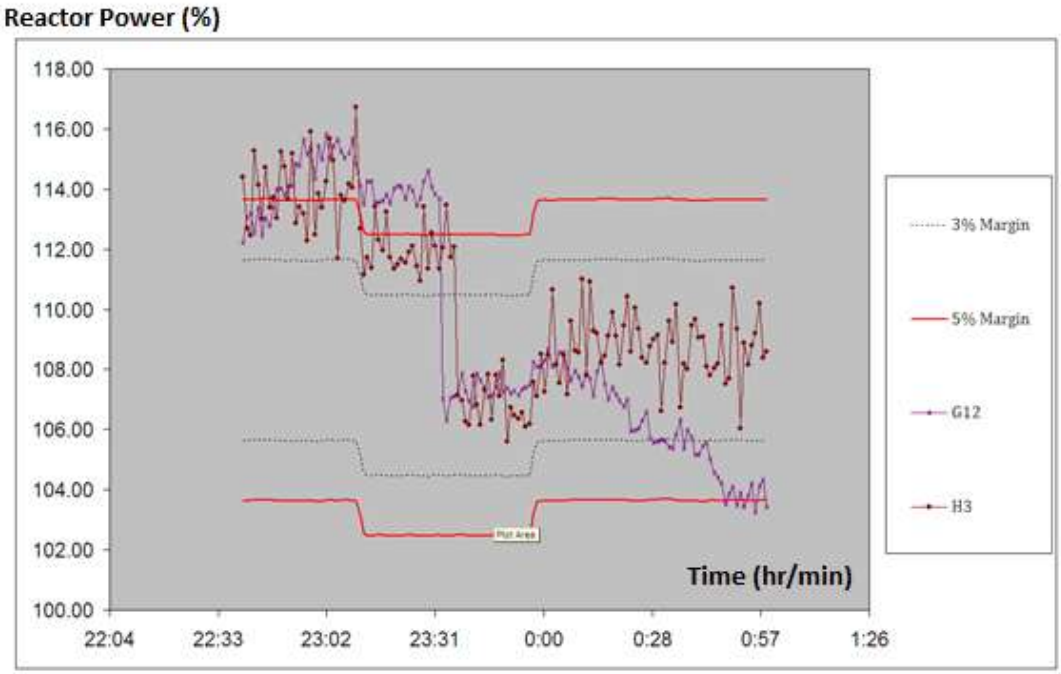

Figure 5.44: Operational response to a high-risk trend developing for detector AF3H. Reactor power is de-rated at 23:02 to increase the available MTT and bring the detector response back into the acceptable band (in red).

Once the model is established using historical data, the detector response data are collected daily and trended to determine the risk factor for all channels. As the new information becomes available, the model is modified to improve accuracy and completeness. The initial channel table is updated, as shown below, along with the channel risk prioritization map. Since enough channels were confirmed to fall under the risk criteria for 1A or 1B, this category was modified into two (2) independent categories, B and C, with the associated risk factors of 10% and 8% risk, respectively. The channel mapping is updated to reflect the latest findings. The risk categorization in Table 5.19 applies any time four (4) bundles are fueled in the four-bundle region or eight (8) bundles are fueled in the eight-bundle region.

Table 5.19: The updated channel table. Channels are updated as the new information becomes available. A4, B4 = four-bundle push; A8, B8 = eight-bundle push; C = four-bundle and eight-bundle push.

Risk Category A (12% MTT)		**Risk Category B (10% MTT)**		**Risk Category C (8% MTT)**
A4-bundle	A8-bundle	B4-bundle	B8-bundle	4/8bundle
J03	D04	K02	F03	G02
J22	D05	K23	F22	G23
K03	D20	M04	J02	S02
K22	D21	M21	J23	S23
L04	E04	O03	Q01	X11
L21	E21	O04	Q24	X14
P03	H02	O21	T03	
P22	H23	O22	T22	
P04	J01	P02	V05	
P21	J24	P23	V20	
	K01	Q03		
	K24	Q22		
	L01	W12		
	L24	W13		
	O01			
	O24			
	P01			
	P24			
	Q02			
	Q23			
	R02			
	R23			
	U04			
	U21			
	Y12			
	Y13			

5.7 Summary of Results

The results of testing new detector models, denoising and dimensionality reduction, PF optimization, and risk estimation results are summarized in Table 5.20, while final

discussions of these results regarding the research objectives, along with conclusions and suggestions for future work, are presented in the next and final chapter of this thesis.

Table 5.20: Results summary table.

Case	Description	Execution	Performance Criteria	Discussion of Results
5.1.1	Model Validation	Detector responses to fueling and oscillations assumed to be 10% of full power and 6% respectively.	Detector response to the power ramp of 16% in ten (10) seconds.	Comparison of old versus new DSC gains and comparison to FUELPIN predictions
5.1.2	DSC Difference	16% Ramp/10 sec for aged detectors	MTT loss ≤1%	The maximum MTT loss due to the gain change was 1.0%
5.2.1	Denoising and Smoothing of Data	LPF	SNR ≥110/1	SNR of 122.9 (Tri), 92.5 (Rec), 142.1 (Gaussian), 92.5 (S-G)
5.2.2	Denoising and Smoothing of Data with WTA	MWT	SNR ≥110/1	Peak SNR = 31.308271, 31.316610, 31.308271
5.3.1	Dimensionality Reduction	PCA	95% of the total variance.	X2 and X6 (calandria inlet temperature and pressure)

5.3.2	Dimensionality Reduction	wPCA	95% of the total variance.	X3, X4 (pump bearing temperature for Pump1 and Pump2)

Table 5.20: Results summary table (continued).

Case	Description	Execution	Performance Criteria	Discussion of Results
5.3.3	Dimensionality Reduction for Non-linear Data	NLPCA	Check for non-linear behavior based on pattern recognition in a 3D PC space.	The training error decreases sharply when the number of iterations increases and reaches a level of 0.6246 at 1200 iteration.
5.4.	DSC Model for Transient Scenarios	Application of the new gains	Residual DSC error ≤1%	Min. residual DSC error = 0.25%, max. residual DSC error =2.1% for transient power case.
5.5	Optimization of DSC gain coefficients	GA solver in MATLAB	Residual DSC error ≤1%	Min. residual DSC error = 0.8%, max. residual DSC error = 0.88% for transient power case.
5.6	Risk Estimation	FSN	Qualitative/quantitative	Case 1: (RI) = 8*10–5/year (significantly above the 0.2*10–5/year). An immediate compensatory action is required. Case 2: (RI) = 6.2% (i.e., less than 10%) of the available margin of 8*10–5/year.

				No immediate compensatory action is required.

Chapter 6: Conclusions and Future Work

This final chapter of the thesis presents conclusions, significance of results, and suggestions for future work.

6.1. Conclusions

With the nuclear energy industry realigning itself toward life-extension projects, additional tools and methods are required to ensure that effective performance optimization methods are available. Commercial awareness is increasingly becoming one of the major business drivers for all utilities. Initiatives that have a real impact on the successful delivery of life-extension projects are a welcome addition to an existing suite of tools and approaches. As discussed in Chapter 1, the main problem to address in this thesis is improving the effective PFs for aged detectors, which may delay the need for detector replacement. Therefore, the overarching target of this research was to propose a methodology for optimization of detector performance to mitigate detector aging effects without adversely affecting the operational MTT. To achieve this objective, the following work was performed:

1. In-core neutron detector design and properties were analyzed, and new detector models were developed using mathematical models. A simulation model for aged in-core neutron detector was developed in Simulink. The model employed two noise reduction techniques, LPF and WTA. Resultant SNRs were used as performance criterion to compare the two methods. LPF yielded the maximum SNR of 142.5 as compared to 31.5 for WTA. For dimensionality reduction of the detector data, three methods were investigated: PCA, wPCA, and NLPCA with ANNs. Both PCAs and NLPCAs were successful at reducing the dimensionality of the dataset and identifying patterns of interest.

2. The model was validated using plant data for the case of 16% power ramp in 10 seconds, which represents the same theoretical scenario as used in the similar case in FUELPIN reference code. The obtained residual DSC error was compared to the

bounding criteria (≤1% loss of MTT) by FUELPIN code. The model performed in agreement with the theoretical predictions with no discrepancies.

3. The model was customized to include three typical plant transient scenarios: detector noise, acyclic detector signal variations, and a full power ramp-up. The three resultant models were validated for the case of maximum DSC gain settings, which represent the worst-case scenario for each transient. The results were compared to the predictions for the maximum residual DSC error. In the first two cases, the residual DSC error was found to be acceptable (≤1% loss of MTT). The maximum loss to MTT in the first case of a noisy detector was ≤0.5%, while the maximum loss to MTT in the second case of a detector signal oscillation was ≤0.25%. The results of the third case (simulating a full power ramp-up maneuver) were poor, i.e., 1.4% DSC error.

4. To translate the maximum DSC error into the effective MTT loss, an equation was developed for calculation of MTT for changing power conditions. The result for this case study was found to be 2.1%.

5. To improve the impact on the MTT, the models were further tuned with the new DSC gain settings, obtained with an enhanced GA. A GA was selected as a heuristic technique for solving optimization and search problem where the DSC function was the objective function and the detector function was the fitness function. Two new sets of DSC gain constants were obtained and used to solve the power ramp-up case. This allowed reduction of the maximum MTT loss to 0.88% and subsequently to 0.8%. In spite of the solution potentially being not optimal because of the application of a heuristic technique, the results indicate that the proposed algorithm was successful at reducing the residual DSC to less than the bounding criteria (≤1% loss of MTT).

6. To integrate the suggested approach for detector life extension, this thesis proposed the use of FSN for estimation of instantaneous risk due to detector degradation. Compared with the PRA, the FSN approach had a significant advantage in the fact that the plant data could be continuously collected, expanded, and transferred as needed. Fault

probabilities calculated by FSN were dynamically updated as new knowledge became available or in cases of missing or incomplete data. This was demonstrated in three case studies where system unavailability statistics based on the assumed component failure rates were used in a qualitative/quantitative manner for risk estimation. In these cases, it was assumed that due to a specific system configuration, a detector system would be required to be placed in an unusual state for a short duration. Risk evaluation could still be performed without waiting for the annual PRA model updates using the instantaneous risk estimated from the FSN and comparing it with the existing margin. The results showed that this approach could be used to enable risk-informed decisions for detector extensions and to delay the need for replacements.

6.2. Significance of Results

All steps in the proposed methodology were validated with actual operational data transients. It is expected that the work in this thesis will:

- Provide NPP staff with additional confidence that the impact on MTT due to degradation in aged detectors' PF is acceptable,
- Support a possible strategy of delaying detector replacement,
- Provide an option to avoid having to take compensatory penalties (with the potential for a reactor power de-rate).

These contributions support several fundamental performance objectives, such as system availability, personnel safety, and economic costs:

1. Availability:

   Findings of this thesis can be used to ensure that neutron detection systems can meet the required reliability and availability goals despite degradation due to aging.

2. Personnel Safety:

Findings of this thesis can be used to justify the option of postponing the detector replacement until the planned refurbishment outage. The additional personnel radiation exposure (necessitated by replacement of neutron detector equipment in radioactive areas) and handling and disposal of additional radioactive wastes (generated by the detector replacement campaign) are expected to be significant. The work in this thesis helps ensure that worker radiation exposure is as low as practical and is comparable to industry peers.

3. Economic Impacts:

   The findings of this thesis can be used to optimize the cost of maintenance as a percentage of the overall plant operation and maintenance cost. Operations control specialists can graphically view the risk state of the station and monitor ongoing and planned activities. The work in this thesis supports the extension to the life cycle of the equipment to obtain the most extended effective service life. A portion of the proposed methodology was used to implement one prototypical modification at an NPP. It is expected that, with time, this pilot implementation will serve as the basis for similar changes to the remaining detectors at the NPP in question. Thus, the need for ad-hoc detector replacement before the planned refurbishment campaign can be eliminated.

6.3. Future Work

The scope of the operational cases analyzed in this thesis was narrowed to Pt-clad Inconel in-core neutron detectors. It can be further extended to perform a similar assessment before implementation of this methodology to other neutron detection instrumentation at NPPs. Trend analyses of the installed noise reduction modification and validation against the theoretical cases would be beneficial for both design validation and long-term aging management. A systematic approach to modeling detector response could be used to optimize ongoing verification of system unavailability models against operating experience. The comparison can be performed between the actual and assumed component failure rates and failure modes based on the near real-time plant performance data rather than information collected in the past to avoid large unexpected discrepancies in the system unavailability assumptions. This is particularly suitable for unavailability assessments

where some FMs are not amenable to numerical treatment, e.g., FMs for which no failure data exists, such as latent design or commissioning faults and or common-mode failures due to human interactions.

Since the primary focus of this work is on the overall methodology, only a brief investigation into optimization of data smoothing and filtering was conducted, and a limited set of filtering techniques was selected to explore the importance of denoising process data before future analysis. LPFs used in this study showed promise in terms of reducing the high-frequency components of a signal. One of the limitations noted for this method is that the low-frequency noise in the process signal is typically omitted in the analysis. Also, smoothing of data using sliding average filters comes at a price of some losses in signal shape, amplitude, and SNR versus the desired SNR values (e.g., 110:1 or better) or distortion of the true signal waveform. This can be further explored in future studies.

The wavelet transform method performed better in terms of computational time, which was an important criterion for real-time applications. Application of wavelet analysis techniques combined with careful optimization of smoothing of derivatives could be further investigated to produce better results in terms of an acceptable SNR and loss of signal amplitude. Thus, this method can produce better capabilities to eliminate the high-frequency components of noise, where most of the white noise energy is concentrated, subsequently leading to SNR improvement. Another future exploration of this method over traditional LPFs can focus on numerically controlling the smoothing strength.

Although the work described in this thesis shows the application of FSN-based troubleshooting methods to a simple problem, the same approach can be expanded to apply to more complex problems and larger systems. Traditional methods such as PRA could benefit from the addition of FSN to address model uncertainties and provide a valuable tool to the implementation of risk and reliability analysis. This can be incorporated as early as the design phase to guide the development and verification of emergency operating procedures and assessment of the risk significance of mitigation systems. Furthermore, after the knowledge base has been sufficiently expanded and the accuracy of the forecasting based on the historical data reaches a certain level, the system can be used for real-time

forecasting fault propagation scenarios based on the real-time data. This can be a valuable path forward for future research and development of this method.

References

[1] R.B. Shields, A Platinum In-core Flux Detector, Nuclear Science, IEEE Transactions on, Volume: 20, Issue: 1, Feb. 1973, pp 603 - 608
[2] C.C. Price and J.R. Harvinen, “Evaluation of Self-Powered Detectors in EBR-II”, A.N.S- Trans. -15, No. 1, 366, 1972
[3] J.W. Hilborn, “Self-Powered Neutron Detectors for Reactor Flux Monitoring”, Nucleonics 22 No. 2, 1964, pp 69
[4] D.P. Roux and S.H. Hanauer, “Use of Reactor Gamma Radiation as a Reactor Control and Safety Parameter”, American Nuclear Society. Trans. 6, 74, 1963
[5] H. Ager-Hanssen and R.D. Smith, “Advanced In-Core Instrumentation from Halden”, Nucleonics 22 No. 4, 1964, pp 49
[6] H. Weiss, “Power measurement and Automatic Reactor Control by Gamma or Cerenkov-Radiation”, IAEA Con. on Nucl. Elect. (Bombay) , STl/PUB/115 , 1951
[7] J.A. Sovka, “Response of Cobalt Neutron Flux Detectors”, AECL-3368, 1969
[8] M. Griffiths, G. Bickel, S. Douglas, “Irradiation-Induced Embrittlement of Inconel 600 Flux Detectors in CANDU Reactors”, Journal of Energy and Power Engineering 6, 2012, pp 188-194
[9] D. P. McAllindon, A. Celli, J. W. Hilborn,”Comparison of Predicted and Measured Performance Characteristics of In-Core Flux Detectors”, COG-95-449, April 1996.
[10] INPO SOER 10-2 “Engaged, Thinking Organization: Case Study – Darlington unit De-Rate due to NOP Margin Reduction”
[11] O. Glöckler, “Reactor Noise Measurements in the Safety and Regulating Systems of CANDU Stations”, 8th Symposium on Nuclear Reactor Surveillance and Diagnostics Göteborg, Sweden, May 27-31, 2002
[12] O. Glockler, K. Kapoor, G. Czuppon, "Effective Prompt Fractions of In-Core Flux Detectors Derived from SDSl-induced Power Rundown Test of Darlington Unit 1 on August 28, 1995, Rep. RND-Q2Rev.3, February, 1996
[13] O. Glockler, K. Kapoor, G. Czuppon "Effective Prompt Fractions of In-Core Flux Detectors Derived from SDS2-induced Power Rundown Test of Darlington Unit 2 on November 18, 1995," Rep. RNDRl-Rev.3, February, 1996
[14] 0. Glockler, K. Kapoor, G. Czuppon "Effective Prompt Fractions of In-Core Flux Detectors Derived from SDS2-induced Power Rundown Test of Darlington Unit 4 on August 23, 1996," Rep. RND-T2Rev.l, October, 1996
[15] O. Glockler, K. Kapoor, G. Czuppon, et al, "Effective Prompt Fractions of In-Core Flux Detectors Derived from SDSl-induced Power Rundown Test of Pickering-B Unit 8 on September 17, 1993," PB-IR-63700-5, 1997
[16] O. Glockler, K. Kapoor, G. Czuppon, et al, "Effective Prompt Fractions of HESIR In-Core Flux Detectors Derived from SDSl-induced Power Rundown Test of Pickering-B Unit 6 on March 18, 1996," PB-IR-63700-30, 1997
[17] O. Glockler, M.V. Tulett, "Application of Reactor Noise Analysis in the CANDU Reactors of Ontario Hydro," IMORN-25, Raleigh NC, June 13-15, 1994. Progress in Nuclear Energy, Vol. 29, No. 3/4, pp. 171-191
[18] O. Glockler, M.V. Tulett, "Development and Application of Noise Analysis in CANDU Reactors: Ontario Hydro's Experience Gained in the Past Three Years," 7th

Symposium on Nuclear Reactor Surveillance and Diagnostics, SMORN-VII, Avignon, France, June 19-23, 1995
[19] Bruce A 37M Integrated Safety Analysis and Assessment Report (ISAAR) 61079/RPJ001 R02, Bruce Power CD# NK21-REP-03503-00005, June 21, 2012, proprietary
[20] I. Martchouk, "FUELPIN User's Manual", Nuclear Instruments and Methods in Physics Research Section A: Accelerators, Spectrometers, Detectors and Associated Equipment, Volume 574, Issue 1, 21 April 2007, Pages 127-132
[21] E. Wilson, M. Anderson, D. Prendergast, D.Cheneler, "Comparison of CdZnTe neutron detector models using MCNP6 and Geant4", in proceedings of ANIMMA 2017 EPJ Web of Conferences 170, 08008 (2018)
[22] M. E. Abhold, M. C. Baker, "MCNP-REN: a Monte Carlo Tool for Neutron Detector Design", Nuclear Instruments and Methods in Physics Research Section A Accelerators Spectrometers Detectors and Associated Equipment 485(3):576-584, June 2002
[23] L. M. Scallan, "Efficiency Modeling for Neutron Detectors", in proceedings of the 58th Annual Meeting of the Health Physics Society, 7-11 July 2013, Madison, WI
[24] D. Bi, D. Xu, J. Bu, "A Unified Framework for Modeling Slow Response Self-Powered Neutron Detectors with Discrete-time State-space Representation", in proceedings of the 3rd International Conference on Advancements in Nuclear Instrumentation Measurement Methods and their Applications (ANIMMA), Marseille, France 2013, IEE Xplore 30 January 2014.
[25] L. Xia, "Development of 3-D Neutronic Kinetic Model and Control for CANDU Reactors", Electrical and Computer Engineering Doctoral Thesis, Electronic Thesis and Dissertation Repository, University of Western Ontario, 2012
[26] J. Yu, "Simulation of Dynamic Response of Self-Powered-Inconel-Neutron-Detector Lead Cables Using a Semi-Empirical Model", Faculty of Energy Systems and Nuclear Science - Master Theses, UOIT, November 2013
[27] G. d'Urso, P. Prieur, C. Vincent, "Blind identification methods applied to Electricite de France's civil works and power plants monitoring", in proceedings of the IEEE Signal Processing Workshop on Higher-Order Statistics, 1997, pp. 82 – 86
[28] D. Donoho, "Nonlinear Wavelet Methods for Recovery of Signals, Densities, and Spectra from Indirect and Noisy Data", Different Perspectives on Wavelets, Proceeding of Symposia in Applied Mathematics, Vol. 47, I. Daubechies ed. Amer. Math. Soc., Providence, R.I., 1993, pp 173-205
[29] B. Buades, C. Morel, J. Morel, "A Review of Image Denoising Algorithms, with a New One", Multiscale Model Simul., Volume 4, No 2, pp. 490–530
[30] P. Lei, "Adaptive Median Filtering", report in proceedings of "Machine Vision: Digital Image Processing", pp 140-429
[31] C. Zhou, D.M. Hepburn, X. Song, et al, "Application of denoising techniques to PD measurement utilizing UHF, HFCT, acoustic sensors and IEC60270", in proceeding of 20th International Conference and Exhibition on Electricity Distribution - Part 1, 2009
[32] L. Wang, M. Wang, L. Zhang, et al, "Kalman Filter's Application in Denoising of Power Spectrum Estimate in AR Process" in proceedings of the International Symposium on Intelligent Information Technology Application Workshops, 2008, pp. 825-828

[33] E. B. Halim, M.A.A.S. Choudhury, S. L. Shah, et al, "Time domain averaging across all scales: A novel method for detection of gearbox faults", Mechanical Systems and Signal Processing 22, 2008, pp. 261–278
[34] F. Combet, L. Gelman, "An automated methodology for performing time synchronous averaging of a gearbox signal without speed sensor", Mechanical Systems and Signal Processing 21, 2007, pp. 2590–2606
[35] X. Zhou, Y. Shao, D. Zhen, et al," Gear Fault Signal Detection based on an Adaptive Fractional Fourier Transform Filter", in proceeding of the 9th International Conference on Damage Assessment of Structures, Journal of Phys. Conference Series, 2011.
[36] K. Clair, J. Stenberg, "Signal Processing Techniques for Determining Powerplant Characteristics", Final Report, Bureau of Reclamation, Denver CO, 2012, http://www.usbr.gov/research/projects/detail.cfm?id=9962
[37] H.M. Hashemian, "Application of Advanced Technology to Improve Plant Performance in Nuclear Power Plants", IAEA MTCD publication, http://www-pub.iaea.org/MTCD/publications/PDF/P1500_CD_Web/htm/pdf/plenary/13KS_H.Hashemian.pdf
[38] Y.X. Zhang, R.B. Randall, "Rolling element bearing fault diagnosis based on the combination of genetic algorithms and fast kurtogram", Mechanical Systems and Signal Processing 23, 2009, pp. 1509–1517
[39] S.W. Lee, B. H. Nam, "Peak Detection of ECG Signal using Wavelet Transform and Radial Bases Functions", in proceedings of the 39th SICE Annual Conference, 1999, pp 1067-1070
[40] K. Goebel, A. Agogino, "Fuzzy sensor fusion for gas turbine power plants", in proceedings of SPIE, Sensor Fusion: Architecture, Algorithms, and Applications III, Vol. 3719, 1999, pp. 52-61
[41] S. Tian, Z. Chena, M. Uedab, et al "Signal processing schemes for Eddy Current Testing of steam generator tubes of nuclear power plants" , Elsevier, Nuclear Engineering and Design, Volume 245, 2012, pp78–88
[42] S. Saha, et al. "Identification of Nonlinear Systems From the Knowledge Around Different Operating Conditions: A Feed-Forward Multi-Layer ANN Based Approach." Parallel Distributed and Grid Computing (PDGC), 2012, 2nd IEEE International Conference on, Dec. 2012, pp 413 - 418
[43] A. Graps, "An introduction to wavelets", Computational Science & Engineering, IEEE, Volume: 2 , Issue: 2 , pp 50 – 61
[44] D. K. Hammond and E.P. Simoncelli, " A machine learning framework for adaptive combination of signal denoising methods", in proceedings of IEEE International Conference on Image Processing, San Antonio, TX, Oct 2007
[45] A. Bakhtazad, A. Palazoglu, J. Romagnoli, "Process trend analysis using wavelet-based de-noising", Control Engineering Practice 8, 2000, pp. 657-663
[46] H. Zamanian and A. Ohadi, "Gearbox Fault Detection through PSO Exact Wavelet Analysis and SVM Classifier", in proceedings of the 18th Annual International Conference on Mechanical Engineering-ISME, 11-13 May, 2010
[47] X. Wang and D. Zhang, "Denoising of Generator Output Power based on the wavelet transform", in proceedings of the 24th Chinese Control and Decision Conference (CCDC), 2012, pp. 3307 – 3310

[48] X. Zhao, and X. Wang, “A Fault Detection Algorithm Based on Wavelet Denoising and KPCA”, Advances in Future Computer and Control Systems, Vol. 1, 2012, pp. 311-317
[49] C.Ji, R. Zhang, S. Wen, et al, “Flame Image of Pint-Sized Power Plant’s Boiler Denoising Using Wavelet-Domain HMT Models”, Springerlink: Advances in Intelligent Computing, Lecture Notes in Computer Science Volume 3645, 2005, pp. 910-919
[50] S. Tian et al, “Signal Processing Schemes for Eddy Current Testing of Steam Generator Tubes of Nuclear Power Plants”, Nuclear Engineering and Design 245 (2012), pp. 78– 88
[51] J. Liu, and P. Pilay, “Application of wavelet analysis in power system disturbance modeling”, in proceeding of: Africon, 1999, IEEE, Volume: 2
[52] I.Yilmazlar, and G. Kokturk, “Power system failure analysis by using the discrete wavelet transform”, IEEE Transactions on Power Delivery 05, 2002
[53] Das, Saptarshi, et al. "A new fractional fourier transform based design of a band-pass FIR filter for power feedback in nuclear reactors under noisy environment." Emerging Trends in Electrical and Computer Technology (ICETECT), 2011 International Conference on. IEEE, 2011
[54] Das, Saptarshi, I. Pan, et al. "Fractional order fuzzy control of nuclear reactor power with thermal-hydraulic effects in the presence of random network induced delay and sensor noise having long range dependence." Energy Conversion and Management 68, 2013, pp. 200-218
[55] E. Nasimi, H. A.Gabbar, “Signal Denoising Methods For Fault Diagnosis and Troubleshooting At CANDU® Stations”, Nuclear Engineering and Design, Elsevier, 280, 2014, pp. 481–492
[56] U. Pareek and I. N. Kar, “Estimating Compressor Discharge Pressure of Gas Turbine Power Plant Using Type-2 Fuzzy Logic Systems,” in Proceedings of the IEEE International Conference on Fuzzy Systems, Vancouver, Canada, July 2006, pp. 649–654
[57] A. C. Rencher, “Methods of Multivariate Analysis”, Second Edition, John Wiley & Sons, Inc, pg 1, 727 pgs.
[58] N. Pettorelli, S. Dray & D. Maillard, “Coupling Principal Component Analysis and GIS to Map Deer Habitats”, Wildlife Biology, 11:4, 2005
[59] R. Goodacre, S. Trew, C. Wrigley-Jones, et al, “Rapid Screening for Metabolite Overproduction in Fermentor Broths Using Pyrolysis Mass Spectrometry with Multivariate Calibration and Artificial Neural Networks”, Biotechnology and Bioengineering 44, 1994, pp. 1205-1216
[60] É.M Timmins, S. A. Howell, B. K. Alsberg, et al, “Rapid Differentiation of Closely Related Candida Species and Strains by Pyrolysis Mass Spectrometry and Fourier Transform Infrared Spectroscopy”, Journal of Clinical Microbiology 36, , 1998, pp. 367-374
[61] U. Demšar, P. Harris, C. Brunsdon, et al, “Principal Component Analysis on Spatial Data: An Overview”, Routledge, Annals of the Association of American Geographers, 05 July 2012
[62] P. Sanguansat, “Principal Component Analysis - Multidisciplinary Applications”, InTech, February 29, 2012, 212 pgs.
[63] S. Yin, “On PCA-based Fault Diagnosis Techniques”, IEEE Conference on Control and Fault-Tolerant Systems (SysTol), 2010, 6-8 Oct. 2010

[64] S. Zhou, J.Zhang, and S.Wang, “Fault Diagnosis in Industrial Processes Using Principal Component Analysis and Hidden Markov Model”, American Control Conference Boston, Massachusetts June 30 - July 2, 2004
[65] L. H. Chiang, E. L. Russell, R.D. Braatz, “Fault Diagnosis in Chemical Processes using Fisher Discriminant Analysis, Discriminant Partial Least Squares, and Principal Component Analysis”, Chemometrics and Intelligent Laboratory Systems 50, 2000, pp. 243–252
[66] C. Rosen and J. Lennox, “Multivariate and Multiscale Monitoring of Wastewater Treatment Operation,” Water research, vol. 35, 2001, pp. 3402– 3410
[67] W. Sandham, M. Leggett (Eds.), “Geophysical Applications of Artificial Neural Networks and Fuzzy Logic”, Kluwer Academic Publishers, 2003
[68] L.A. Zadeh, O. Kaynak, B. Turksen, et al, “Roles of Soft Computing and Fuzzy Logic in the Conception, Design and Deployment of Information/Intelligent Systems”, Computational Intelligence: Soft Computing and Fuzzy-Neuro Integration with Applications, (Eds.), 1998, pp. 1-9
[69] E. Nasimi, H.A. Gabbar, “Application of Principal Component Analysis for the Diagnosis of Neutron Overpower System Oscillations in CANDU reactors”, Elsevier Nuclear Engineering and Design, 270, 2014, pp. 238-248
[70] X. Peng, Q. Li, Kan Wang, “Fault Detection and Isolation for Self-Powered Neutron Detectors based on Principal Component Analysis”, Annals of Nuclear Energy
Volume 85, November 2015, pp. 213–219
[71] J. Kennedy; R. Eberhart, “Particle swarm optimization”, in proceedings of IEEE Conference on Neural Networks, 1995
[72] Y. Shi ; R. Eberhart, “A modified Particle Swarm Optimizer”, Evolutionary Computation Proceedings, 1998, IEEE World Congress on Computational Intelligence, 1995
[73] IAEA-TECDOC-1383, “Guidance for optimizing nuclear power plant maintenance programmes”, Report prepared within the framework of the Technical Working Group on Life Management of Nuclear Power Plants, December 2003
[74] A. Teyssedoua, J. Dipamaa, W. Hounkonnoua, et al, “Modeling and Optimization of a Nuclear Power Plant Secondary Loop”, Nuclear Engineering and Design, Volume 240, Issue 6, June 2010, pp. 1403–1416
[75] Volkanovski and L. Cizelj, “Nuclear Power Plant Maintenance Optimization with Heuristic Algorithm”, Science and Technology of Nuclear Installations, Volume 2014 (2014), Article ID 458016, 13 pages
[76] D. Babazadeha, MBoroushakia, C. Lucasb, “Optimization of fuel core loading pattern design in a VVER nuclear power reactors using Particle Swarm Optimization (PSO)’, Annals of Nuclear Energy, Volume 36, Issue 7, July 2009, pp. 923–930
[77] K. G. Felker, A. R. Siegel, and S. F. Siegel, “Optimizing Memory Constrained Environments in Monte Carlo Nuclear Reactor Simulations”, International Journal of High Performance Computing Applications, April, 2012
[78] T. Aoki, N. Kodama, K. Takase, et al, “Study of the Optimization of Maintenance Plan for Nuclear Power Plants”, E-Journal of Advanced Maintenance, Japan Society of Maintenology, Vol.6 2014, pp.1-13

[79] A. Zolfaghari, H. Minuchehr, A. Noroozy, et al, “PWR Nuclear Power Plants Fuel Management Optimization”, Conference Paper, 17th International Conference on Nuclear Engineering, January 2009
[80] Rasmussen, Norman C.; et al. (1975-10). "Reactor safety study. An assessment of accident risks in U. S. commercial nuclear power plants. Executive Summary", WASH-1400 (NUREG-75/014), Rockville, MD, USA: Federal Government of the United States, U.S. Nuclear Regulatory Commission.
[81] Harold Lewis, “Risk Assessment Review Group Report to the U. S. Nuclear Regulatory Commission, NRC”, Nuclear Age, Black Inc., 1978, p. 288.
[82] Andrews, J. D. and S. J. Dunnett, “Event Tree Analysis Using Binary Decision Diagrams”, IEEE Trans. Reliability, 49(2):230–238 (2000).
[83] Henley, E. J. and H. Kumamoto, “Probabilistic Risk Assessment and Management for Engineers and Scientists”, 2nd ed., IEEE Press, 1996.
[84] Kapan, S. and B. J. Garrick, “On the Quantitative Definition of Risk, Risk Analysis”, 1:11–37 (1981).
[85] NASA, “Fault Tree Handbook with Aerospace Applications”, version 1.1. NASA, August 2002.
[86] M. Kalantarnia, F. Khan, and K. Hawboldt, K., “Modelling of BP Texas City Refinery Accident Using Dynamic Risk Assessment Approach”, Process Safety and Environmental Protection 88, 2010, pp. 191-199
[87] L. H. Chiang, and R. D. Braatz, “Process Monitoring Using Causal Map and multivariate Statistics: Fault detection and Identification”, Chemometrics and Intelligent Laboratory Systems 65, 2003, pp. 159– 178
[88] S. W.Choia, C. Lee, J-M. Lee, et al, “Fault Detection and Identification of Nonlinear Processes Based on Kernel PCA”, Chemometrics and Intelligent Laboratory Systems (75), 2005, pp. 55– 67
[89] R. Rengaswamy, V.Venkatasubramanian, ”A Fast Training Neural Network and its Updation for Incipient Fault Detection and Diagnosis”, Computers and Chemical Engineering (24) 43, 2000, pp. l-437
[90] Y. Zhou, J. Hahn, and M. S. Mannan, “Fault Detection and classification in Chemical Processes Based on Neural Networks with Feature Extraction”, ISA Transactions 42, 2003, pp. 651–664
[91] Z. Zheng et al, “A Practical Failure Prediction with Location and Lead Time for Blue Gene/P”, International Conference on Dependable Systems and Networks Workshops, 2010, pp. 15-22
[92] J. Gu et al, “Dynamic Meta-Learning for Failure Prediction in Large-Scale Systems: A case Study”, International Conference on Parallel Processing, 2008, pp. 157-164
[93] R. Sahoo and A. Oliner, “Critical Event Prediction for Proactive Management in Large-scale Computer Clusters”, SIGKDD International Conference on Knowledge Discovery and Data mining, 2003, pp. 426-435
[94] M. Kalantarnia, F. Khan, K. Hawboldt, “Dynamic risk assessment using failure assessment and Bayesian Theory”, Journal of Loss Prevention in the Process Industries 22, 2009, pp. 600–606
[95] M. S. Gönül, D. Önkal, M. Lawrence, “The Effects of Structural characteristics of Explanations on Use of a DSS”, Decision Support Systems (42), 2006, pp. 1481–1493

[96] S.M. Virk, A. Muhammad, A.M. Martinez-Enriquez, “Fault Prediction Using Artificial Neural Network and Fuzzy Logic”, MICAI '08: Seventh Mexican International Conference on Artificial Intelligence , 27-31 Oct. 2008, pp. 149 - 154
[97] W. Sandham, M. Leggett (Eds.), “Geophysical Applications of Artificial Neural Networks and Fuzzy Logic”, Kluwer Academic Publishers, 2003
[98] L.A. Zadeh, O. Kaynak, B. Turksen, et al, “Roles of Soft Computing and Fuzzy Logic in the Conception, Design and Deployment of Information/Intelligent Systems”, Computational Intelligence: Soft Computing and Fuzzy-Neuro Integration with Applications, (Eds.), 1998, pp. 1-9
[99] J.S.R. Jang, “ANFIS: Adaptive Network based Fuzzy Inference Systems”, IEEE Transactions Systems, Man & Cybernetics, 1991
[100] M. Sugeno, “Industrial Applications of Fuzzy Control”, Elsevier Science Pub Co., 1985
[101] V. Cherkassky, O.Kayak, L.A. Zadeh et al (Eds.), “Fuzzy Inference Systems: A Critical Review”, Computational Intelligence: Soft Computing and Fuzzy-Neuro Integration with Applications”, Springer, 1998, p. 177-197
[102] K. E. Holbert, K.Lin, “Nuclear Power Plant Instrumentation Fault Detection Using Fuzzy Logic”, Science and Technology of Nuclear Installations, Volume 2012, 2012, pp. 11
[103] F. R. Rubio, M. Berenguel, and E. F. Camacho, “Fuzzy Logic control of a Solar Power Plant,” IEEE Transactions on Fuzzy Systems, vol. 3, no. 4, 1995, pp. 459–468
[104] A. Flores, D. Sáez, J. Araya, et al, “Fuzzy Predictive control of a Solar Power Plant,” IEEE Transactions on Fuzzy Systems, vol. 13, no. 1, 2005, pp. 58–68
[105] C. M. Leuba, M. Abdalla, C. E. Ford, et al, “Hybrid Fuzzy-PI Adaptive control for U-tube Steam Generators,” Control, Theory and Advanced Technology, vol. 8, no. 3, 1992, pp. 567–575
[106] N. Na, K. Kwon, C. Ham, et al, “A Study on Water Level control of PWR Steam Generator at Low Power and the Self-tuning of its Fuzzy Controller,” Fuzzy Sets and Systems, vol. 74, no. 1, 1995, pp. 43–51
[107] G. Y. Park and P. H. Seong, “Application of a Fuzzy Learning Algorithm to Nuclear Steam generator Level control,” Annals of Nuclear Energy, vol. 22, no. 3-4, 1995, pp. 135–146
[108] G. Wang and K. E. Holbert, “Hybrid Classical-fuzzy Controller for a Power Plant Water Supply System,” in Proceedings of the 34th Annual North American Power Symposium, Tempe, Ariz, USA, October 2002, pp. 352–359
[109] W. Yang, K. Y. Lee, S. T. Junker, et al, “Fuzzy Fault Diagnosis and Accommodation System for Hybrid Fuel-cell/Gas-turbine Power Plant,” IEEE Transactions on Energy Conversion, vol. 25, no. 4, 2010, pp. 1187–1194
[110] R. Berrios, F. Núñez, and A. Cipriano, “Fault Tolerant Measurement System Based on Takagi-Sugeno Fuzzy Models for a gas Turbine in a Combined Cycle Power Plant,” Fuzzy Sets and Systems, vol. 174, no. 1, 2011, pp. 114–130
[111] U. Pareek and I. N. Kar, “Estimating Compressor Discharge Pressure of Gas Turbine Power Plant Using Type-2 Fuzzy Logic Systems,” in Proceedings of the IEEE International Conference on Fuzzy Systems, Vancouver, Canada, July 2006, pp. 649–654
[112] H.A. Gabbar, “Qualitative Fault Propagation Analysis”, Journal of Loss Prevention in the Process Industries, Vol. 20, No. 3, 2007, pp. 260–270

[113] H. A. Gabbar, "Improved Qualitative Fault Propagation Analysis", Journal of Loss Prevention in the Process Industries 20, 2007, pp. 260-270
[114] H.E. Sayed and H. A. Gabbar, and S. Miyazaki, “Faults Forecasting System”, World Academy of Science, Engineering and Technology 29, 2009
[115] H. A. Gabbar, “Fault Semantic Networks for Accident Forecasting of LNG Plants”, Knowledge-Based and Intelligent Information and Engineering Systems, Lecture Notes in Computer Science, Volume 6277/2010, pp. 427-437
[116] H. A. Gabbar and P. Sauer , “Knowledgebase and Acquisition System for Failure and Accident Analysis of Gas Processing Facilities”, in proceedings of International Workshop on Real Time Measurement, Instrumentation & Control [RTMIC] 19 – 1, IEEE NPSS (Toronto), UOIT, Oshawa, ON, 25 & 26 June, 2010
[117] E. Nasimi, H.A. Gabbar, “Development Of Design Support Tool Using Hierarchical Control Chart (HCC) and IEC61131 for Nuclear Power Plant Control”, Journal of Process Systems Engineering (Mar-2010)
[118] H.A. Gabbar and R. Bedard, “Hazard Analysis and Accident Prediction for LNG Plants”, In proceedings of International Workshop on Real Time Measurement, Instrumentation & Control [RTMIC] 18 – 1, IEEE NPSS (Toronto), UOIT, Oshawa, ON, 25 & 26 June, 2010
[119] H. A. Gabbar and F. I. Khan, “Design of Fault Semantic Networks to Integrate Fault, Failure, Hazard, and Accident Models for LNG Plants”, 21st European Symposium on Computer Aided Process Engineering, 1st Edition, Pistikopoulos, Georgiadis and Kokossis (Eds), Elsevier, 07 July 2011
[120] S. Hussain, A. Hossein, H.A. Gabbar, “Tuning of fault semantic network using Bayesian theory for probabilistic fault diagnosis in process industry”, in proceedings of 2013 International Conference on Quality, Reliability, Risk, Maintenance, and Safety Engineering (QR2MSE), 2013
[121] J. J. Downs and E. F. Vogel, “A plant wide industrial process control problem”, Computers chem. Engng. Vol. 17, No.3 , 1993, pp. 245-255
[122] C. Westbury and L. Buchanan, M. Sanderson, et al, “Using Genetic Programming to Discover Nonlinear Variable Interactions”, Behavior Research Methods, Instruments, & Computers 2003, 35(2), pp. 202-216
[123] A. H. Hosseini, S. Hussain, H. A. Gabbar, “Detecting Nonlinear Interrelation Patterns among Process Variables Using Genetic Programming and its application in Fault semantic Network”, Soft Computing - Methodologies and Application, Volume 18, Issue 7, July 2014, pp. 1283-1292
[124] H. A. Gabbar, P.W.H. Chung, K. Suzuki, et al, “Utilization of unified modeling language (UML) to represent the artifacts of the plant design model”, International Symposium on Design, Operation and Control of Next Generation Chemical Plants (PSE Asia), PS54, 2000, pp. 387-92
[125] H. A. Gabbar, K. Suzuki, Y. Shimada, “Study on plant object-oriented model formalization - case study: HDS plant design”, Journal of Design Studies, Vol. 24 No. 1, 2003, pp. 101-8
[126] T. Azad and H. A. Gabbar, “Fault semantic network for micro grid diagnosis and control”, in proceeding of IEEE International Conference on Smart Grid Engineering (SGE), 27-29 Aug. 2012, pp.1-8

[127] E. Nasimi, H. A. Gabbar, “FSN-Based Fault Modeling in CANDU ® Stations”, in Annals of Nuclear Energy 65: March 2014, pp. 325–337
[128] A. Savitzky A., M. J. E. Golay, “Analytical Chemistry”, vol. 36, 1964, pp. 1627–1639
[129] T. O’Haver, “A Pragmatic Introduction of Signal Processing with Applications in Scientific Measurement”, An illustrated essay, 1997, available from https://terpconnect.umd.edu/~toh/spectrum/IntroToSignalProcessing.pdf
[130] A. Graps, “An introduction to wavelets”, Computational Science & Engineering, IEEE, Volume: 2 , Issue: 2 , pp 50 – 61
[131] H. Qiu, J. Lee, J. Lin, G.Yu, "Wavelet filter-based weak signature detection method and its application on rolling element bearing prognostics", Journal of Sound and Vibration, 2006, pp. 1066–1090
[132] A. Bakhtazad, A. Palazoglu, J. Romagnoli, “Process trend analysis using wavelet-based de-noising”, Control Engineering Practice 8, 2000, pp. 657-663
[133] R. Rengaswamy, V.Venkatasubramanian, ”A Fast Training Neural Network and its Updation for Incipient Fault Detection and Diagnosis”, Computers and Chemical Engineering (24) 43, 2000, pp. l-437
[134] S. W. Choia, C. Lee, J-M. Lee, et al, “Fault Detection and Identification of Nonlinear Processes Based on Kernel PCA”, Chemometrics and Intelligent Laboratory Systems (75), 2005, pp. 55– 67
[135] Y. Zhou, J. Hahn, and M. S. Mannan, “Fault Detection and classification in Chemical Processes Based on Neural Networks with Feature Extraction”, ISA Transactions 42, 2003, pp. 651–664
[136] K. P. Kording and D. M. Wolpert, “Bayesian decision theory in sensorimotor control”, TRENDS in Cognitive Sciences, Vol.10, No.7, July 2006, Elsevier, Special Issue: Probabilistic models of cognition.
[137] J. G. Ziegler and N. B. Nichols, “Optimum Settings for Automatic Controllers”, Trans. ASME, Vol. 64, 1942, pp. 759-768
[138] A. E. Summers, “Introduction to Layer of Protection Analysis”, Sis-Tech Solutions, published In Journal Of Hazardous Materials, LP, presented At The Mary Kay O’Conner Process Safety Center Symposium, Texas A&M University, October 2002, 2002
[139] V. J. Pohjola, R. Koivisto, M. K. Alha, “Conceptual association of safety with process design and operation, in proceedings of Proceedings of the Second International Conference on Foundations of Computer-Aided Process Operations, Crested Butte, Colorado, July 18-23,1993 pp. 457-462
[140] N. Wahba, V.Mehdi-Nejad, “Review of Expert Reports Investigating the Moderator Temperature Fluctuations and Impact on Fuel Channel Integrity”, COG OP-06-2056, May 2007, protected.